Early transcriptional changes in neutrophil-mediated processes following recanalization after ischemic stroke

Truong An Bui[1,2], Yonglie Ma[1], Glen C Jickling[2,3], Ian R Winship[1,2,*]

[1]Neurochemical Research Unit, Department of Psychiatry, Faculty of Medicine and Dentistry, University of Alberta, Edmonton, Alberta, Canada

[2]Neuroscience and Mental Health Institute, University of Alberta, Edmonton, Alberta, Canada

[3]Department of Medicine, Faculty of Medicine and Dentistry, University of Alberta, Edmonton, Alberta, Canada

* Corresponding Author: Ian Winship, Email: iwinship@ualberta.ca

Abstract

Background: Ischemic stroke is a leading cause of mortality and long-term disability globally. Recanalization therapies restore blood flow by thrombolysis and/or mechanical thrombectomy. Despite successful recanalization, many patients still experience poor clinical outcomes. This phenomenon, known as futile recanalization, may result from reperfusion injury and microcirculatory failure. Given the short therapeutic window for ischemic stroke, it is critical to identify early biomarkers that could be targeted to minimize pathology and extend the therapeutic window to improve clinical outcomes.

Methods: Using a murine middle cerebral occlusion (MCAO) model that mimics a large vessel occlusion with recanalization, a comprehensive microarray analysis of gene expression from blood samples collected immediately and 3 hours after recanalization (N=44) was performed. Differentially expressed genes (DEGs), enrichment pathways, immune cell proportions, enriched cell markers, and predicted miRNAs and transcription factors were identified using RStudio. Findings in mice were validated in datasets of rat MCAO stroke (GSE21136) and human stroke patients (GSE16561) to confirm transcriptional changes in peripheral blood post-recanalization.

Results: *Il1r2, Cd55, Mmp8, Cd14,* and *Cd69* were identified as early biomarkers in blood after stroke and recanalization. Further, cross-validation revealed *Vcan* as a DEG conserved across species, making it a novel marker of ischemia detected as early as 3 hours post-recanalization (4 hours post-MCAO) in mice, 24 hours after recanalization in rats (MCAO-thrombectomy), and within 24 hours from onset in humans receiving rtPA-thrombolysis. Using human (CIBERSORTx) and murine (ImmuCellAI-mouse) cell deconvolution reference datasets, neutrophil was elevated post-recanalization. Leukocyte and neutrophil activation pathways were significantly enriched early after stroke in mouse and human samples, with a stronger upregulation observed in females of both species. The analysis revealed several key miRNAs involved in gene regulation following recanalization; NFE4 and MTF1 emerged as essential transcription factors in these processes. Based on these data, a coregulatory network underlying neutrophil activity was constructed, highlighting its central role in early responses to ischemia and recanalization, which was enriched in females.

Conclusions: This study identified new early genomic markers in the blood for ischemia and recanalization, as well as critical age- and sex-specific factors. By mapping a coregulatory network of interacting genes and neutrophil-related pathways, as well as identifying the novel

marker *Vcan*, the data provides insights to inform future research and develop targeted therapies. Such therapies can improve treatment efficacy or modulate neutrophils to reduce futile recanalization, ultimately enhancing clinical outcomes for ischemic stroke patients.

Keywords: recanalization, ischemic stroke, biomarkers, neutrophil, peripheral response, reperfusion injury

Graphical Abstract

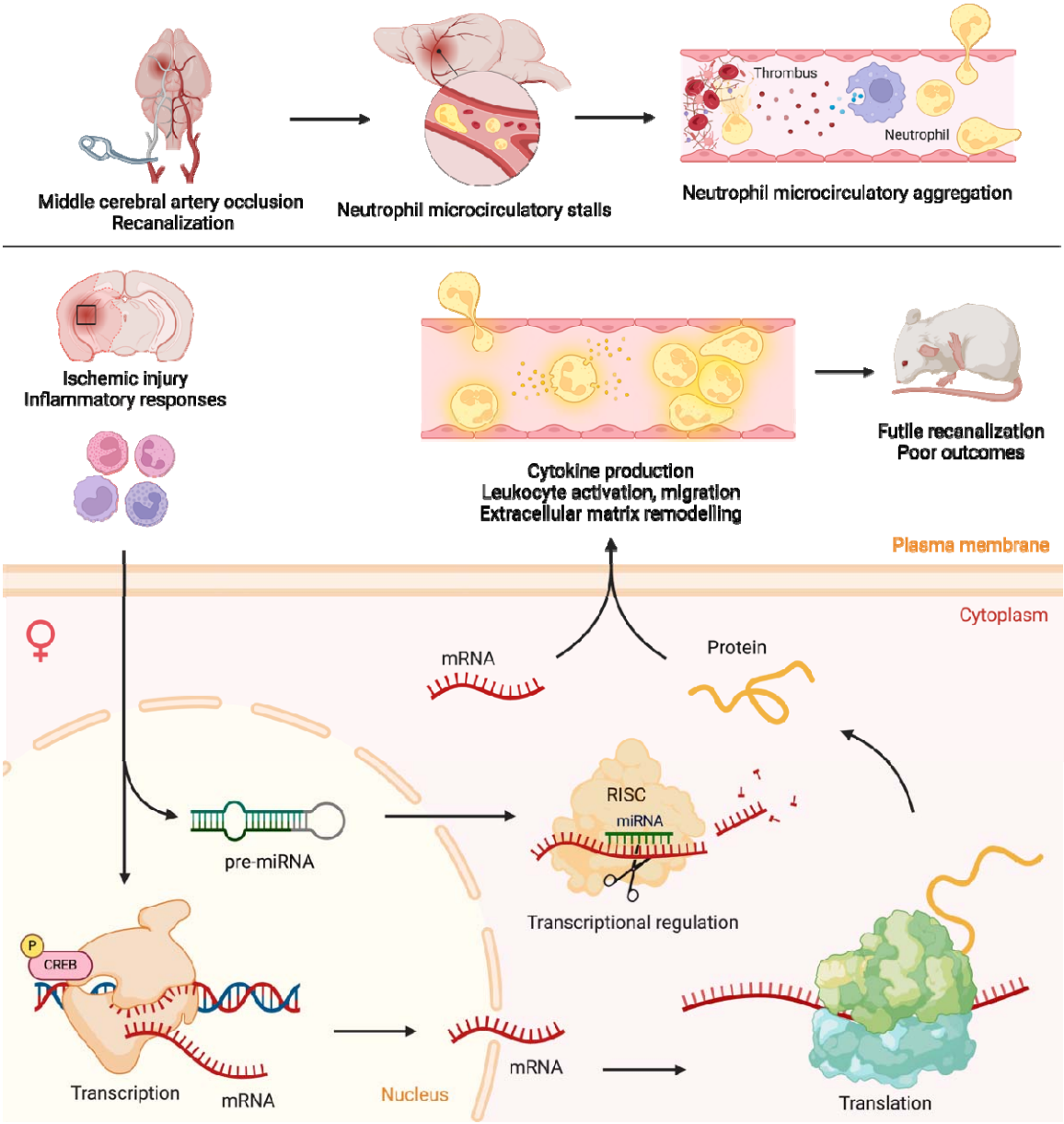

Clinical and research perspectives

This study identifies *Il1r2*, *Cd55*, *Mmp8*, *Cd14*, *Cd69*, and *Vcan* as novel, early blood biomarkers of ischemic stroke and reperfusion injury following recanalization. Notably, *Vcan* was conserved across rodent and human models, underscoring its translational potential. These peripheral hemo-genomic signatures hold promise as biomarkers to help identify patients at higher risk of futile recanalization, thereby enabling earlier, more tailored clinical interventions to reduce reperfusion injury and improve recovery. The significant increase in neutrophil proportions, demonstrated through deconvolution of both human and murine reference datasets, supports prior evidence implicating neutrophil aggregation in reperfusion failure and highlights this cell type as a key target for further investigation. Moreover, the pronounced neutrophil-related transcriptional responses in females suggest that sex-specific mechanisms may influence stroke outcomes and warrant consideration in therapeutic design in acute stroke management. At the mechanistic level, the study reveals a core gene regulatory network—centred on neutrophil-associated genes, transcription factors NFE4 and MTF1, and stroke-associated miRNAs—that orchestrates early immune responses to ischemia and recanalization. Collectively, these findings suggest potentially predictive molecular signatures of reperfusion failure following recanalization. Future studies could investigate whether targeting these regulatory elements can prevent futile recanalization, thus improving long-term functional outcomes.

Introduction

In the 2021 Global Burden of Diseases, Injuries, and Risk Factors Study, stroke was identified as the third leading cause of mortality worldwide, following ischemic heart disease and COVID-19 (1). Ischemic stroke, the predominant subtype, accounts for approximately 75-80% of all stroke cases (2). In 2021, stroke also resulted in an estimated 3,870,000 deaths globally (1,3) and contributed to 160.4 million disability-adjusted life years (4). The epidemiology of stroke reveals a pronounced age-related incidence, predominantly affecting individuals aged 65 and older (2). Notably, there is a sex disparity in the age of onset, with women experiencing strokes 4 to 6 years later than men (5). However, women under 35 years old have a 44% higher likelihood of ischemic stroke relative to men and women overall have a greater lifetime risk of ischemic events and transient ischemic attacks (6). After middle age, the incidence and long-term risks of ischemic stroke rise more steeply in women, paralleled by an increase in the severity of resultant disabilities (7). This heightened risk with increasing age contributes to a significant public health challenge, given the global demographic shifts towards the aging populations (8).

The best available treatment for ischemic stroke is recanalization therapy via thrombolysis with recombinant tissue plasminogen activator (alteplase) (r-tPA) or tenecteplase (9) and/or endovascular therapy (EVT) (10). While recanalization restores flow in the occluded vessel, this does not always extend into the microcirculation that nourishes brain tissue. This can result from collateral failure, whereby cerebral ischemia in penumbral regions worsens over time due to the collapse of the collateral circulation (11). It also results from microcirculatory failure, where dysfunction in the small blood vessels within the brain tissue impairs microcirculation, despite the large vessels being recanalized (12). A key contributor to this dysfunction is the post-ischemic “stalling” of neutrophils within cerebral microvessels. After recanalization, neutrophils can adhere to endothelial cells and aggregate in microvessels, thereby preventing blood flow, becoming activated, and releasing pro-inflammatory cytokines, which amplify tissue damage and drive further inflammation (for review, see (13)).

Ischemic stroke progression follows a well-defined time course, beginning with the immediate occlusion of a major cerebral artery, leading to a rapid depletion of oxygen and glucose, energy failure, and excitotoxicity in the infarct core, while the surrounding penumbra remains metabolically active but vulnerable (14–16). Without timely intervention, the penumbra undergoes irreversible damage as collateral circulation fails and inflammation escalates (17). The

therapeutic window for recanalization is highly restricted—thrombolysis with r-tPA is only approved within 4.5 hours of stroke onset, and EVT is most effective within 6-24 hours for select patients (18–20). Furthermore, while recanalization aims to restore blood flow, alleviate tissue hypoxia, and salvage ischemic tissue, restoration of flow can paradoxically cause tissue damage. This complication, known as reperfusion injury, happens when blood flow is abruptly restored to previously ischemic tissue after a period of oxygen deprivation. This causes a rush of molecular oxygen, leading to the rapid production of reactive oxygen species. This, in turn, causes oxidative stress, prolonged inflammation, and activation of immune cells in the blood and brain and can potentiate microcirculatory failure (21).

Although the success rate of recanalization has improved over time, many patients still experience poor long-term outcomes, as measured by the modified Rankin Scale (mRS) at 90 days and the National Institutes of Health Stroke Scale. This phenomenon, known as futile recanalization—where patients remain functionally dependent despite successful recanalization (mRS $\geq$ 3)—occurs in 32-57% of ischemic stroke patients who undergo EVT (22,23) and is exacerbated by collateral failure, microcirculatory failure, and reperfusion injury (11,24).

Patterns of gene expression following ischemic stroke offer valuable insights into the underlying causes of reperfusion injury and potential outcomes of recanalization. Comparative analyses of gene expression profiles across different types of blood cells in stroke patients reveal that transcriptional alterations primarily occur in neutrophils as early as 15 minutes after ischemic onset (25). These transcriptional shifts are modulated by interactions among neutrophils, platelets, and cytokines, which can amplify the inflammatory response and influence stroke outcomes (13). This suggests neutrophils can be an early peripheral and genomic signature of post-recanalization microcirculatory failure (26). Changes in gene expression profiles may indicate ongoing inflammatory and repair processes, potentially serving as biomarkers to assess the severity and progression of stroke, as well as the risks and mechanisms of futile recanalization.

There remains a critical need to identify novel biomarkers that can reliably predict which patients are at the highest risk of microcirculatory failure and futile recanalization. Current clinical assessment tools are insufficient in capturing the complex interplay between immune responses, endothelial dysfunction, and reperfusion injury at a molecular level (27). A deeper understanding of the transcriptomic landscape of circulating immune cells, particularly

neutrophils, could reveal novel prognostic markers and therapeutic targets to mitigate post-recanalization complications. Moreover, integrating high-throughput gene expression analyses with single-cell RNA sequencing and proteomics could uncover previously unrecognized pathways that drive neutrophil-mediated microvascular dysfunction.

A rapidly measurable blood-based biomarker panel is invaluable for informing clinical decisions during initial triage and acute care to reduce the risks of futile recanalization. By incorporating novel molecular markers into point-of-care diagnostics, clinicians can better stratify patients based on their likelihood of responding to recanalization therapies and tailor interventions accordingly. Future studies should focus on identifying gene expression patterns that differentiate beneficial immune responses from pathological inflammation, paving the way for targeted therapies that could extend the therapeutic window and improve stroke recovery outcomes.

This study explored early transcriptional changes occurring in peripheral blood following stroke with or without recanalization in a mouse model. Dynamic gene expression patterns were analyzed to uncover regulatory pathways responding to MCAO and recanalization. The analyses identified several critical genes that could serve as new biomarkers or predictors of ischemic/reperfusion injury following recanalization. Notably, sex- and age-specific differences in gene expression were observed, with female mice and aged mice displaying unique leukocyte and neutrophil-related gene activation patterns. *Vcan* emerged as a novel biomarker for ischemic stroke and recanalization, and the only gene conserved across mice, rats, and humans. *Vcan*'s distinct expression in aged animals, especially as a central miRNA regulatory node, points to a previously unexplored aspect of ischemic stroke and reperfusion injury biology. Finally, a coregulatory network composed of rich interactions between identified differentially expressed genes, miRNAs, and their transcription factors in neutrophil-centred pathways linked to reperfusion injury was compiled for the first time. These discoveries open new avenues for understanding the molecular mechanisms driving stroke recovery and may provide insights for developing therapies tailored to age and sex.

Methods

1. Middle cerebral artery occlusion (MCAO) surgery

Experimental methods are outlined in **Supplementary Figure 1**. Wild-type mice (C57BL/6J) were obtained from the University of Alberta North Campus Animal Services and housed in the university facility's pathogen-free animal room at 18-22°C and 60% humidity, with free access to food and water. Standard diet and husbandry conditions were maintained. Proximal middle cerebral artery occlusion (MCAO) was modelled by transecting the external carotid artery, ligating the common carotid artery, and inserting a Doccol monofilament through the internal carotid artery to occlude the origin of the middle cerebral artery. The MCAO model closely mimics the pathophysiology of human ischemic stroke, blocking the major middle cerebral artery, with controlled recanalization/reperfusion. Body temperature was monitored throughout the surgery using a rectal probe and maintained at 37.0 ± 0.5°C by a heating pad. The suture was placed for 60 minutes before removal to mimic complete recanalization.

Three experimental groups (N=44), sham (SHAM, N=16), 1-hour MCAO (MCAO, N=17), and 1-hour MCAO with 3-hour recovery post-recanalization (MCAO+Recan, N=11), were included in the dataset. Both young adult (3-6 months old, N=20) and aged (18-24 months old, N=24), male (N=20) and female (N=24) mice were used. Randomization was used to assign treatment. To limit potential confounders, each cage also has all SHAM, MCAO, and MCAO+Recan groups. MCAO mice were euthanized immediately 60 minutes after surgery, blood samples were collected, and the suture causing MCAO was removed. In the MCAO+Recan group, the suture was removed 60 minutes after the onset of occlusion and mice were allowed to recover for an additional 3 hours before euthanasia. SHAM mice were subjected to only anesthesia and the manipulation of surrounding tissues and arteries, with 4 hours of recovery before sample collection. Saline and buprenorphine (0.03mg/kg) were administered subcutaneously after MCAO surgery for pain management. Animals were kept under anesthesia during surgery (2.0-2.5% isoflurane (70:30, O_2:N_2O)).

All mice were anesthetized with an intraperitoneal injection of 20% urethane at the point of sample collection. Blood samples were obtained immediately with retro-orbital sampling, collected in 500µL RNAprotect animal blood tubes (Qiagen, Germany), and stored at -20°C until RNA purification. Mice were then euthanized by decapitation. ARRIVE (Animal pre-clinical studies) checklist was completed (**Supplementary Table 3**) (28). All experiments were

approved by the University of Alberta's Health Sciences Animal Care and Use Committee (Protocol AUP361) and adhered to the guidelines set by the Canadian Council for Animal Care.

2. Sample collection and microarray analysis

Total RNA was isolated from blood samples using the RNeasy Kits, a process that was automated by the QIAcube (Qiagen, Germany). RNA was cleaned, and contaminants were removed using the RNeasy MinElute CleanUp Kit (Qiagen, Germany). NanoDrop 2000 (Thermo Fisher Scientific, U.S.) and Agilent Bioanalyzer 2100 (Agilent Technologies, U.S.) were used to measure RNA yield and detect integrity before microarray analysis. Samples with an RNA integrity number (RIN) of less than 7, A260/A280 ratio of less than 1.8, and volume of less than 35uL each at 50ng/uL were excluded from the dataset (ThermoFisher Scientific, U.S.). Reads were measured by Affymetrix Clariom S microarray (Affymetrix, ThermoFisher Scientific) by North American Genomics. Experimenters and technicians were blinded during sample processing. 58 blood samples were obtained, and 44 samples passed RIN, A260/A280 ratio, and volume cutoff.

3. Expression data analysis

All expression analysis was performed in RStudio. The limma package, which allows for variance stabilization, was used to normalize reads and identify differentially expressed genes (DEGs) across sex and age from raw data CEL files ($|\log_2 FC| \geq 1.5$, p-vale ≤ 0.05) (29). An ExpressionSet object containing expression and phenotype data was created and used in all downstream analyses. Exploratory data analysis techniques, including heatmaps, principal component analysis (PCA), and clustering, were employed to examine data. The volcano plot and heatmap for DEGs were plotted with the R packages ggplot2 and ComplexHeatmap. Sample clustering was performed. We used Pearson's Chi-squared test with Yates' continuity correction to evaluate the associations between these sample clusters and the categorical variables of treatment, sex, and age.

DEGs were exported to Cytoscape Version 3.9.1 to visualize their interactive network. Protein-protein interaction networks (PPIs) of DEGs were constructed with STRING (https://string-db.org). MCODE V1.5.1 was used to identify significant modules (MCODE score ≥ 4). Hub genes were selected using CytoHubba. GeneCards was used to look up previous finding and

gene functions (30). R/Bioconductor package gProfiler was used for functional enrichment analysis. gProfiler computes the enrichment of a pathway from the input gene list using Fisher's exact test and multiple-test correction (31). NetworkAnalyst platform and miRTarbase were used to predict miRNA–gene interaction (32). ChIP Enrichment Analysis (ChEA) was used to obtain transcription factors (TFs). ChEA results help identify candidate TFs that likely regulate the gene set based on experimentally derived TF target profiles, along with statistics and gene overlap details, but without TF expression, activity status, or mechanisms (33). Additional graphs were visualized in BioRender.

4. Integrative cellular profiling

Both deconvolution methods (CIBERSORT for humans and ImmuCellAI for mice) and cell marker dataset enrichment (CellMarker) were used since they provide complementary insights into the cellular composition and transcriptional activity of bulk microarray samples.

Cell Marker 2.0 and clusterProfiler were used to infer the cell types in which the DEGs might be found (34,35). Cell-type associations were identified based on lists of DEGs. Upregulated and downregulated DEGs for each condition were separately analyzed using over-representation analysis (ORA) via enricher, mapping to annotated cell types. This method enables a deeper understanding of the functional changes within specific cell types or to identify potential cell types that contribute to differential gene expression.

To estimate the relative abundance of known immune cell populations in our samples, we employed both ImmuCellAI-mouse (36) and CIBERSORTx using the LM22 leukocyte gene signature matrix (37–40). ImmuCellAI-mouse was selected for its optimized performance in quantifying 36 distinct mouse immune cell subtypes, providing high-resolution deconvolution tailored to our murine datasets (36). In parallel, CIBERSORTx, which leverages the human-specific LM22 signature, was applied to facilitate cross-species comparison through orthologous gene mapping (37–40). Analyses were conducted in high-resolution mode, restricted to protein-coding transcripts to enhance specificity. The resulting immune cell proportion estimates from both platforms were statistically compared across experimental groups using the Kruskal–Wallis test with Benjamini-Hochberg adjustment, followed by Dunn’s post hoc correction, with a false discovery rate (FDR) threshold of 0.05 (41,41,42). Aligned rank transform analysis of variance (ART ANOVA) with Benjamini-Hochberg adjustment (FDR ≤ 0.05) was used to identify

interactions between treatment, species differences, age, and sex that influence changes in cell proportions. These combined strategies obtain a comprehensive picture: quantitative cell type proportions from deconvolution, and mechanistic insights into cell type-specific transcriptional activity from marker enrichment, ultimately strengthening the ability to interpret complex biological differences between mouse and human models.

5. Cross-validation

The findings were compared to those from previous studies in the Gene Expression Omnibus (GEO) database to validate the results. The search query [ischemic stroke AND (reperfusion OR middle cerebral occlusion) AND peripheral blood] was used to obtain studies surveying transcriptional changes in peripheral blood post-recanalization. Datasets GSE16561 (43) and GSE21136 (44) were collected from the GEO database.

GSE16561 comprises clinical data analyzing blood expression from patients with MRI-diagnosed ischemic stroke, including those who received rt-PA (within 3 hours from onset) and controls (43). The median time from symptom onset to blood draw in these subjects was 7.4 hours (45). GSE21136 includes microarray analysis on rats that received MCAO+Recan with and without rtPA (44). Similar differential gene expression and functional enrichment analyses were performed on these datasets in R. All data in this study are available in the GEO database under accession number GSE278554.

Results

Following the reading of raw CEL files and normalization with rma, the entire dataset was assigned to an ExpressionSet object, which consists of 44 samples and 29,129 quantified transcripts. A heatmap plot identified four clusters of genes, with clusters seeming to correspond primarily to sex differences **(Figure 1A**). Pearson's Chi-squared test with Yates' continuity correction was conducted to determine whether sample clustering based on gene expression profiles was significantly associated with treatment, sex, or age. Treatment ($\chi^2 = 2.7904$, df = 2, p-value = 0.2478), age ($\chi^2 = 0.23653$, df = 1, p-value = 0.6267), and sex ($\chi^2 = 1.2449$, df = 1, p-value = 0.2645), however, were not significantly associated with cluster sampling.

PCA showed that the SHAM group and the MCAO group (i.e. MCAO with blood sampled 1 hour after ischemic onset, prior to recanalization) were closely clustered and had less

internal variation. In contrast, the MCAO+Recan group (i.e. blood samples 3 hours after recanalization or 4 hours after ischemic onset) has a greater internal variation and heterogeneous responses (**Figure 1B**). Nevertheless, PC1 (22.99%) and PC2 (8.81%) indicate that these biological variations were not significant.

Using an exploratory approach to allow for a broader survey of potential associations or relationships in these early transcriptional changes, differential gene expression (MCAO vs. SHAM and MCAO+Recan vs. SHAM) was analyzed. The comparison MCAO+Recan vs. MCAO (Recan group) was also examined for any notable recanalization effect. DEGs with a less conservative filter ($|\log_2 FC| \geq 1.5$, $p \leq 0.05$) were identified and reported with adjusted p-values along with raw p-values (**Supplementary Table 1**).

1. Differential expression analysis

i. Identification of novel early ischemic stroke and recanalization markers

Differential gene expression analysis identified 4 significantly upregulated genes in the MCAO group compared to SHAM: *Plet1*, *Krt13*, *Psca*, and *Gsto1* ($|\log_2 FC| \geq 1.5$, $p \leq 0.05$) (**Figure 1C**; **Supplementary Table 1**). These genes have been previously associated with tumour, cancer, and tissue damage (46–49). *Plet1* is a progenitor cell marker predicted to be involved in cell-matrix adhesion, cell migration, and wound healing (47). *Krt13* is related to inflammation, tissue damage, and epithelial proliferation and differentiation (50). *Gsto1* has previously been associated with inflammatory responses (51). However, to date, these genes, which showed significant upregulation only 1 hour after ischemic onset, have not been associated with ischemic stroke.

Samples from the MCAO+Recan group had an increased number of DEGs, with 12 significantly upregulated genes (*Il1r2*, *Hdc*, *Tarm1*, *Mrgpra2a*, *Mrgpra2b*, *Mt1*, *Mmp8*, *Ngp*, *Vcan*, *Lrg1*, *Cd14*, and *Ms4a6d*) and 7 significantly downregulated genes (*Cd55*, *Cd69*, *Pou2af1*, *Ly6d*, *H2-Oa*, *Ptprcap*, and *Ms4a1*) ($|\log_2 FC| \geq 1.5$, $p \leq 0.05$) (**Figure 1C**; **Supplementary Table 1**). Among these, *Il1r2* (52,53), *Hdc* (54,55), *Mt1* (56), *Mmp8* (57–59), *Ngp* (60–62), *Vcan* (63–65), *Lrg1* (66–68), *Cd14* (69–71), *Ms4a4a* (72–74), *Ms4a6d* (75–77), and *Cd69* (78–80) have been previously linked to ischemic stroke and inferred in immune-related pathogenesis but have not been identified as early as 4 hours after ischemic onset or after recanalization.

Additionally, Recan group (MCAO+Recan vs. MCAO) had 19 DEGs: *B3gnt5, Ms4a1, Slc15a4, Blk, Stap1, Nfkbid, Srpk1, Cd55, Ly6d, P2ry10b, Pgap1, Cd69, Pou2af1, Cd79b, Vcan, P2ry10, Ifi203, Lnx2,* and *Ms4a6d*, 7 of which were shared with MCAO+Recan group (**Supplementary Figure 2A**). The majority of DEGs in Recan were downregulated, especially B-cell and immune signalling genes, such as *Ms4a1, Cd79b, Pou2af1, Cd55, Cd69,* and *Blk*. *Vcan* and *Ms4a6d* were upregulated, implicating ECM changes and myeloid responses (**Supplementary Table 1**). *Vcan* is consistently upregulated in both MCAO+Recan and Recan groups, supporting its role in tissue remodelling and neuroinflammation post-stroke and recanalization. *Cd55* and *Cd69* were downregulated in both MCAO+Recan and Recan, indicating reduced T-cell and complement activity with reperfusion. *Ms4a1* (B-cell marker) was significantly downregulated in both MCAO+Recan and Recan, suggesting reperfusion might suppress adaptive immune responses (**Supplementary Table 1**).

We also performed multivariate analyses to examine the two-way interactions of Sex × Treatment and Age × Treatment. There were no significant interactions in the MCAO group; however, in the MCAO+Recan, we found 127 DEGs showing Age × Treatment interactions and 14 DEGs showing Sex × Treatment ($|\log_2 FC| \geq 1.5$, FDR ≤ 0.05) (**Supplementary Table 1**). These two groups share 9 DEGs: *Nexmif, Or8d23, Fam171b, Map3k1, Klc1, Vmn1r70, Dsg1b, Atp8b5,* and *Dgkz.* Only *Mrgpra2a* was shared between MCAO+Recan and Sex × MCAO+Recan with FDR < 0.05 cutoff. When using p-value < 0.05, Sex × MCAO+Recan shared *Mrgpra2a, Mrgpra2b, Lrg1, Tarm1, Mmp8, Mt1, Hdc,* and *Pou2af1* with MCAO+Recan and Age × MCAO+Recan shared *Cd14* with MCAO+Recan (**Supplementary Figure 2B**)

ii. Females and young animals showed greater transcriptional changes

We next examined how sex and age influence transcriptional changes following ischemia. Sex differences were evident. In the MCAO group, females had more DEGs than males (31 vs. 0, the latter had 12 differentially expressed transcripts with no mapped genes). In the MCAO+Recan group, females exhibited 118 DEGs, while males had only 9. Females in the MCAO and MCAO+Recan groups shared 14 DEGs, including *Asprv1, Cbr2, Cxcr2, Emp1, Gsto1, Hdc, Il1b, Il1rn, Lrg1, Mmp8, Mrgpra2a, Plet1, Prg4,* and *Sirpb1a*. Additionally, the female MCAO+Recan group shared *Ly6d* and *Ptprcap* with their male counterparts (**Figure 2A**).

This trend persisted when comparing MCAO+Recan with Recan groups: female Recan animals had 85 DEGs, 44 of which overlapped with female MCAO+Recan DEGs: *Mrgpra2a, Retnlg, Lcn2, Mrgpra2b, Il1r2, Ccr1, Mmp8, Il13ra1, Lrg1, Fpr2, Socs3, Cd33, Tarm1, Ifitm6, Bst1, Clec4e, Il1rap, Vcan, Nfyb, S100a8, Ptprcap, Cd14, Trim7, Ly6d, Cd83, Cyb561a3, Chil3, Ms4a1, Ms4a6d, Pou2af1, Cd55, Ngp, Nop56, Wfdc21, Mafb, Ets1, Mt1, Cxcr5, Macf1, Pax5, Cd79b, Pgap1, Blk*, and *Cd69*. On the contrary, male MCAO+Recan and Recan only shared 4 DEGs, including *Stap1, Plp1, Cd3g,* and *Cxcr4*. Between female and male Recan groups, 5 DEGs overlapped: *Ms4a1, B3gnt5, Srpk1, Pgap1,* and *Cd69*. Across all conditions, MCAO+Recan animals consistently showed the highest number of DEGs and females had more extensive transcriptional changes compared to males (**Supplementary Figure 2C**).

Overall, young animals displayed more pronounced transcriptional responses than aged animals. In the MCAO group, young animals had 47 DEGs compared to only 2 in aged animals. Similarly, in the MCAO+Recan group, young animals exhibited 89 DEGs, whereas aged animals had 21. Thus, at both 1 and 4 hours after ischemic onset, young animals showed substantially stronger gene expression changes than aged animals. When comparing MCAO and MCAO+Recan groups, young animals shared 6 common DEGs: *Asprv1, Hdc, Il1r2, Il1rn, Mmp8,* and *Pla2g7*; whereas aged animals had no common genes. When comparing young and aged animals in the MCAO+Recan group, the only shared gene is interleukin-1 receptor type II (*Il1r2*) (**Figure 2B**).

Young MCAO+Recan and Recan animals shared 34 DEGs, including *Aurkaip1, Pdpk1, Ndufa12, Cenpx, Med11, Spopl, Rbm6, Wtap, Usp16, Pafah1b2, Mapkap1, Derl2, Polr3k, Dusp5, D8Ertd738e, Tmem183a, Cenpv, Micu1, Slc25a4, S1pr4, Atp5f1e, Ppid, Taf9, Med21, Cep63, Mtmr14, Hmbs, Zfp367, Taf1d, Mier1, Cd3g, P2ry10, Ifi203*, and *P2ry10b*. Aged MCAO+Recan and Recan animals shared 17 DEGs, namely *Cd14, Vcan, Ly6d, Gpr18, Fcgr1, Cd79b, Mafb, Stap1, Il1r2, Cd55, Ms4a1, Ms4a6d, Cxcr5, Lrg1, Chil3, Tarm1,* and *Ngp.* Only one DEG, *Slc15a4*, was common between young and aged Recan animals (**Supplementary Figure 2D**).

GeneCards verification revealed that these DEGs included inflammation-associated genes such as *Il1r2, Cd244, Il1rn, Mmp8, Ccr2, Tnfaip2, Gsto1* (young MCAO), *Ifi203* (aged MCAO), *Cxcr2, Il1f9, Ifi203, Romo1, Pdcd5, Cd33, Hsbp1, Mmp8* (young MCAO+Recan), *Tarm1, Cxcr5, Cd79b,* and *Cd14* (aged MCAO+Recan) (30). Some of these genes, such as *Mmp8* (24 hours

after onset) (57), *Ccr2* (3 days after onset) (81), and *Cxcr2* (6 hours after onset) (82), have been previously associated with ischemic stroke, but never as early as 4 hours after onset.

It is important to note that, despite the identification of 19 unique DEGs in MCAO+Recan, not all of them exhibited uniform expression trends across treatment groups. *Mrgpra2a, Mrgpra2b, Lrg1, Tarm1, Mmp8, Mt1, Hdc*, and *Pou2af1* showed sex-specific and *Cd14* showed age-specific expression patterns ($|\log_2 FC| \geq 1.5$, $p \leq 0.05$) (**Supplementary Table 2**). The upregulation of *Cd14* post-recanalization was mainly driven by the aged group. *Mrgpra2a* and *Mrgpra2b* increased expression levels were primarily observed in female MCAO+Recan animals. Additionally, the differential changes in *Ly6d, Vcan*, and *Mt1* expression levels were observed in all subgroups within MCAO+Recan except for young males (**Supplementary Figure 2E**).

2. Enrichment analysis

i. Differentially expressed genes post-recanalization conserved across species

The PPI network of 19 DEGs of the MCAO+Recan group was constructed with STRING. The hub genes *Il1r2, Cd55, Mmp8, Cd14*, and *Cd69* were identified using the DMNC algorithm of the plug-in CytoHubba (**Figure 3A**). Since the number of DEGs in the MCAO group was low, the analysis for this group yielded no results.

To gain further biological and cell-specific context, the 19 DEGs from the MCAO+Recan group were assessed with gProfiler. The analysis showed that these DEGs were mainly involved in leukocyte activation (*Cd55, Tarm1, Mmp8, Pou2af1, Ly6d, H2-Oa, Ms4a1*), cytokine production (*Il1r2, Cd55, Tarm1, Mmp8, Pou2af1, Cd14*), and lymphocyte activation (*Cd55, Tarm1, Pou2af1, Ly6d, H2-Oa, Ms4a1*) (**Figure 3B**).

The GSE16561 and GSE21136 datasets, consisting of human and rat ischemic and recanalization samples, were used to validate the expression of the MCAO+Recan DEGs (**Figure 3C**). *Vcan* was the only DEG found in all three datasets of recanalization: GSE1656 (humans), GSE21136 (rats), and this mouse data. This suggests that *Vcan* is an important and novel marker of ischemic stroke and recanalization that is highly conserved across species. *Il1r2* and *Vcan* were shared between MCAO+Recan mice and rats. *Vcan* and *Cd14* were shared between MCAO+Recan mice and human samples. Proinflammatory *Il1r2* and *Cd14* were both

hub genes, suggesting they may play a critical role in reperfusion injury and early recanalization responses.

ii. Sex- and age-specific inflammatory pathways post-recanalization

When breaking the MCAO+Recan enrichment analysis down to age- and sex-specific groups, many pathways are shared among the groups, and the immune system process was significantly enriched in the MCAO+Recan (**Figure 4-5; Supplementary Figure 3**). This included downregulated genes in female (*Cd55, Prg4, Ets1, Pou2af1, Cxcr5, Cd79b, Cd83, Blk, Ly6d, H2-Oa, Mzb1, Ms4a1*) (**Figure 4A**) and aged animals (*Cd55, Stap1, Cxcr5, Cd79b, Gpr18, Ly6d, Ms4a1*) (**Figure 5B**). The immune system process was also linked to upregulated genes in the female (*Cxcr2, Gpr35, Cd244a, Il36g, Il1rn, Lcn2, Il1b, Mafb, S100a8, Sirpb1a, Tlr2, S100a9, Csf3r, Bst1, Clec4d, Clec4e, Ifitm1, Nlrp12, Tarm1, Trim30b, Adam8, Ifitm2, Ifitm6, Hmox1, Hp, Mmp8, Ccr2, Alas1, Myd88, Ccr1, Tlr13, Trpm2, Lilrb4b, Lilrb4a, Osm, Wfdc17, Wfdc21, Cd300lf, Arg2, Olfm4, Acod1, Il1rap, Retnlg, App, Fpr2, Pla2g7, Trem1, Fpr1, Dusp1, Cd14, Slc15a3*) (**Figure 4A**), aged (*Gpr35, Mafb, Fcgr1, Tarm1, Ctsl, Acod1, Pram1, Cd14, Il1r2*) (**Figure 5B**), and young animals (*Cxcr2, Il36g, Il1rn, Lcn2, Hp, Mmp8, Rab27a, Pla2g7*) (**Figure 5A**). Many DEGs were shared between these groups, such as the downregulated *Cd55, Cxcr5, Cd79b, Ly6d, Ms4a1* and the upregulated *Cxcr2, Gpr35, Il1r2,* and *Arg2* (**Supplementary Table 2**).

Females and young MCAO+Recan also saw an enrichment in cytokine production and regulation. These pathways were driven by upregulated *Il1r2, Cxcr2, Gpr35, Chil1, Il1rn, Il1b, Tlr2, Csf3r, Ifitm1, Nlrp12, Ifitm2, Ifitm6, Ccr2, Myd88, Ccr1, Il13ra1, Osm, Wfdc21, Cd300lf, Socs3, Il1rap, App, Dusp1, Cd14, Csf2ra* in females (**Figure 4A**), and *Il1r2, Cxcr2, Il36g, Il1rn* in young animals (**Figure 5A**).

Other inflammatory pathways, such as lymphocyte activation and differentiation, were enriched in female and aged MCAO+Recan. Lymphocyte activation was driven by downregulated *Cd55, Cxcr5, Cd79b, Gpr18, Ly6d, Ms4a1* in the aged group (**Figure 5B**) and upregulated *Cd244a, Il1b, Mafb, Sirpb1a, Clec4d, Clec4e, Tarm1, Adam8, Ccr2, Myd88, Lilrb4b, Lilrb4a, Arg2* in the female group (**Figure 4A**). On the other hand, lymphocyte differentiation was observed in the female group with downregulated *Pou2af1, Cd79b, Cd83, Ly6d, H2-Oa, Ms4a1* (**Figure 4A**) and the aged group (**Figure 5B**) with the same genes and an

additional *Gpr18*. Mononuclear cell differentiation and migration was significantly enriched in downregulated aged MCAO+Recan (*Cd79b, Gpr18, Ly6d, Ms4a1*) (**Figure 5B**) and upregulated female MCAO+Recan (*Nlrp12, Adam8, Ccr2, Ccr1, Trpm2, Retnlg, App, Fpr2, Pla2g7, Trem1, Dusp1, Pou2af1, Cd79b, Cd83, Blk, Ly6d, H2-Oa, Ms4a1*) (**Figure 4A**). Monocellular proliferation was also found in the upregulated female MCAO+Recan (*Cd244a, Il1b, Tarm1, Ccr2, Myd88, Lilrb4b, Lilrb4a, Arg2*) (**Figure 4A**).

iii. Neutrophil and leukocyte-based pathways upregulated in females across species

Using ImmunCellAI-mouse algorithm, our dataset showed significant changes in macrophages (M1 and M2), neutrophils, and T-cells (Tregs, T cells CD4 T gamma delta) proportion at 3 hours after reperfusion (**Supplementary Figure 4**). However, not all these cell types were observed in human orthologs by CIBERSORTx (**Figure 6**). For instance, only neutrophils had their proportion significantly increased in MCAO+Recan group in both mouse (i.e., ImmunCellAI-mouse) and human orthologs (i.e., CIBERSORTx). Notably, the proportion of neutrophils also showed both a significant main treatment effect (adj p-value = 0.0465) and a treatment × sex interaction (adj p-value = 0.0201) (**Figure 6**; **Table 1**).

ART ANOVA identified significant treatment effects that differ between human and mouse for B cells memory (adj p-value = 0.0175), T cells CD4 naïve (adj p-value = 0.0223), T cells gamma delta (adj p-value = 4.7912e-06), monocytes (adj p-value = 0.0471), and macrophages M1 (adj p-value = 3.3698e-07) and M2 (adj p-value = 4.8789e-06). In humans, the proportion of monocytes showed a significant treatment effect (adj p-value = 0.0465), with the highest proportion observed in the MCAO+Recan group. However, this trend was not seen in mice (**Figure 6**). These findings validate previous observations of differing immune cell proportions between mice and humans (83,84).

Furthermore, several cell types showed significant age- and sex-specific differences. For example, macrophages M1 in mice showed not only substantial treatment effects but also treatment × age (adj p-value = 0.0086) and treatment × age × sex interactions (adj p-value = 0.0174), which aligns with human data and further emphasizes their importance. Macrophages M2 showed a similar pattern (**Table 1**; **Supplementary Figure 4**). Follicular helper T cells were notable for significant changes across all interaction terms in the human data. B cells in mice had

a substantial treatment × sex × age interaction. T cells CD4 showed a significant treatment × sex interaction (**Table 1**).

Table 1. Kruskal-Wallis and ART ANOVA analyses with Benjamini-Hochberg adjustment of CIBERSORTx and ImmunCellAI-mouse results (*adj-p≤0.05, **adj-p≤0.01, ***adj-p≤0.001).

Cell Type	Species	Treatment effect Kruskal-Wallis p-val [adj p]	Treatment:Species ART ANOVA p-val [adj p]	Treatment:Sex ART ANOVA p-val [adj p]	Treatment:Age ART ANOVA p-val [adj p]	Treatment:Age:Sex ART ANOVA p-val [adj p]
B cells naive	Human	0.0448 [0.1112]		0.6807 [0.9621]	0.7923 [0.9640]	0.1655 [0.4966]
B cells memory	Human	0.0249 [0.0801]	***0.0053 [0.0175]**	0.5132 [0.8436]	0.0786 [0.3255]	0.5955 [0.9010]
B cells memory	Mouse	0.1187 [0.2220]		0.9097 [0.9887]	0.5952 [0.9010]	0.1919 [0.5346]
Plasma cells	Human	0.2910 [0.4220]	0.1620 [0.2700]	0.8301 [0.9857]	0.8508 [0.9857]	0.5783 [0.8984]
Plasma cells	Mouse	0.7324 [0.8330]		0.4892 [0.8395]	0.0400 [0.2048]	0.9145 [0.9887]
T cells CD8	Human	0.0309 [0.0899]	0.2639 [0.3299]	0.5374 [0.8579]	0.6357 [0.9454]	0.9454 [0.9621]
T cells CD8	Mouse	0.1274 [0.2310]		0.8430 [0.9857]	0.7537 [0.9621]	0.9622 [0.9887]
T cells CD4 naive	Human	0.2541 [0.3780]	***0.0089 [0.0223]**	0.1526 [0.4830]	0.9830 [0.9887]	0.7488 [0.9621]
T cells CD4 naive	Mouse	0.1994 [0.3212]		****0.0002 [0.0051]**	0.2252 [0.5724]	0.1736 [0.5119]
T cells CD4 memory resting	Human	0.7936 [0.8389]		0.3720 [0.7526]	0.5739 [0.8984]	0.9145 [0.9887]
T cells CD4 memory activated	Human	0.0416 [0.1096]		0.3238 [0.6787]	0.1856 [0.5295]	0.3018 [0.6483]
T cells follicular helper	Human	0.4169 [0.5256]		*****7.2266e-08 [3.1436e-06]**	*****1.1697e-06 [3.3922e-05]**	*****1.3801e-07 [4.8028e-06]**
T cells regulatory (Tregs)	Human	0.7955 [0.8389]	0.2234 [0.3192]	0.9781 [0.9887]	0.9750 [0.9887]	0.9677 [0.9887]
T cells regulatory (Tregs)	Mouse	0.0654 [0.1375]		0.0346 [0.1882]	0.0060 [0.0563]	0.1121 [0.4178]
T cells gamma delta	Human	***0.0105 [0.0485]**	*****1.3067e-06 [4.7912e-06]**	0.2360 [0.5785]	0.2544 [0.5831]	0.0264 [0.1532]
T cells gamma delta	Mouse	***0.0109 [0.0485]**		0.9590 [0.9887]	0.6615 [0.9591]	0.1436 [0.4812]
NK cells resting	Human	0.0195 [0.0706]		0.7378 [0.9621]	0.9829 [0.9887]	0.4261 [0.7857]
NK cells activated	Human	***0.0033 [0.0465]**		0.4137 [0.7857]	0.0103 [0.0852]	0.0140 [0.0955]
Monocytes	Human	***0.0077 [0.0465]**	***0.0236 [0.0471]**	0.0148 [0.0955]	0.0109 [0.0866]	0.7202 [0.9621]
Monocytes	Mouse	0.2317 [0.3536]		0.8165 [0.9857]	0.1582 [0.4830]	0.1198 [0.4255]
Macrophages M0	Human	0.6082 [0.7055]		0.2232 [0.5724]	0.0420 [0.2088]	0.0759 [0.3255]
Macrophages M1	Human	0.2231 [0.3498]	*****3.3698e-08 [3.3698e-07]**	*****4.8272e-12 [3.7417e-10]**	*****6.4512e-12 [3.7417e-10]**	*****2.7188e-12 [3.7417e-10]**
Macrophages M1	Mouse	***0.0057 [0.0465]**		0.2270 [0.5724]	****0.0004 [0.0086]**	***0.0011 [0.0174]**
Macrophages M2	Human	0.7533 [0.8389]	*****9.7579e-07 [4.8789e-06]**	0.0061 [0.0563]	0.0128 [0.0938]	***0.0028 [0.0305]**
Macrophages M2	Mouse	***0.0080 [0.0465]**		0.0314 [0.1761]	***0.0016 [0.0201]**	***0.0012 [0.0174]**
Dendritic cells resting	Human	0.5842 [0.6915]		0.3957 [0.7737]	0.2014 [0.5456]	0.2083 [0.5491]
Dendritic cells activated	Human	0.1859 [0.3080]		0.5327 [0.8579]	0.0667 [0.3138]	0.5051 [0.8436]
Mast cells resting	Human	***0.0008 [0.0243]**		0.7137 [0.9621]	0.9129 [0.9887]	0.0767 [0.3255]

Mast cells activated	Human	0.0343 [0.0948]		0.4769 [0.8357]	0.5058 [0.8436]	0.0369 [0.1946]
Eosinophils	Human	0.8616 [0.8923]	0.8171 [0.8171]	0.8752 [0.9887]	0.9154 [0.9887]	0.5232 [0.8509]
Eosinophils	Mouse	0.9028 [0.9187]		0.9442 [0.9887]	0.1438 [0.4812]	0.3208 [0.6787]
Neutrophils	Human	0.0275 [0.0841]	0.6477 [0.7197]	0.0129 [0.0938]	0.3844 [0.7688]	0.4188 [0.7857]
Neutrophils	Mouse	***0.0025 [0.0465]**		***0.0017 [0.0201]**	0.2743 [0.6119]	0.9912 [0.9912]
B cells	Mouse	***0.0059 [0.0465]**		0.6536 [0.9557]	0.0716 [0.3194]	***0.0032 [0.0329]**
Dendritic cells	Mouse	0.4907 [0.6055]		0.3932 [0.7737]	0.1128 [0.4178]	0.1936 [0.5346]
Granulocytes	Mouse	0.0181 [0.0699]		0.4290 [0.7857]	0.7830 [0.9621]	0.7280 [0.9621]
Macrophages	Mouse	***0.0068 [0.0465]**		0.1098 [0.4178]	****0.0005 [0.0093]**	****0.0010 [0.0174]**
NK cells	Mouse	0.3161 [0.4472]		0.7293 [0.9621]	0.4064 [0.7856]	0.1007 [0.3981]
T cells	Mouse	***0.0068 [0.0465]**		0.4921 [0.8395]	0.5139 [0.8436]	0.2341 [0.5785]
T cells CD4	Mouse	0.1394 [0.2378]		***0.0015 [0.0195]**	0.5455 [0.8629]	0.2486 [0.5831]
NKT	Mouse	0.1386 [0.2378]		0.0566 [0.2738]	0.1824 [0.5289]	0.0228 [0.1367]
B1 cells	Mouse	***0.0007 [0.0244]**		0.2967 [0.6454]	0.2038 [0.5456]	0.2547 [0.5831]
Follicular B cells	Mouse	0.0143 [0.0593]		0.7046 [0.9621]	0.8536 [0.9857]	0.1301 [0.4527]
Germinal center B cells	Mouse	0.5122 [0.6189]		0.6341 [0.9454]	0.7613 [0.9621]	0.2924 [0.6440]
Marginal zone B cells	Mouse	0.0246 [0.0801]		0.6681 [0.9607]	0.4803 [0.8357]	0.3307 [0.6799]
cDC1	Mouse	0.3748 [0.4970]		0.0932 [0.3772]	0.2439 [0.5813]	0.7839 [0.9621]
cDC2	Mouse	0.9410 [0.9410]		0.6839 [0.9621]	0.1581 [0.4830]	0.0696 [0.3185]
MoDC	Mouse	0.0891 [0.1723]		0.6506 [0.9557]	0.9558 [0.9887]	0.2413 [0.5813]
pDC	Mouse	***0.0102 [0.0485]**		0.1176 [0.4255]	0.0170 [0.1056]	0.1545 [0.4830]
Basophils	Mouse	0.0647 [0.1375]		0.2641 [0.5969]	0.7626 [0.9621]	0.7644 [0.9621]
Mast cells	Mouse	0.0664 [0.1375]		0.8909 [0.9887]	0.8438 [0.9857]	0.4675 [0.8300]
CD4 Tm cells	Mouse	0.0868 [0.1723]		0.0144 [0.0955]	0.4404 [0.7937]	0.1502 [0.4830]
T cells helper	Mouse	0.3771 [0.4970]		0.0093 [0.0809]	0.7663 [0.9621]	0.3321 [0.6799]
CD8 Tc	Mouse	0.7713 [0.8389]		0.7852 [0.9621]	0.8554 [0.9857]	0.6969 [0.9621]
CD8 Tcm	Mouse	0.0472 [0.1112]		0.8325 [0.9857]	0.7635 [0.9621]	0.9682 [0.9887]
CD8 Tem	Mouse	0.0479 [0.1112]		0.7152 [0.9621]	0.5953 [0.9010]	0.4207 [0.7857]
CD8 Tex	Mouse	0.3906 [0.5034]		0.4425 [0.7937]	0.9816 [0.9887]	0.9612 [0.9887]
T cells CD8 naive	Mouse	0.3458 [0.4776]		0.8699 [0.9887]	0.9270 [0.9887]	0.9340 [0.9887]

The Cell Marker 2.0 database was used to identify cell types in which the DEGs were enriched. This approach provided valuable tissue and cell-specific context for the observed transcriptional changes. In this dataset, the marker with the highest gene count was for neutrophils, with all genes being significantly upregulated and driven by the MCAO+Recan group, and the greatest expression in female and aged mice (**Figure 7A**). This suggests that neutrophil markers were highly expressed and contributed to ischemic pathogenesis post-

recanalization. Downregulated DEGs were mostly markers of macrophages, lymphocytes, T cells, B cells, and arterial cells (**Figure 7A**).

The female MCAO+Recan also showed the highest number of enriched pathways related to neutrophil activity, such as neutrophil migration (*Cxcr2, Il1b, Bst1, Adam8, Myd880*), chemotaxis (*Cxcr2, Il1b, S100a8, S100a9, Csf3r, Bst1, Trem1*), aggregation (*Il1b, S100a8, S100a9, Adam8*), and degranulation (*Cxcr2, Chil1, Cd55, Lcn2, S100a8, Sirpb1a, S100a9, Clec4d, Tarm1, Cd33, Adam8, Mcemp1, Hp, Mmp8, Trpm2, Lilrb4b, Lilrb4a, Olfm4, Fpr2, Fpr1, Cd14*) (**Figure 7B**).

Other potential pathways that may connect to reperfusion injury and futile recanalization in this group were leukocyte activation (*Cxcr2, Cd244a, Cd55, Il1b, Mafb, Sirpb1a, Tlr2, Clec4d, Clec4e, Tarm1, Adam8, Hmox1, Mmp8, Pou2af1, Ccr2, Cxcr5, Myd88, Lilrb4b, Lilrb4a, Cd79b, Cd300lf, Arg2, Cd83, Blk, Ly6d, App, H2-Oa, Mzb1, Ms4a1), leukocyte cell-cell adhesion (Cd244a, Cd55, Il1b, S100a8, Sirpb1a, S100a9, Tarm1, Adam8, Ets1, Ccr2, Lilrb4b, Lilrb4a, Arg2, Cd83, H2-Oa, Lrg1*), and leukocyte proliferation (*Cd244a, Cd55, Il1b, Tarm1, Ccr2, Myd88, Lilrb4b, Lilrb4a, Arg2, Blk, Mzb1, Csf2ra*). In addition, significant leukocyte differentiation (*Mafb, Cd79b, Ctsl, Gpr18, Ly6d, Ms4a1*), leukocyte chemotaxis (*Gpr35, Stap1, Cxcr5, Gpr18*), and leukocyte activation (*Cd55, Mafb, Stap1, Tarm1, Cxcr5, Cd79b, Ctsl, Gpr18, Ly6d, Pram1, Ms4a1*) were found in the aged MCAO+Recan (**Figure 7B**).

The high degree of expression in neutrophil-associated pathways in these samples was then compared with other datasets related to recanalization after stroke. The female MCAO+Recan group was compared to the human female samples GSE1656 (GSE21136 was excluded as it consists of only male samples), and 37 shared orthologues, including the hub genes *Il1r2, Mmp8, Cd14,* and *Cd55,* were identified (**Figure 8A**). Notably, *Vcan* was also significantly upregulated in both female mice and female patients. Furthermore, the two groups shared a considerable number of enriched pathways (**Figure 8B**), many of which were related to neutrophil and leukocyte activity (**Figure 8C**). This indicates a highly conserved pattern of post-recanalization leukocyte- and neutrophil activities across species that can be linked to reperfusion injury.

3. Regulatory network analysis

Using NetworkAnalyst, the miRNAs that regulated DEGs in the MCAO+Recan group were predicted. The top regulated nodes (degree ≥ 10) were identified to be *Clec7a, Cd69, Ets1, Cxcr2, Macf1, Csf3r, Csf1, Btc, Vcan, Entpd1, Slc11a2, Cxcr2, Fitm2, Lmbrd1, Pafah1b2*, and *Gsk3b* (**Supplementary Figure 6)**.

Notably, *Vcan* was the sole node identified in aged MCAO+Recan animals and one of the central nodes in female MCAO+Recan animals. It was regulated by mmu-mir-450b-5p, mmu-mir-143-3p, mmu-mir-340-5p, mmu-mir-680, mmu-mir-690, mmu-mir-185-5p, mmu-mir-203-5p, mmu-mir-129-5p, mmu-mir-3079-5p, mmu-mir-434-3p in the aged group, and the additional mmu-mir-203-5p and mmu-mir-185-5p in female group (**Supplementary Figure 6**). *Vcan* was an upregulated gene involved in the cell adhesion pathway and cell periphery in females and in the extracellular region for both the female and aged groups. It is also regulated by the NF-κB factor (motif: GGGRATTTCC) (**Supplementary Table 2**). This suggests that *Vcan* plays a role in remodelling the extracellular matrix (ECM) during neutrophil migration and adhesion in reperfusion injury.

The top 50 TFs that regulated DEGs in MCAO+Recan groups were exported from ChEA3. NFE4 and MTF1 had the highest confidence score, 9.0 and 10.0, respectively, and regulated genes in females from the MCAO+Recan group **(Supplementary Figure 7)**. NFE4 regulated mostly proinflammatory genes, namely *P2ry13, Ifitm2, Csf3R, Fpr1, Mcemp1, Fpr2, Csf2Ra, Trem1, Bst1, Nlrp12, Clec4D, Cxcr2, Adam8, Clec4E, Cd300Lf, Myd88, Cd33, Ccr2,* and *Tlr2*. MTF1 targeted more specific leukocyte differentiation and leukocyte aggregation and migration, including *Il1rn, Csf3R, Fpr1, Tnfaip2, Fpr2, Csf2ra, Trem1, Pla2g7, Socs3, Clec7A, Cxcr2, Upp1, Cd14, Cd300lf, Slc15A3, Slc16A3, Ier3, Ccr1, Osm, Acod1, Il36G, Cyb561A3, Fosl2, Bst1, Nlrp12, Clec4D, Mafb, Il1B, Adam8, Clec4E, S100A9, Myd88*, and *Tlr2*. These two TFs co-regulated multiple genes, namely *Cd300lf, Csf2ra, Nlrp12, Clec4d, Csf3r, Trem1, Cxcr2, Adam8, Fpr1, Fpr2,* and *Bst1*.

Among the regulated genes, 16/19 of NFE4 targeted genes (*Csf3R, Fpr1, Mcemp1, Fpr2, Csf2Ra, Trem1, Bst1, Nlrp12, Clec4d, Cxcr2, Adam8, Clec4e, Cd300lf, Myd88, Cd33, Ccr2, Tlr2*) and 17/33 of MTF1 targeted genes (*Csf3R, Fpr1, Tnfaip2, Fpr2, Csf2Ra, Trem1, Pla2G7, Socs3, Clec7A, Cxcr2, Upp1, Cd14, Cd300lf, Slc15A3, Slc16A3, Ier3, Ccr1, Osm, Acod1, Il36g, Cyb561A3, Fosl2, Bst1, Nlrp12, Clec4d, Mafb, Il1b, Adam8, Clec4e, S100A9, Myd88, Tlr2*) were

implicated in neutrophil migration, degranulation, chemotaxis, and migration, both involved in neutrophil migration and degranulation (**Figure 4A; Supplementary Table 2**). Combining these multifaceted data, a network illustrating how DEGs, miRNAs, and TFs interact to upregulate neutrophil activity, implicating reperfusion injury, particularly in females, was constructed (**Figure 9**).

Discussion

1. Novel biomarkers of recanalization and reperfusion failure

Several blood biomarkers have been identified with high sensitivity for stroke diagnosis, such as S100B (glial activation), vWF (thrombosis), MMP9, and VCAM (inflammation), and are used to discriminate stroke from healthy controls (85). As the number of candidate biomarkers continues to rise, they offer additional insights into clinical responses to medical interventions and outcome predictions. However, there are currently no biomarkers for the early prediction of the risks of poor recovery following recanalization in ischemic stroke. The requirements for such biomarkers, including high sensitivity, specificity, and rapid turnaround time, make their development challenging. Identifying blood biomarkers could revolutionize stroke care, enhancing prognosis and recovery with personalized treatment. At-risk patients can then benefit from early additional therapies such as neuroprotective or anti-inflammatory. Moreover, early biomarkers could help stratify patients in clinical trials, offering better insights into the mechanisms of injury and recovery. The quest for reliable biomarkers is, therefore, critical to improving post-recanalization outcomes and reducing long-term disability in stroke survivors.

This study investigated the regulation of genes associated with ischemia and recanalization by transcription factors and miRNAs, uncovering early changes associated with neutrophil activity that may drive pathophysiology related to reperfusion injury and futile recanalization. In the co-regulatory network, several nodes exhibited high centrality, including five hub genes—*Il1r2, Cd55, Mmp8, Cd14, and Cd69*—along with two transcription factors, MTF1 and NFE4, and multiple miRNAs. These regulatory elements were predominantly associated with neutrophil activity, offering a deeper understanding of gene regulatory mechanisms involved in reperfusion injury and recovery post-stroke and recanalization.

Further analysis of the hub genes suggests *Il1r2* expression may play a regulatory role in modulating the inflammatory response by reducing IL-1 activity, potentially influencing stroke

outcomes by limiting excessive inflammation (86). *Cd55*, downregulated following recanalization, can protect brain tissue in ischemic stroke by inhibiting the complement system, preventing excessive inflammation and complement-mediated damage to neurons, glial cells, and the blood-brain barrier. This regulation helps preserve tissue integrity and reduce secondary injury following the initial ischemic event (87–89). *Mmp8*, primarily produced by neutrophils, facilitates neutrophil migration and plays a role in degrading the ECM components, thereby modulating inflammation. *Mmp8* expression is associated with high risks of ischemia, contributes to the breakdown of the blood-brain barrier and tissue remodelling, and decreased MMP8 protein levels improve neurological functions and reduce MCAO infarct size in rats (57,90). Additionally, *Cd69* and *Cd14* are integral components of the core inflammatory program governing neutrophil activity during ischemic stroke. For instance, *Cd69* dampens endothelial activation during ischemic events, and its deficiency in mouse models is linked to increased neutrophil infiltration and larger infarct volumes (91). *Cd14*, on the other hand, triggers neutrophil responses through toll-like receptors, amplifying the inflammatory response. Elevated *Cd14* expression has been associated with worse stroke outcomes due to increased inflammation (92). Notably, a limitation of this study is that its design cannot distinguish between transcriptional changes driven by recanalization and/or reperfusion injury or whether they primarily reflect the length of time (i.e., 4 hours) from ischemic onset.

miRNAs, which directly influence mRNA expression, also play a crucial role in this regulatory network. The most connected genes in this miRNA analyses were *Clec7a, Cd69, Ets1, Cxcr2, Macf1, Csf3r, Csf1, Btc, Vcan, Entpd1, Slc11a2, Cxcr2, Fitm2, Lmbrd1, Pafah1b2*, and *Gsk3b*. The genes *Cxcr2, Vcan, Gsk3b, Csf3r*, and *Ets1* were particularly relevant to neutrophil migration and ECM remodelling, the critical processes of ischemic stroke. For instance, CXCR2 is a chemokine receptor critical for neutrophil migration. It binds to chemokines like CXCL1 and CXCL8, directing neutrophils to sites of inflammation during ischemic stroke. CXCR2 has a direct role in recruiting neutrophils to damaged brain tissue, contributing to inflammation and stroke pathology (13). CSF3R is the receptor for granulocyte colony-stimulating factor, which regulates neutrophil production and release (93). The roles of other genes are less clear. GSK3B is a kinase involved in cell migration, proliferation, and apoptosis and also regulates ECM components and may therefore be involved in stroke recovery by modulating tissue remodelling (94). MACF1 is involved in cytoskeleton dynamics, essential for cell migration and structural

integrity (95). Though its direct role in ischemic stroke is unclear, MACF1 could affect cell migration, including neutrophil motility and tissue repair processes.

2. Growing evidence of neutrophils' central role in reperfusion injury

The functional enrichment analysis and cell deconvolution analysis here highlighted that the biological processes regulated by these genes were primarily related to leukocyte and neutrophil activity. Neutrophil microcirculatory stalls represent an emerging area of research in ischemic stroke and futile recanalization. While some *in vivo* imaging studies have shown neutrophil stalls in the microvasculature are the driving cause of microcirculatory failure, much remains to be learned (13).

The baseline immune composition differs profoundly between humans and mice, most notably in the proportions of neutrophils and lymphocytes. Humans have a neutrophil-dominant profile (50–70% of white blood cells), whereas mice are lymphocyte-rich (70–90%) with far fewer circulating neutrophils (10–30%) (96–99). These inherent disparities extend to other immune subsets, including transitional B cells, memory T cells, and macrophage populations, and must be considered when interpreting cross-species immune responses. Our transcriptomic deconvolution analysis revealed apparent species-specific treatment effects. Monocytes exhibited a significant treatment response in humans but not in mice, whereas neutrophils responded in both species, with comparable treatment-driven patterns, despite their markedly different baseline abundances. This highlights the strong potential of neutrophils for translational research in studying reperfusion injury or futile recanalization. This also suggests that the observed neutrophil-driven biomarkers have a high probability of translating to clinical studies. Several mouse-restricted subsets, such as B1 cells, pDCs, and specific macrophage subtypes, also exhibited significant treatment effects, underscoring the need for cell-type– and species–specific analyses.

After stroke, neutrophils heavily rely on the ECM to migrate, extravasate, and aggregate in small capillaries. Ischemic injury triggers inflammatory cytokines and chemokines, upregulating ICAM-1 and VCAM-1 on endothelial cells. Neutrophils bind to these adhesion molecules via integrins (e.g., α2β1, α4β1), and secrete MMP-9, degrading ECM components like collagen and fibronectin, facilitating extravasation. Once inside the brain parenchyma, neutrophils follow chemokine gradients (e.g., CXCL1) to migrate, but as they accumulate, they

release neutrophil extracellular traps that trap more neutrophils and platelets, leading to microvascular plugging and obstruction, particularly in small vessels within the ischemic core and penumbra. The interaction between neutrophils and the altered ECM thus plays a crucial role in their ability to migrate and aggregate after a stroke, causing reperfusion injury and potential futile recanalization.

3. *Vcan* as a conserved recanalization marker between different animal models

Vcan, encoding the large extracellular matrix chondroitin sulfate proteoglycan versican, emerged from this study as a novel player in ECM-driven neutrophil-mediated microcirculatory failure or reperfusion injury. Interestingly, *Vcan* has not been previously investigated in the context of ischemic stroke or futile recanalization, despite this study's observation of its significantly conserved increased expression across species that underwent recanalization treatment. In traumatic brain injury, it was shown that FOXO1 protein is induced in neutrophils after injury, and FOXO1 upregulates cytoplasmic *Vcan*. These FOXO1-high neutrophils infiltrate the brain, promoting the aggregation and activation of other immune cells, exacerbating brain damage (100). In other pathologies, *Vcan* and other ECM proteoglycans play a crucial role in ECM remodelling during recovery, interacting with proteins and molecules to maintain ECM structure and stability. *Vcan* not only acts as a biomarker of peripheral ECM remodelling but also serves as a repository for cytokines that regulate immune cell behaviour (101). These dynamic interactions between ECM and neutrophils, where neutrophils contribute to ECM remodelling via enzymes like neutrophil elastase and matrix metalloproteinases, while the ECM influences neutrophil function, highlight the bidirectional relationship that drives inflammation and recovery. *Vcan*'s role in this process emphasizes its significance in shaping the inflammatory microenvironment, influencing both neutrophil activity and ECM integrity, which are vital to stroke progression and post-reperfusion outcomes. Beyond these connections, however, little is known regarding *Vcan*'s role in stroke or recanalization outcomes, marking it as an intriguing target for further research.

Previous single-cell RNA sequencing (scRNA-seq) data identified monocytes, but not neutrophils, as the primary leukocyte population expressing *Vcan* (102). This study, however, employed a 35-minute MCAO mouse model and collected blood samples for scRNA-seq analysis at days 2 and 14 post-stroke, which differ from the model and sampling strategy used in

this study. Differences in both experimental design (i.e., 35-minute MCAO being a less severe model) and temporal resolution likely contribute to the observed discrepancies. Neutrophil and monocyte dynamics after ischemic stroke follow distinct temporal patterns: neutrophil counts increase rapidly within hours, reach a peak within the first 24 hours, and decline within approximately one week, whereas monocyte counts increase more gradually and remain elevated for an extended period (103–105). These kinetics may explain why *Vcan* expression was previously associated with monocytes at later stages, while this study linked it to neutrophils at earlier time points. Together, these findings suggest that the cellular sources of *Vcan* expression may vary across different phases of ischemic stroke and reperfusion. Additional scRNA-seq studies with refined temporal sampling are required to determine whether *Vcan* expression is differentially regulated by neutrophils in the acute phase and by monocytes at later stages.

In aged animals, *Vcan* was significantly regulated by mmu-mir-450b-5p, mmu-mir-143-3p, mmu-mir-340-5p, mmu-mir-680, mmu-mir-690, mmu-mir-185-5p, mmu-mir-203-5p, mmu-mir-129-5p, mmu-mir-3079-5p, mmu-mir-434-3p, and the additional mmu-mir-203-5p and mmu-mir-185-5p for female MCAO+Recan. Some of these miRNAs already have established roles in ischemic stroke. miR-143-3p and miR-185-5p are highly sensitive markers of ischemic stroke in clinical patients (106,107). miR-143-3p plays a role in vascular remodelling, integrity, and angiogenesis by regulating vascular smooth muscle cells, which are crucial for stroke recovery and reperfusion (106). Meanwhile, miR-185-5p demonstrates neuroprotective effects in ischemic stroke by targeting genes involved in oxidative stress and apoptosis. Overexpression of miR-185-5p has been shown to protect neurons from ischemic injury by inhibiting pro-apoptotic genes like Caspase-3 and reducing oxidative stress through the NF-κB pathway (107).

Additionally, miR-450b-5p is highly expressed in thrombi retrieved via EVT from stroke patients (108), while miR-340-5p exhibits anti-inflammatory properties, inhibiting pro-inflammatory cytokines such as TNF-α and IL-1β. Overexpression of miR-340-5p in stroke models reduces infarct size and improves functional recovery by mitigating inflammation (109). miR-129-5p further enhances ischemic brain recovery by binding to SIAH1 and activating the mTOR signalling pathway, preventing neuronal apoptosis (110). Together, these findings suggest that these miRNAs, specifically those found to be modulating *Vcan*, represent potential therapeutic targets, offering promising avenues for future interventions to improve clinical outcomes following recanalization.

4. Key transcriptional regulators in reperfusion injury

ChEA analysis showed that NFE4 and MTF1 were the TFs with the highest scores in the entire dataset, regulating 19 and 33 genes, respectively, in the female MCAO+Recan group. Among these, 16/19 and 17/33 were implicated in neutrophil migration, degranulation, chemotaxis, and migration. The high number of genes linked to neutrophil function suggests that NFE4 and MTF1 were central regulators in mediating the recruitment and activity of neutrophils, which could profoundly affect stroke recovery and outcomes, positioning them as key players in the reperfusion injury after ischemic stroke. Previous studies demonstrated that in brain ischemia induced by transient middle cerebral occlusion, MTF-1 was triggered by a subsequent temporary femoral artery occlusion (i.e. treatment via remote ischemic conditioning), mediating neuroprotective mechanisms against oxidative and hypoxic stress. MTF-1 also translocate to the nucleus and induces NCX1 upregulation, which has been demonstrated to be neuroprotective (111). NFE4, however, has not been linked to stroke previously.

TFs function as regulators that modulate transcriptional output, thereby controlling cell fate decisions and inflammatory responses. Previous studies showed that TFs instruct a transcriptional program that allows the developmental transition from neutrophil precursors into mature neutrophils (112). However, the molecular mechanisms underlying neutrophil differentiation and function during inflammation remain largely uncharacterized. By regulating genes involved in neutrophil migration, degranulation, chemotaxis, and cellular migration, NFE4 and MTF1 likely influence the timing, intensity, and localization of neutrophil activity in the ischemic brain. For instance, genes under their control could dictate how quickly neutrophils are recruited to the injury site, the extent to which they degranulate to release enzymes that break down damaged tissue, and how they move through the damaged brain microenvironment. Such regulation is critical because an excessive or prolonged neutrophil response can lead to blood-brain barrier disruption, increased infarct size, and further neuronal death.

In contrast, a finely tuned response can promote tissue repair and resolution of inflammation. Thus, the role of NFE4 and MTF1 in modulating neutrophil-related genes highlights their importance in balancing these opposing outcomes. On one hand, they facilitate necessary immune functions that clear damaged cells and initiate healing, while on the other, they must restrain excessive inflammation to prevent further injury. The ability of these

transcription factors to tightly regulate neutrophil behaviour may be critical in determining whether stroke recovery proceeds in a neuroprotective or detrimental direction, influencing both short-term recovery and long-term neurological outcomes. Understanding the precise mechanisms by which NFE4 and MTF1 control these processes could open avenues for developing targeted therapies that modulate neutrophil responses, potentially minimizing damage and enhancing recovery in stroke patients.

While ChEA effectively infers the activity of these TFs based on the enrichment of their target genes, it is important to note that this analysis does not directly indicate whether the transcription factors themselves are deregulated at the mRNA or protein expression level. Post-translational modifications, such as phosphorylation, acetylation, ubiquitination, or sumoylation can also modulate TF localization, stability, DNA-binding affinity, and interaction with co-factors, thereby fine-tuning TF regulatory functions without necessitating changes in gene expression. An altered activity inferred by ChEA could arise from changes in the candidate TF's own expression, but it could also stem from more complex regulatory mechanisms. For instance, MTF1 is known to be activated by zinc binding and can be regulated by phosphorylation, illustrating how such modifications can dictate its functional state (113,114). Therefore, even if NFER4, MTF1, or SPI1 potentially had no significant changes in their expression, their inferred hub status through ChEA strongly suggests that their activity is altered, potentially through critical post-translational modification events. To fully ascertain their direct deregulation, further investigation into their respective mRNA expression (e.g., via RNA-seq or qRT-PCR data) and protein abundance (e.g., through Western blotting or mass spectrometry) in our specific experimental conditions would be necessary.

Limitations

Inherent limitations, including a moderate sample size, should be considered when interpreting the findings of this study. While larger sample sizes can enhance statistical power, our study was designed as an exploratory investigation to capture early and rapid transcriptional changes following ischemia and recanalization at time points that had not previously been studied. Supporting evidence from previous studies suggests meaningful results can be obtained even with relatively small sample sizes (e.g., between 8 and 16) for microarray studies (115–117). A permutation method that accounts for correlation and effect size heterogeneity among

genes shows that a small pilot dataset with 4-6 samples per group is sufficient (118). Furthermore, analyses of the main effects comparing SHAM (N=16) versus MCAO+Recan (N=11) groups were sufficiently powered to define changes in gene expression associated with stroke and recanalization. Nevertheless, more extensive studies on subgroup analyses (such as sex and age) could benefit from a larger sample size.

These findings identify early genomic indicators of ischemia and recanalization for further investigation in future studies. The data reveal consistent molecular patterns across different biological conditions that can inform age and sex-specific gene expression and be further investigated as modulators of pathology and outcome. With multiple age and sex groups, the consistency of findings across groups suggests that the observed gene expression changes are robust and meaningful, providing a strong foundation for further investigation. Given the extensive number of gene expression changes observed, comprehensively validating all differentially expressed genes within a single study would be impractical. However, our exploratory approach allowed for efficient identification of the most relevant genes for further validation using functional and outcome-related measures. Validation studies incorporating a larger sample size, additional assays of leukocyte activation and function during and after ischemia, and additional time points will further inform the functional importance of gene expression patterns and enhance translational relevance.

Our study is unable to conclusively demonstrate whether observed transcriptomic differences arise from changes in gene expression within a given cell type or from shifts in immune cell composition—such as stroke-induced leukocytosis—captured in bulk RNA-seq data. For example, increased detection of canonical neutrophil genes (e.g., *Il1r2*, *Mmp8*) shortly after ischemia may reflect higher circulating neutrophil counts rather than transcriptional activation within individual neutrophils (119–121). While our use of computational deconvolution provides an improved estimate of cell type abundance, it cannot fully resolve cell type–specific transcriptional programs. Future studies incorporating scRNA-seq or single-nucleus approaches would enable direct discrimination between compositional shifts and actual within-cell transcriptional changes, providing a more precise understanding of the molecular mechanisms driving immune responses after stroke.

Another key consideration in the study design was the selection of early time points, specifically 1 hour after ischemic onset and 3 hours after recanalization (4 hours after onset).

This decision was guided by the need to capture rapid transcriptional changes within the therapeutic window, which holds the most significant potential to inform acute therapeutic strategies. Currently, intravenous thrombolysis with r-tPA is most effective within 3-4.5 hours of stroke onset, while mechanical thrombectomy benefits select patients for up to 24 hours based on advanced imaging criteria (18,19,122,123). Later time points, such as 24 hours post-recanalization, were not included because they fall outside the window for meaningful acute interventions and may primarily reflect secondary injury processes rather than immediate molecular responses. Identifying the earliest transcriptional responses is, therefore, crucial for developing interventions that can be administered adjunctively with recanalization therapies to prevent irreversible neuronal loss and enhance functional recovery. Moreover, previous research has demonstrated that gene expression changes can occur as early as 15 minutes after stimulation, reinforcing the relevance of capturing early-phase transcriptional dynamics (25). Neutrophils are known to respond rapidly to ischemic and inflammatory cues, making this timeframe appropriate for examining their involvement in stroke microcirculatory failure and futile recanalization (13,24). Future studies could incorporate time-course analyses extending beyond the acute phase to determine whether early gene expression changes translate into sustained neuroprotection or contribute to delayed injury mechanisms.

The study did not compare gene expression between venous and arterial blood samples but rather focused on peripheral transcriptional changes in venous blood. Arterial blood, being directly oxygenated and closer to the site of cerebral events, may exhibit different gene expression patterns than venous blood (124,125). Moreover, arterial blood reflects systemic physiological responses and oxygenation status more directly, while venous blood may better capture localized tissue responses and metabolic byproducts (126). Studying peripheral changes is especially valuable in clinical settings where rapid, minimally invasive, and repeatable sampling is required. Unlike arterial sampling, which is more invasive and technically challenging, venous blood draws are routinely performed and can facilitate the identification of early biomarkers predictive of stroke outcomes. Nevertheless, future research could explore potential differences in transcriptional profiles between venous and arterial blood to determine their relative utility in biomarker discovery and stroke prognosis.

The absence of behavioural or functional outcome in this study does not allow direct correlation of behaviour with gene expression changes. This study was not designed as an

outcome-based investigation but rather as an exploratory study to identify early molecular patterns following recanalization. By prioritizing early transcriptional changes, our study provides a necessary first step in understanding the mechanisms that drive post-stroke repair. This allows future research to take a more targeted approach to investigate the functional impacts of individual therapeutic targets (genes and gene products), focusing on the most promising molecular pathways identified here. This study provides a strong foundation by identifying key gene expression changes that occur immediately after recanalization, offering potential early indicators of stroke recovery that can be explored in subsequent studies incorporating longitudinal behavioural measures, imaging modalities, and long-term follow-up such as with the use of knock-out/knock-in models.

Conclusion

This study illuminates the critical role of gene regulatory networks in the pathophysiology of ischemic stroke, particularly in early recanalization responses. By identifying essential hub genes—*Il1r2, Cd55, Mmp8, Cd14,* and *Cd69*—and the novel marker *Vcan*, this study uncovered genomic indicators of recanalization that are highly conserved across species, from mice to humans. *Vcan* presents a promising target for future investigation, as its interaction with neutrophils during microcirculatory stalls and a high degree of conservation across species may offer new therapeutic avenues. Neutrophil was the only cell type with deconvoluted cell proportion significantly increased in both human and murine reference data. The functional enrichment analysis also revealed that pathways related to leukocyte migration, neutrophil activation, and phagocytosis were enriched in female mice and conserved in human recanalization models, pointing to potential sex-specific differences in reperfusion injury and stroke recovery mechanisms. The discovery of transcription factors NFE4 and MTF1, alongside miRNAs involved in reperfusion and recanalization injury, provides deeper insight into the regulatory dynamics of post-stroke recovery. These findings underscore the importance of targeting these molecular interactions in future therapeutic strategies. Experimental validation of these associations is essential, as it will advance understanding of stroke pathogenesis and potentially lead to novel, more effective treatments for ischemic stroke. By focusing on these molecular mechanisms, future research may enhance the efficacy of recanalization therapies, minimize futile recanalization, and ultimately improve patient outcomes in stroke recovery.

Sources of funding

This project is funded by a Canadian Institutes of Health Research Project Grant (CIHR PS 180244, IRW and GCJ) and Heart and Stroke Foundation Grant-in-Aid (HSFC GIA G-24-0036377, IRW).

Availability of data and materials

The dataset supporting the conclusions of this article is available in the GEO repository accession GSE278554.

Author contributions

T.A.B., I.R.W, Y.M., and G.C.J designed experiments. T.A.B. and Y.M performed experiments and collected data, T.A.B. analyzed data. T.A.B., G.C.J. and I.R.W. wrote the main manuscript text, and T.A.B. prepared all the figures. All authors reviewed and revised the manuscript.

Acknowledgements

The authors thank Sima Abbasi Habashi and Patricia Kent for their continual support.

Ethics declaration

All experiments were approved by the University of Alberta's Health Sciences Animal Care and Use Committee (Protocol AUP361) and adhered to the guidelines set by the Canadian Council for Animal Care.

Conflict of interest disclosures

The authors declare no competing interests.

References

1. Brauer M, Roth GA, Aravkin AY, Zheng P, Abate KH, Abate YH, et al. Global burden and strength of evidence for 88 risk factors in 204 countries and 811 subnational locations, 1990–2021: a systematic analysis for the Global Burden of Disease Study 2021. The Lancet. 2024 May 18;403(10440):2162–203.

2. Benjamin EJ, Blaha MJ, Chiuve SE, Cushman M, Das SR, Deo R, et al. Heart Disease and Stroke Statistics-2017 Update: A Report From the American Heart Association. Circulation. 2017 Mar 7;135(10):e146–603.

3. Vaduganathan M, Mensah GA, Turco JV, Fuster V, Roth GA. The Global Burden of Cardiovascular Diseases and Risk. J Am Coll Cardiol. 2022 Dec 20;80(25):2361–71.

4. GBD 2019 Stroke Collaborators. Global, regional, and national burden of stroke and its risk factors, 1990-2019: a systematic analysis for the Global Burden of Disease Study 2019. Lancet Neurol. 2021 Oct;20(10):795–820.

5. Madsen TE, Khoury JC, Leppert M, Alwell K, Moomaw CJ, Sucharew H, et al. Temporal Trends in Stroke Incidence Over Time by Sex and Age in the GCNKSS. Stroke. 2020 Apr;51(4):1070–6.

6. Leppert MH, Burke JF, Lisabeth LD, Madsen TE, Kleindorfer DO, Sillau S, et al. Systematic Review of Sex Differences in Ischemic Strokes Among Young Adults: Are Young Women Disproportionately at Risk? Stroke. 2022 Feb;53(2):319–27.

7. Petrea RE, Beiser AS, Seshadri S, Kelly-Hayes M, Kase CS, Wolf PA. Gender Differences in Stroke Incidence and Poststroke Disability in the Framingham Heart Study. Stroke. 2009 Apr;40(4):1032–7.

8. Kanasi E, Ayilavarapu S, Jones J. The aging population: demographics and the biology of aging. Periodontol 2000. 2016 Oct;72(1):13–8.

9. Roth JM. Recombinant tissue plasminogen activator for the treatment of acute ischemic stroke. Proc Bayl Univ Med Cent. 2011 July;24(3):257–9.

10. Bhatia K, Bhagavan S, Bains N, French B, Siddiq F, Gomez CR, et al. Current Endovascular Treatment of Acute Ischemic Stroke. Mo Med. 2020;117(5):480–9.

11. Pham M, Bendszus M. Facing Time in Ischemic Stroke: An Alternative Hypothesis for Collateral Failure. Clin Neuroradiol. 2016 June;26(2):141–51.

12. Dalkara T, Arsava EM. Can restoring incomplete microcirculatory reperfusion improve stroke outcome after thrombolysis? J Cereb Blood Flow Metab Off J Int Soc Cereb Blood Flow Metab. 2012 Dec;32(12):2091–9.

13. Bui TA, Jickling GC, Winship IR. Neutrophil dynamics and inflammaging in acute ischemic stroke: A transcriptomic review. Front Aging Neurosci. 2022;14:1041333.

14. Woodruff TM, Thundyil J, Tang SC, Sobey CG, Taylor SM, Arumugam TV. Pathophysiology, treatment, and animal and cellular models of human ischemic stroke. Mol Neurodegener. 2011 Jan 25;6(1):11.

15. Saver JL. Time Is Brain—Quantified. Stroke. 2006 Jan;37(1):263–6.

16. Hui C, Tadi P, Khan Suheb MZ, Patti L. Ischemic Stroke. In: StatPearls [Internet]. Treasure Island (FL): StatPearls Publishing; 2025 [cited 2025 Feb 28]. Available from: http://www.ncbi.nlm.nih.gov/books/NBK499997/

17. Liu S, Levine SR, Winn HR. Targeting ischemic penumbra: part I - from pathophysiology to therapeutic strategy. J Exp Stroke Transl Med. 2010 Mar 15;3(1):47–55.

18. Li J, Li F, Li Z, Wu M, Dai L, Wang J, et al. Time-Dependent Endovascular Treatment Effect According to Collateral Status in Basilar Artery Occlusion. Neurotherapeutics. 2023 Jan 1;20(1):220–9.

19. Liu J, Zhuo N, Wei J, Fan Y, Jiang C. Endovascular treatment of stroke in the late time window with large vessel occlusion using the ASPECTS as an imaging screening criterion. Sci Rep. 2024 May 29;14(1):12285.

20. Stemer A, Lyden P. Evolution of the Thrombolytic Treatment Window for Acute Ischemic Stroke. Curr Neurol Neurosci Rep. 2010;10(1):29–33.

21. Cowled P, Fitridge R. Pathophysiology of Reperfusion Injury. In: Fitridge R, Thompson M, Fitridge R, Thompson M, editors. Mechanisms of Vascular Disease: A Reference Book for Vascular Specialists [Internet]. Adelaide (AU); 2011 [cited 2022 June 29]. Available from: http://www.ncbi.nlm.nih.gov/books/NBK534267/

22. Goyal M, Menon BK, van Zwam WH, Dippel DWJ, Mitchell PJ, Demchuk AM, et al. Endovascular thrombectomy after large-vessel ischaemic stroke: a meta-analysis of individual patient data from five randomised trials. Lancet Lond Engl. 2016 Apr 23;387(10029):1723–31.

23. Shen H, Killingsworth MC, Bhaskar SMM. Comprehensive Meta-Analysis of Futile Recanalization in Acute Ischemic Stroke Patients Undergoing Endovascular Thrombectomy: Prevalence, Factors, and Clinical Outcomes. Life. 2023 Sept 26;13(10):1965.

24. El Amki M, Glück C, Binder N, Middleham W, Wyss MT, Weiss T, et al. Neutrophils Obstructing Brain Capillaries Are a Major Cause of No-Reflow in Ischemic Stroke. Cell Rep. 2020 Oct 13;33(2):108260.

25. Jickling GC, Liu D, Ander BP, Stamova B, Zhan X, Sharp FR. Targeting neutrophils in ischemic stroke: translational insights from experimental studies. J Cereb Blood Flow Metab. 2015 June;35(6):888–901.

26. Tang Y, Xu H, Du XL, Lit L, Walker W, Lu A, et al. Gene Expression in Blood Changes Rapidly in Neutrophils and Monocytes after Ischemic Stroke in Humans: A Microarray Study. J Cereb Blood Flow Metab. 2006 Aug;26(8):1089–102.

27. de la Riva P, Marta-Enguita J, Rodríguez-Antigüedad J, Bergareche A, de Munain AL. Understanding Endothelial Dysfunction and Its Role in Ischemic Stroke After the Outbreak of Recanalization Therapies. Int J Mol Sci. 2024 Oct 29;25(21):11631.

28. Percie du Sert N, Hurst V, Ahluwalia A, Alam S, Avey MT, Baker M, et al. The ARRIVE guidelines 2.0: Updated guidelines for reporting animal research. Br J Pharmacol. 2020 Aug;177(16):3617–24.

29. Ritchie ME, Phipson B, Wu D, Hu Y, Law CW, Shi W, et al. limma powers differential expression analyses for RNA-sequencing and microarray studies. Nucleic Acids Res. 2015 Apr 20;43(7):e47.

30. Stelzer G, Rosen N, Plaschkes I, Zimmerman S, Twik M, Fishilevich S, et al. The GeneCards Suite: From Gene Data Mining to Disease Genome Sequence Analyses. Curr Protoc Bioinforma. 2016 June 20;54:1.30.1-1.30.33.

31. Raudvere U, Kolberg L, Kuzmin I, Arak T, Adler P, Peterson H, et al. g:Profiler: a web server for functional enrichment analysis and conversions of gene lists (2019 update). Nucleic Acids Res. 2019 July 2;47(W1):W191–8.

32. Zhou G, Soufan O, Ewald J, Hancock REW, Basu N, Xia J. NetworkAnalyst 3.0: a visual analytics platform for comprehensive gene expression profiling and meta-analysis. Nucleic Acids Res. 2019 July 2;47(W1):W234–41.

33. Lachmann A, Xu H, Krishnan J, Berger SI, Mazloom AR, Ma'ayan A. ChEA: transcription factor regulation inferred from integrating genome-wide ChIP-X experiments. Bioinformatics. 2010 Oct 1;26(19):2438–44.

34. Wu T, Hu E, Xu S, Chen M, Guo P, Dai Z, et al. clusterProfiler 4.0: A universal enrichment tool for interpreting omics data. Innov Camb Mass. 2021 Aug 28;2(3):100141.

35. Hu C, Li T, Xu Y, Zhang X, Li F, Bai J, et al. CellMarker 2.0: an updated database of manually curated cell markers in human/mouse and web tools based on scRNA-seq data. Nucleic Acids Res. 2023 Jan 6;51(D1):D870–6.

36. Miao YR, Xia M, Luo M, Luo T, Yang M, Guo AY. ImmuCellAI-mouse: a tool for comprehensive prediction of mouse immune cell abundance and immune microenvironment depiction. Bioinformatics. 2022 Jan 12;38(3):785–91.

37. Avila Cobos F, Vandesompele J, Mestdagh P, De Preter K. Computational deconvolution of transcriptomics data from mixed cell populations. Bioinforma Oxf Engl. 2018 June 1;34(11):1969–79.

38. Akthar M, Nair N, Carter LM, Vital EM, Sutton E, McHugh N, et al. Deconvolution of whole blood transcriptomics identifies changes in immune cell composition in patients with systemic lupus erythematosus (SLE) treated with mycophenolate mofetil. Arthritis Res Ther. 2023 June 30;25(1):111.

39. Chen B, Khodadoust MS, Liu CL, Newman AM, Alizadeh AA. Profiling tumor infiltrating immune cells with CIBERSORT. Methods Mol Biol Clifton NJ. 2018;1711:243–59.

40. Newman AM, Liu CL, Green MR, Gentles AJ, Feng W, Xu Y, et al. Robust enumeration of cell subsets from tissue expression profiles. Nat Methods. 2015 May;12(5):453–7.

41. Chen B, Khodadoust MS, Liu CL, Newman AM, Alizadeh AA. Profiling Tumor Infiltrating Immune Cells with CIBERSORT. Methods Mol Biol Clifton NJ. 2018;1711:243–59.

42. Akthar M, Nair N, Carter LM, Vital EM, Sutton E, McHugh N, et al. Deconvolution of whole blood transcriptomics identifies changes in immune cell composition in patients with systemic lupus erythematosus (SLE) treated with mycophenolate mofetil. Arthritis Res Ther. 2023;25:111.

43. Barr TL, Conley Y, Ding J, Dillman A, Warach S, Singleton A, et al. Genomic biomarkers and cellular pathways of ischemic stroke by RNA gene expression profiling. Neurology. 2010 Sept 14;75(11):1009–14.

44. Jickling GC, Zhan X, Ander BP, Turner RJ, Stamova B, Xu H, et al. Genome response to tissue plasminogen activator in experimental ischemic stroke. BMC Genomics. 2010 Apr 21;11:254.

45. O'Connell GC, Treadway MB, Petrone AB, Tennant CS, Lucke-Wold N, Chantler PD, et al. Peripheral blood AKAP7 expression as an early marker for lymphocyte-mediated post-stroke blood brain barrier disruption. Sci Rep. 2017 Apr 26;7:1172.

46. Uotani T, Sugimoto M, Ichikawa H, Tanaka S, Nagashima H, Uchida T, et al. Prostate stem cell antigen gene TT genotype and development of intestinal metaplasia in Helicobacter pylori infection. J Dig Dis. 2016 Jan;17(1):20–7.

47. Zepp JA, Zhao J, Liu C, Bulek K, Wu L, Chen X, et al. IL-17A-Induced PLET1 Expression Contributes to Tissue Repair and Colon Tumorigenesis. J Immunol Baltim Md 1950. 2017 Dec 1;199(11):3849–57.

48. Menon D, Innes A, Oakley AJ, Dahlstrom JE, Jensen LM, Brüstle A, et al. GSTO1-1 plays a pro-inflammatory role in models of inflammation, colitis and obesity. Sci Rep. 2017 Dec 19;7:17832.

49. Lian F, Xing X, Yuan G, Schäfer C, Rauser S, Walch A, et al. Farnesoid X receptor protects human and murine gastric epithelial cells against inflammation-induced damage. Biochem J. 2011 Sept 1;438(2):315–23.

50. Park EJ, Choi K, Park K. Induction of inflammatory responses and gene expression by intratracheal instillation of silver nanoparticles in mice. Arch Pharm Res. 2011 Feb;34(2):299–307.

51. Peddareddygari LR, Dutra AV, Levenstien MA, Sen S, Grewal RP. An analysis of methylenetetrahydrofolate reductase and glutathione S-transferase omega-1 genes as modifiers of the cerebral response to ischemia. BMC Neurol. 2009 July 22;9:37.

52. Chen Q, Li Z, Wang M, Li G. Over-expression of IL1R2 in PBMCs of Patients with Coronary Artery Disease and Its Clinical Significance. Anatol J Cardiol. 2022 Sept 1;26(9):710–6.

53. Stamova B, Ander BP, Jickling G, Hamade F, Durocher M, Zhan X, et al. The intracerebral hemorrhage blood transcriptome in humans differs from the ischemic stroke and vascular risk factor control blood transcriptomes. J Cereb Blood Flow Metab. 2019 Sept 1;39(9):1818–35.

54. Chen X, Takemoto Y, Deng H, Middelhoff M, Friedman RA, Chu TH, et al. Histidine decarboxylase (HDC)-expressing granulocytic myeloid cells induce and recruit Foxp3+ regulatory T cells in murine colon cancer. Oncoimmunology. 2017 Feb 10;6(3):e1290034.

55. Esposito E, Ahn BJ, Shi J, Nakamura Y, Park JH, Mandeville ET, et al. Brain-to-cervical lymph node signaling after stroke. Nat Commun. 2019 Nov 22;10(1):5306.

56. Dai H, Wang L, Li L, Huang Z, Ye L. Metallothionein 1: A New Spotlight on Inflammatory Diseases. Front Immunol. 2021 Nov 5;12:739918.

57. Palm F, Pussinen PJ, Safer A, Tervahartiala T, Sorsa T, Urbanek C, et al. Serum matrix metalloproteinase-8, tissue inhibitor of metalloproteinase and myeloperoxidase in ischemic stroke. Atherosclerosis. 2018 Apr;271:9–14.

58. Zhao Y, Zhang Q, Zhang X, Zhang Y, Lu Y, Ma X, et al. The roles of MMP8/MMP10 polymorphisms in ischemic stroke susceptibility. Brain Behav. 2022 Dec;12(12):e2797.

59. Hsieh FI, Chiou HY, Hu CJ, Jeng JS, Lin HJ, Lee JT, et al. Combined Effects of MMP-7, MMP-8 and MMP-26 on the Risk of Ischemic Stroke. J Clin Med. 2019 Nov 18;8(11):2011.

60. Hong J, Qu P, Wuest TR, Huang H, Huang C, Lin PC. Neutrophilic Granule Protein Is a Novel Murine LPS Antagonist. Immune Netw. 2019 Oct 17;19(5):e34.

61. Liu K, Tian L xing, Tang X, Wang J, Tang W qi, Ma Z fu, et al. Neutrophilic granule protein (NGP) attenuates lipopolysaccharide-induced inflammatory responses and enhances phagocytosis of bacteria by macrophages. Cytokine. 2020 Apr 1;128:155001.

62. Kalafati L, Kourtzelis I, Schulte-Schrepping J, Li X, Hatzioannou A, Grinenko T, et al. Innate Immune Training of Granulopoiesis Promotes Anti-tumor Activity. Cell. 2020 Oct 29;183(3):771-785.e12.

63. Song J, Wei R, Huo S, Liu C, Liu X. Versican enrichment predicts poor prognosis and response to adjuvant therapy and immunotherapy in gastric cancer. Front Immunol [Internet]. 2022 Sept 20 [cited 2024 May 20];13. Available from: https://www.frontiersin.org/journals/immunology/articles/10.3389/fimmu.2022.960570/full

64. Wight TN, Kang I, Evanko SP, Harten IA, Chang MY, Pearce OMT, et al. Versican—A Critical Extracellular Matrix Regulator of Immunity and Inflammation. Front Immunol. 2020 Mar 24;11:512.

65. Emmerich P, Matkowskyj KA, McGregor S, Kraus S, Bischel K, Qyli T, et al. VCAN accumulation and proteolysis as predictors of T lymphocyte-excluded and permissive tumor microenvironments. J Clin Oncol. 2020 May 20;38(15_suppl):3127–3127.

66. O'Connor MN, Kallenberg DM, Camilli C, Pilotti C, Dritsoula A, Jackstadt R, et al. LRG1 destabilizes tumor vessels and restricts immunotherapeutic potency. Med N Y N. 2021 Nov 12;2(11):1231-1252.e10.

67. Camilli C, Hoeh AE, De Rossi G, Moss SE, Greenwood J. LRG1: an emerging player in disease pathogenesis. J Biomed Sci. 2022 Jan 21;29(1):6.

68. Lund AW, De Palma M. Targeting LRG1 boosts immunotherapy. Med. 2021 Nov 12;2(11):1195–7.

69. Sharygin D, Koniaris LG, Wells C, Zimmers TA, Hamidi T. Role of CD14 in human disease. Immunology. 2023 July;169(3):260–70.

70. Na K, Oh BC, Jung Y. Multifaceted role of CD14 in innate immunity and tissue homeostasis. Cytokine Growth Factor Rev. 2023 Dec 1;74:100–7.

71. Keerthivasan G, Mei Y, Zhao B, Zhang L, Harris CE, Gao J, et al. Aberrant overexpression of CD14 on granulocytes sensitizes the innate immune response in mDia1 heterozygous del(5q) MDS. Blood. 2014 July 31;124(5):780–90.

72. Li Y, Shen Z, Chai Z, Zhan Y, Zhang Y, Liu Z, et al. Targeting MS4A4A on tumour-associated macrophages restores CD8+ T-cell-mediated antitumour immunity. Gut. 2023 Nov 24;72(12):2307–20.

73. Mattiola I, Mantovani A, Locati M. The tetraspan MS4A family in homeostasis, immunity, and disease. Trends Immunol. 2021 Sept 1;42(9):764–81.

74. Lightfoot YL, Botte A, Trinh RTP, Ding GS, McReynolds M, Allen JK, et al. Anti-MS4A4A Antibody Modulates Myeloid Cell Biology and TREM2 Signaling. Alzheimers Dement. 2023;19(S21):e072144.

75. Chen Y, Li S, Huang X, Wang C, Pan Y, Xiang Q, et al. Tetraspan MS4A6D is a coreceptor of MHC class II antigen (MHC-II) that promotes macrophages-derived inflammation. Mol Immunol. 2023 Aug 1;160:121–32.

76. Guo J, Wang C, Xiang Q, Feng Z, Fei L, Guo G, et al. MS4A6D Promotes carrageenan-induced footpad swelling in mice through enhancing macrophages-derived inflammation. Mol Immunol. 2024 May 1;169:28–36.

77. Cao Z, Lu P, Li L, Geng Q, Lin L, Yan L, et al. Bioinformatics-led discovery of liver-specific genes and macrophage infiltration in acute liver injury. Front Immunol [Internet]. 2023 Dec 7 [cited 2024 May 20];14. Available from: https://www.frontiersin.org/journals/immunology/articles/10.3389/fimmu.2023.1287136/full

78. Koyama-Nasu R, Wang Y, Hasegawa I, Endo Y, Nakayama T, Kimura MY. The cellular and molecular basis of CD69 function in anti-tumor immunity. Int Immunol. 2022 Oct 5;34(11):555–61.

79. Marzio R, Mauël J, Betz-Corradin S. CD69 and regulation of the immune function. Immunopharmacol Immunotoxicol. 1999 Aug;21(3):565–82.

80. Gorabi AM, Hajighasemi S, Kiaie N, Gheibi Hayat SM, Jamialahmadi T, Johnston TP, et al. The pivotal role of CD69 in autoimmunity. J Autoimmun. 2020 July 1;111:102453.

81. Fang W, Zhai X, Han D, Xiong X, Wang T, Zeng X, et al. CCR2-dependent monocytes/macrophages exacerbate acute brain injury but promote functional recovery after ischemic stroke in mice. Theranostics. 2018 June 6;8(13):3530–43.

82. Luo X. CXCR2 antagonism attenuates neuroinflammation after subarachnoid hemorrhage. J Stroke Cerebrovasc Dis. 2023 Sept 1;32(9):107266.

83. Eruslanov EB, Singhal S, Albelda SM. Mouse versus human neutrophils in cancer–a major knowledge gap. Trends Cancer. 2017 Feb;3(2):149–60.

84. Bjornson-Hooper ZB, Fragiadakis GK, Spitzer MH, Chen H, Madhireddy D, Hu K, et al. A Comprehensive Atlas of Immunological Differences Between Humans, Mice, and Non-Human Primates. Front Immunol [Internet]. 2022 Mar 11 [cited 2025 Aug 12];13. Available from: https://www.frontiersin.org/journals/immunology/articles/10.3389/fimmu.2022.867015/full

85. Jickling GC, Sharp FR. Blood biomarkers of ischemic stroke. Neurother J Am Soc Exp Neurother. 2011 July;8(3):349–60.

86. Boraschi D, Italiani P, Weil S, Martin MU. The family of the interleukin-1 receptors. Immunol Rev. 2018;281(1):197–232.

87. Kang L, Kohen M, McCarthy I, Hammelef E, Kim HS, Bapputty R, et al. Critical Role of CD55 in Controlling Wound Healing. J Immunol. 2024 Feb 19;212(7):1142–9.

88. VanLandingham JW, Cekic M, Cutler S, Hoffman SW, Stein DG. Neurosteroids reduce inflammation after TBI through CD55 induction. Neurosci Lett. 2007 Sept 25;425(2):94–8.

89. Tradtrantip L, Duan T, Yeaman MR, Verkman AS. CD55 upregulation in astrocytes by statins as potential therapy for AQP4-IgG seropositive neuromyelitis optica. J Neuroinflammation. 2019 Mar 9;16(1):57.

90. Bai Y, Du Y, Yang Y, Wälchli T, Constanthin PE, Li F. Ultrasound-Targeted Microbubble Destruction Increases BBB Permeability and Promotes Stem Cell-Induced Regeneration of Stroke by Downregulating MMP8. Cell Transplant. 2024;33:9636897231223293.

91. Brait VH, Miró-Mur F, Pérez-de-Puig I, Notario L, Hurtado B, Pedragosa J, et al. CD69 Plays a Beneficial Role in Ischemic Stroke by Dampening Endothelial Activation. Circ Res. 2019 Jan 18;124(2):279–91.

92. Zhou M, Wang CM, Yang WL, Wang P. Microglial CD14 activated by iNOS contributes to neuroinflammation in cerebral ischemia. Brain Res. 2013 Apr 19;1506:105–14.

93. Liu Y, Song R, Lu Z, Zhao L, Zhan X, Li Y, et al. The RNA m6A demethylase ALKBH5 drives emergency granulopoiesis and neutrophil mobilization by upregulating G-CSFR expression. Cell Mol Immunol. 2024 Jan;21(1):6–18.

94. Hajka D, Budziak B, Pietras Ł, Duda P, McCubrey JA, Gizak A. GSK3 as a Regulator of Cytoskeleton Architecture: Consequences for Health and Disease. Cells. 2021 Aug 14;10(8):2092.

95. Cusseddu R, Robert A, Côté JF. Strength Through Unity: The Power of the Mega-Scaffold MACF1. Front Cell Dev Biol. 2021 Mar 18;9:641727.

96. Eruslanov EB, Singhal S, Albelda SM. Mouse versus human neutrophils in cancer–a major knowledge gap. Trends Cancer. 2017 Feb;3(2):149–60.

97. Gibbons DL, Spencer J. Mouse and human intestinal immunity: same ballpark, different players; different rules, same score. Mucosal Immunol. 2011 Mar 1;4(2):148–57.

98. Nauseef WM. Human neutrophils ≠ murine neutrophils: does it matter? Immunol Rev. 2023 Mar;314(1):442–56.

99. Conley HE, Sheats MK. Targeting Neutrophil β2-Integrins: A Review of Relevant Resources, Tools, and Methods. Biomolecules. 2023 June;13(6):892.

100. Zhou M, Liu YWY, He YH, Zhang JY, Guo H, Wang H, et al. FOXO1 reshapes neutrophils to aggravate acute brain damage and promote late depression after traumatic brain injury. Mil Med Res. 2024 Mar 31;11(1):20.

101. Islam S, Watanabe H. Versican: A Dynamic Regulator of the Extracellular Matrix. J Histochem Cytochem. 2020 Sept 10;68(11):763.

102. Garcia-Bonilla L, Shahanoor Z, Sciortino R, Nazarzoda O, Racchumi G, Iadecola C, et al. Analysis of brain and blood single-cell transcriptomics in acute and subacute phases after experimental stroke. Nat Immunol. 2024 Feb;25(2):357–70.

103. Carmona-Mora P, Ander BP, Jickling GC, Dykstra-Aiello C, Zhan X, Ferino E, et al. Distinct peripheral blood monocyte and neutrophil transcriptional programs following intracerebral hemorrhage and different etiologies of ischemic stroke. J Cereb Blood Flow Metab Off J Int Soc Cereb Blood Flow Metab. 2021 June;41(6):1398–416.

104. Carmona-Mora P, Knepp B, Jickling GC, Zhan X, Hakoupian M, Hull H, et al. Monocyte, neutrophil, and whole blood transcriptome dynamics following ischemic stroke. BMC Med. 2023 Feb 20;21(1):65.

105. Qiu YM, Zhang CL, Chen AQ, Wang HL, Zhou YF, Li YN, et al. Immune Cells in the BBB Disruption After Acute Ischemic Stroke: Targets for Immune Therapy? Front Immunol. 2021;12:678744.

106. Tiedt S, Prestel M, Malik R, Schieferdecker N, Duering M, Kautzky V, et al. RNA-Seq Identifies Circulating miR-125a-5p, miR-125b-5p, and miR-143-3p as Potential Biomarkers for Acute Ischemic Stroke. Circ Res. 2017 Sept 29;121(8):970–80.

107. Wang Y, Su X, Leung GHD, Ren B, Zhang Q, Xiong Z, et al. Circulating microRNAs as diagnostic biomarkers for ischemic stroke: evidence from comprehensive analysis and real-world validation. Int J Med Sci. 2023 June 4;20(8):1009.

108. Kim JM, Byun JS, Kim J, Park MS, Hong SA, Nam TK, et al. Analysis of microRNA signatures in ischemic stroke thrombus. J Neurointerventional Surg. 2022 May;14(5):neurintsurg-2021-017597.

109. Zheng Y, Zhao P, Lian Y, Li S, Chen Y, Li L. MiR-340-5p alleviates oxygen-glucose deprivation/reoxygenation-induced neuronal injury via PI3K/Akt activation by targeting PDCD4. Neurochem Int. 2020 Mar 1;134:104650.

110. Lei Y, Jin X, Sun M, Ji Z. miR-129-5p Ameliorates Ischemic Brain Injury by Binding to SIAH1 and Activating the mTOR Signaling Pathway. J Mol Neurosci. 2021 Sept 1;71(9):1761–71.

111. Valsecchi V, Laudati G, Cuomo O, Sirabella R, Del Prete A, Annunziato L, et al. The hypoxia sensitive metal transcription factor MTF-1 activates NCX1 brain promoter and participates in remote postconditioning neuroprotection in stroke. Cell Death Dis. 2021 Apr 30;12(5):423.

112. Ai Z, Udalova IA. Transcriptional regulation of neutrophil differentiation and function during inflammation. J Leukoc Biol. 2020 Mar;107(3):419–30.

113. Tavera-Montañez C, Hainer SJ, Cangussu D, Gordon SJV, Xiao Y, Reyes-Gutierrez P, et al. The classic metal-sensing transcription factor MTF1 promotes myogenesis in response to copper. FASEB J. 2019 Dec;33(12):14556–74.

114. Günther V, Lindert U, Schaffner W. The taste of heavy metals: Gene regulation by MTF-1. Biochim Biophys Acta BBA - Mol Cell Res. 2012 Sept 1;1823(9):1416–25.

115. Wang SJ, Chen JJ. Sample size for identifying differentially expressed genes in microarray experiments. J Comput Biol J Comput Mol Cell Biol. 2004;11(4):714–26.

116. Tsai CA, Wang SJ, Chen DT, Chen JJ. Sample size for gene expression microarray experiments†. [cited 2025 Feb 15]; Available from: https://dx.doi.org/10.1093/bioinformatics/bti162

117. Androvic P, Kirdajova D, Tureckova J, Zucha D, Rohlova E, Abaffy P, et al. Decoding the Transcriptional Response to Ischemic Stroke in Young and Aged Mouse Brain. Cell Rep. 2020 June 16;31(11):107777.

118. Lin WJ, Hsueh HM, Chen JJ. Power and sample size estimation in microarray studies. BMC Bioinformatics. 2010 Jan 25;11(1):48.

119. Shepherd HM, Gauthier JM, Terada Y, Li W, Krupnick AS, Gelman AE, et al. Updated Views on Neutrophil Responses in Ischemia–Reperfusion Injury. Transplantation. 2022 Dec;106(12):2314.

120. Jordan JE, Zhao ZQ, Vinten-Johansen J. The role of neutrophils in myocardial ischemia-reperfusion injury. Cardiovasc Res. 1999 Sept;43(4):860–78.

121. Mehta J, Dinerman J, Mehta P, Saldeen TG, Lawson D, Donnelly WH, et al. Neutrophil function in ischemic heart disease. Circulation. 1989 Mar;79(3):549–56.

122. del Zoppo GJ, Saver JL, Jauch EC, Adams HP. Expansion of the Time Window for Treatment of Acute Ischemic Stroke With Intravenous Tissue Plasminogen Activator. Stroke J Cereb Circ. 2009 Aug;40(8):2945–8.

123. Kobeissi H, Ghozy S, Adusumilli G, Kadirvel R, Brinjikji W, Rabinstein AA, et al. Endovascular Therapy for Stroke Presenting Beyond 24 Hours. JAMA Netw Open. 2023 May 4;6(5):e2311768.

124. Niklason L, Dai G. Arterial Venous Differentiation for Vascular Bioengineering. Annu Rev Biomed Eng. 2018 June 4;20:431–47.

125. Corada M, Morini MF, Dejana E. Signaling Pathways in the Specification of Arteries and Veins. Arterioscler Thromb Vasc Biol. 2014 Nov;34(11):2372–7.

126. Saberian L, Sharif M, Aarabi M, Broumand B, Shafiee MA. Arterial Versus Venous Blood Gas Analysis Comparisons, Appropriateness, and Alternatives in Different Acid/Base Clinical Settings: A Systematic Review. Cureus. 2023;15(7):e41707.

Figures

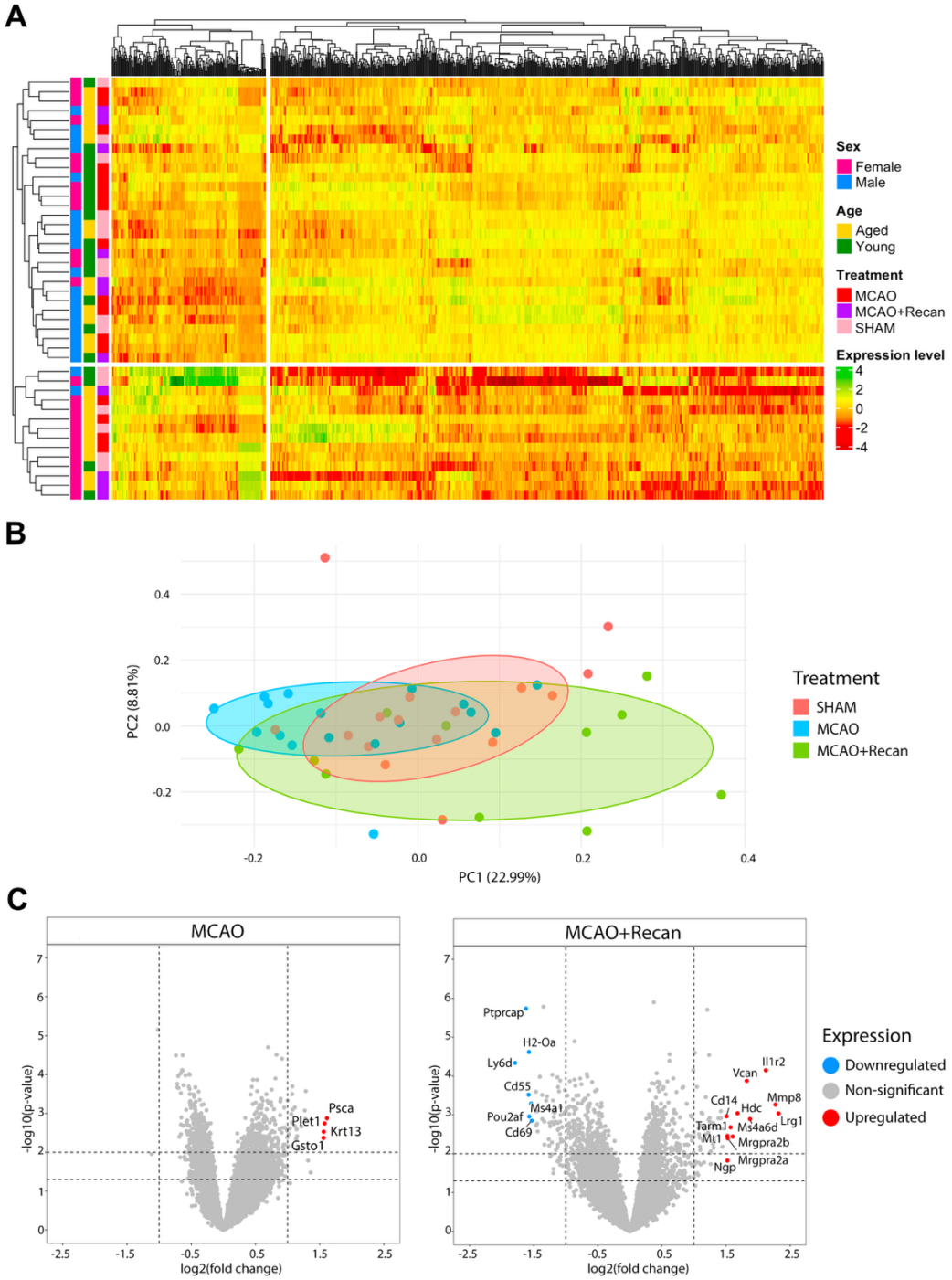

Figure 1 (A) Hierarchical clustering of gene expression patterns across all samples. The cluster dendrograms represent Canberra distance-based hierarchical clustering, which organizes samples (columns) and genes (rows) based on similarities in their expression. The dendrograms on the left and top of the heatmap display the clustering structure, visually grouping samples and genes with similar expression profiles. **(B)** Principal component analysis (PCA) of 44 samples. The

PCA plot illustrates the expression variability among the samples, with each point representing the combined expression of all differentially expressed genes (DEGs) for a given sample. Samples are grouped by experimental condition (SHAM, MCAO, and MCAO+Recan), as indicated by the coloured ellipses. The x-axis represents the first principal component, which explains 22.99% of the total variance, while the y-axis represents the second principal component, explaining 8.81% of the variance. **(C)** Volcano plots of DEGs in MCAO and MCAO+Recan group. The plots depict the significantly upregulated (red) and downregulated (blue) genes in the MCAO (left) and MCAO+Recan (right) groups ($|\log2FC| \geq 1.5$, p-value ≤ 0.05). The plots compare the magnitude and significance of gene expression changes. Differential gene expression analysis was performed using the limma package in RStudio and Bioconductor.

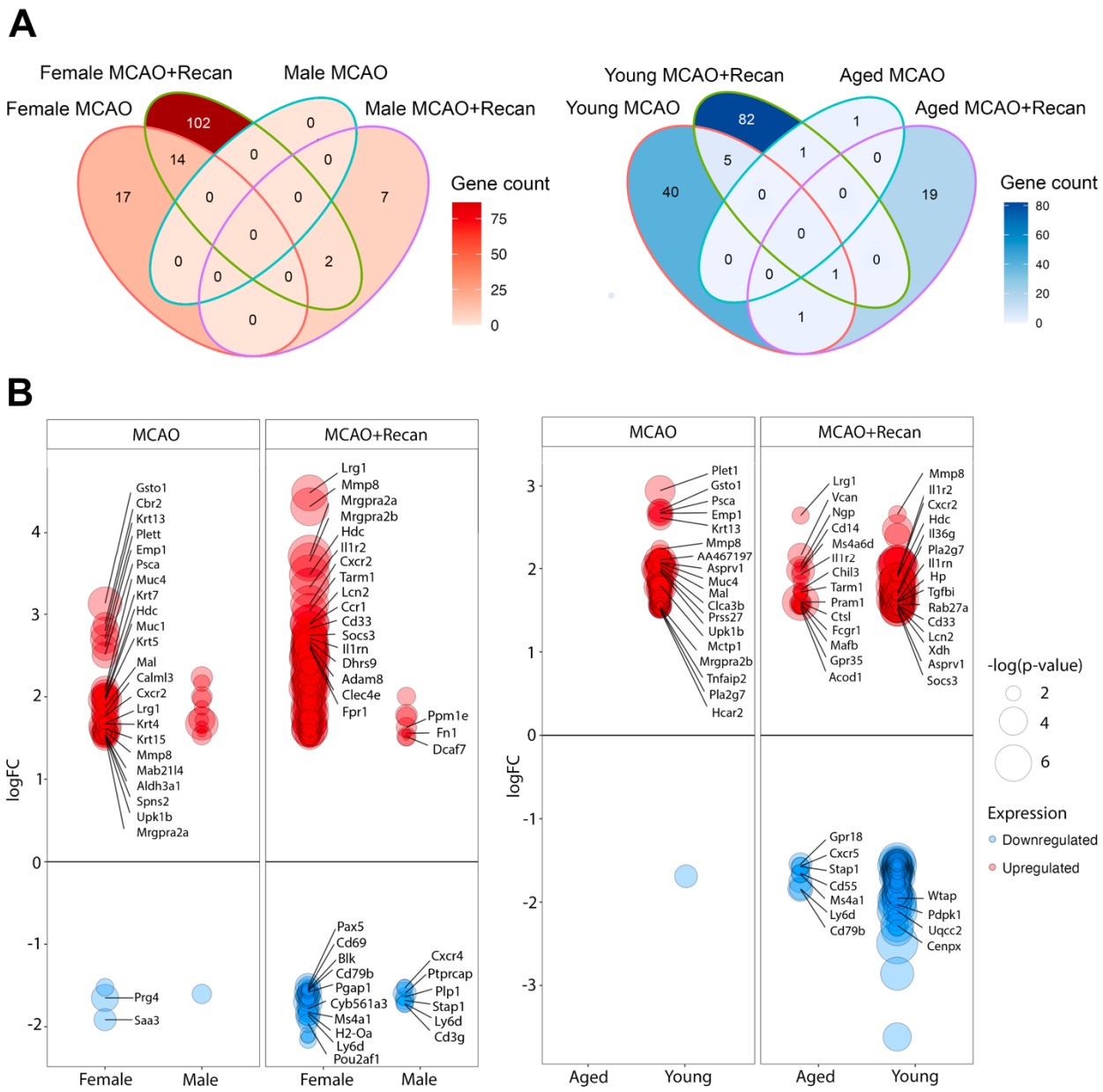

Figure 2. Age- and sex-specific differentially expressed genes (DEGs). Differential gene expression analysis was performed using the limma package from RStudio and Bioconductor. **(A)** Venn diagram showing the overlap of DEGs between sex-specific and age-specific groups ($|\log_2 FC| \geq 1.5$, p-value ≤ 0.05). **(B)** Bar plots depict the up and downregulated genes in age-specific and sex-specific groups ($|\log_2 FC| \geq 1.5$, p-value ≤ 0.05). These analyses highlight the unique and shared transcriptional changes based on age and sex in MCAO+Recan models.

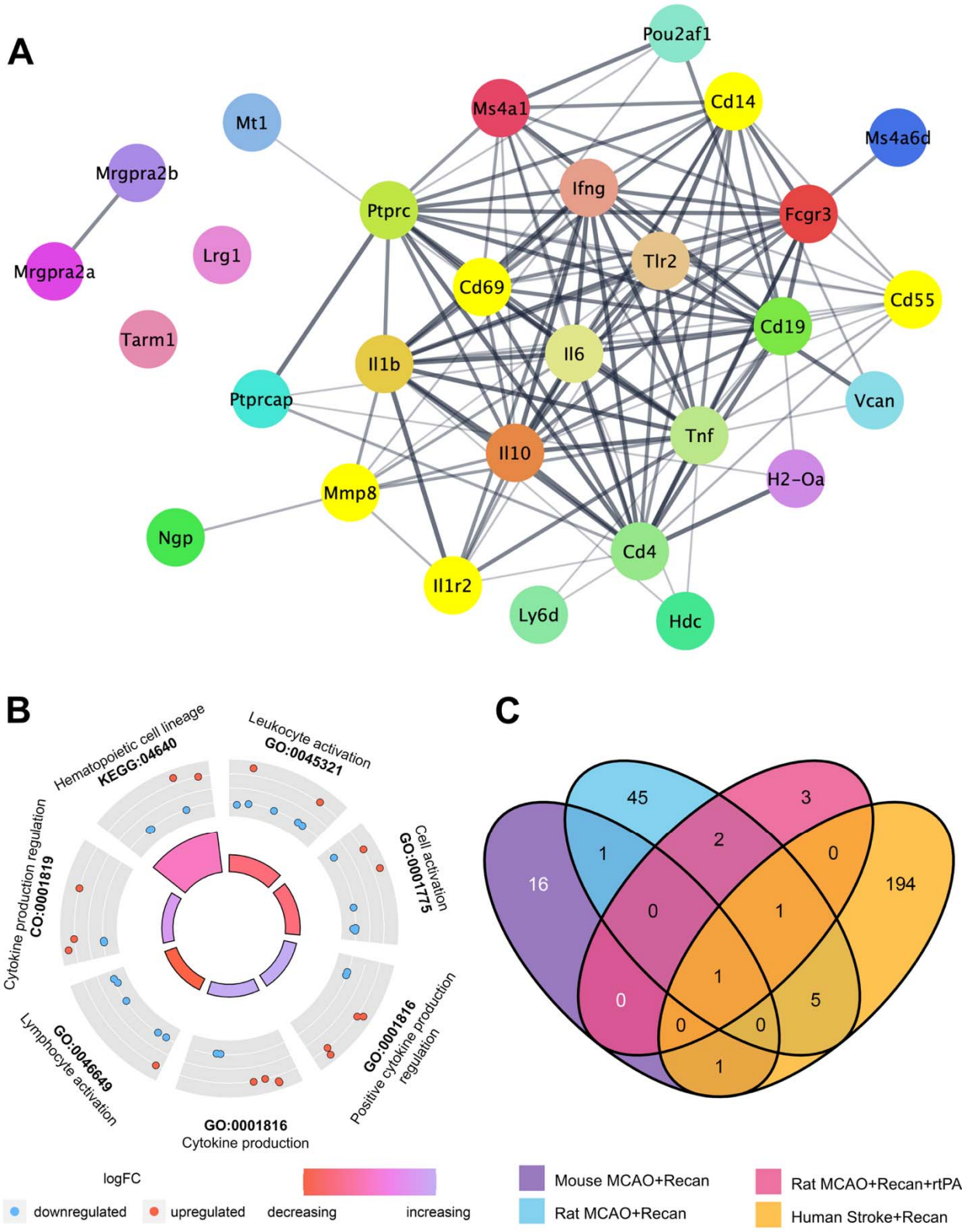
A
Pou2af1
Ms4a1
Cd14
Mt1
Ms4a6d
Mrgpra2b
Ifng
Ptprc
Fcgr3
Lrg1
Mrgpra2a
Tlr2
Cd69
Cd55
Cd19
Tarm1
Il1b
Il6
Ptprcap
Vcan
Tnf
Il10
H2-Oa
Mmp8
Ngp
Cd4
Il1r2
Ly6d
Hdc
B
Hematopoietic cell lineage
KEGG:04640
Leukocyte activation
GO:0045321
Cell activation
GO:0001775
Cytokine production regulation
CO:0001819
GO:0001816
Positive cytokine production regulation
GO:0046649
Lymphocyte activation
GO:0001816
Cytokine production
logFC
downregulated
upregulated
decreasing
increasing
C
45
3
16
1
2
0
194
0
1
1
0
5
0
0
1
Mouse MCAO+Recan
Rat MCAO+Recan
Rat MCAO+Recan+rtPA
Human Stroke+Recan

Figure 3 (A) STRING protein-protein interaction (PPI) network of differentially expressed genes (DEGs). The network was generated with a confidence level of 0.4 and a maximum of 10 additional interactors. Nodes represent DEGs, while edges indicate their interactions. Hub genes identified by the DMNC algorithm within the CytoHubba plugin are highlighted. **(B)** Circular visualization of gene annotation enrichment analysis results (GOCircle) for MCAO+Recan. Differentially expressed genes were selected ($|\log_2 FC| \geq 1.5$, p-value ≤ 0.05). The inner ring features a bar plot, where bar colour corresponds to the z-score (green for downregulation and yellow for upregulation), and the height of each bar represents the significance of the pathway based on log(adj p-value). The outer ring displays scatter plots of gene expression levels (logFC) for each term, with blue indicating downregulation and red indicating upregulation. **(C)** Cross-validation of all DEGs across three datasets. The analysis included mouse, GSE2113 rat samples, and GSE1656 human samples, focusing on DEGs meeting the criteria ($|\log_2 FC| \geq 1.5$, p-value $\leq$ 0.05). This comparison underscores the consistency of DEGs across different species and datasets.

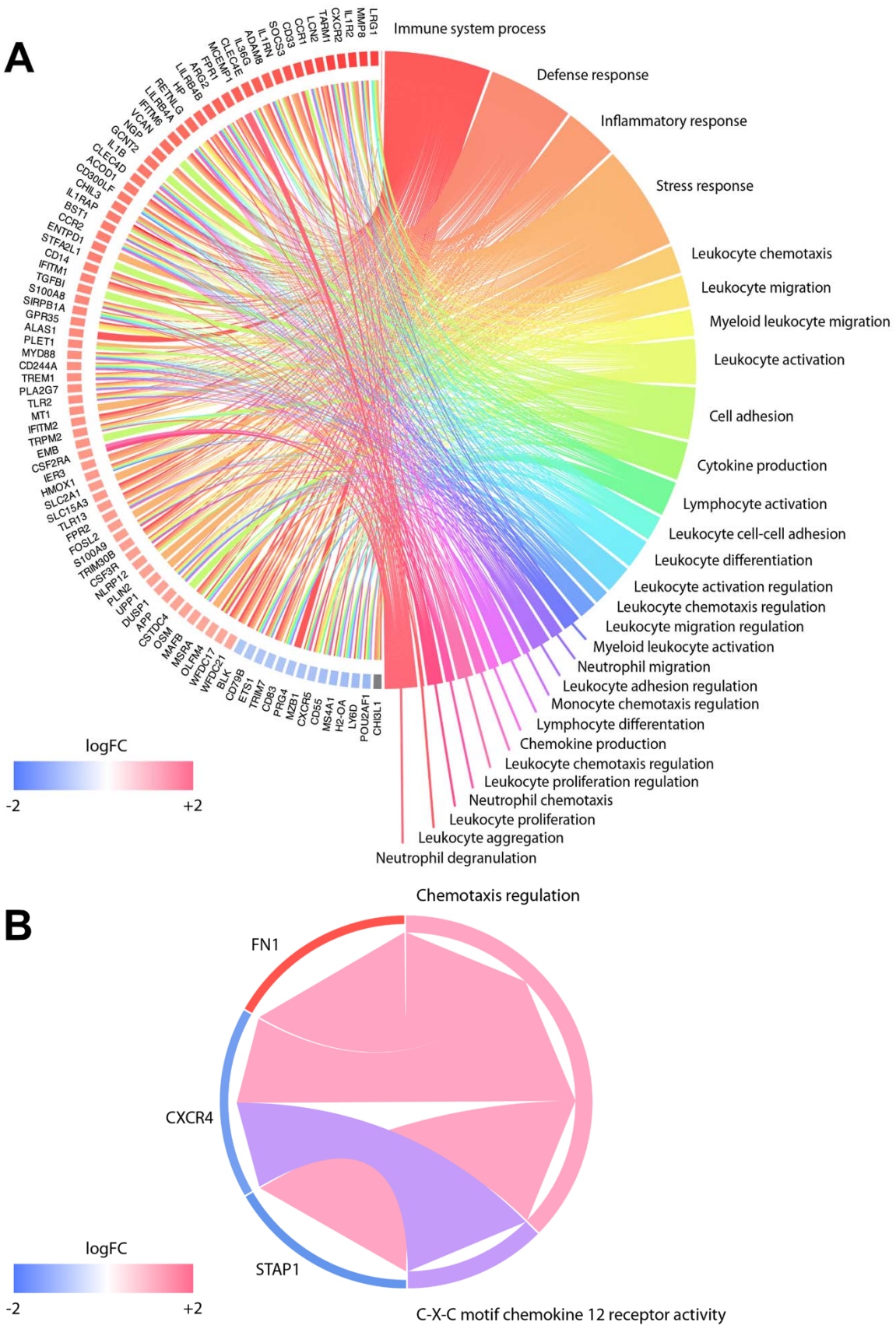
A
Immune system process
Defense response
Inflammatory response
Stress response
Leukocyte chemotaxis
Leukocyte migration
Myeloid leukocyte migration
Leukocyte activation
Cell adhesion
Cytokine production
Lymphocyte activation
Leukocyte cell-cell adhesion
Leukocyte differentiation
Leukocyte activation regulation
Leukocyte chemotaxis regulation
Leukocyte migration regulation
Myeloid leukocyte activation
Neutrophil migration
Leukocyte adhesion regulation
Monocyte chemotaxis regulation
Lymphocyte differentation
Chemokine production
Leukocyte chemotaxis regulation
Leukocyte proliferation regulation
Neutrophil chemotaxis
Leukocyte proliferation
Leukocyte aggregation
Neutrophil degranulation
LRG1 MMP8 IL1R2 CXCR2 TARM1 LCN2 CCR1 CD33 SOCS3 IL1RN ADAM8 IL36G CLEC4E MCEMP1 FPR1 ARG2 LILRB4B HP LILRB4A RETNLG IFITM6 VCAN NGP GCNT2 IL1B CLEC4D ACOD1 CD300LF CHIL3 IL1RAP BST1 CCR2 ENTPD1 STFA2L1 CD14 IFITM1 TGFBI S100A8 SIRPB1A GPR35 ALAS1 PLET1 MYD88 CD244A TREM1 PLA2G7 TLR2 MT1 IFITM2 TRPM2 EMB CSF2RA IER3 HMOX1 SLC2A1 SLC15A3 TLR13 FPR2 FOSL2 S100A9 TRIM30B CSF3R NLRP12 PLIN2 UPP1 DUSP1 APP CSTDC4 OSM MAFB MSRA OLFM4 WFDC17 WFDC21 BLK CD79B ETS1 TRIM7 CD83 PRG4 MZB1 CXCR5 CD55 MS4A1 H2-QA LY6D POU2AF1 CH3L1
logFC
-2
+2
B
Chemotaxis regulation
FN1
CXCR4
STAP1
C-X-C motif chemokine 12 receptor activity
logFC
-2
+2

Figure 4. Gene ontology chord diagram illustrating core genes of significant pathways in **(A)** female and **(B)** male MCAO+Recan mice. Significant pathways are displayed on the right, while core genes are shown on the left, with their log fold change (logFC) represented by colored squares. Connections from left to right indicate gene membership within a pathway's leading-edge subset. The gost() function was employed to analyze gene ontology using gene identifiers from the differential expression results. The analysis was conducted for Mus musculus, with parameters set to evcodes=TRUE and significant=TRUE (p-value ≤ 0.05) to highlight relevant pathways and genes.

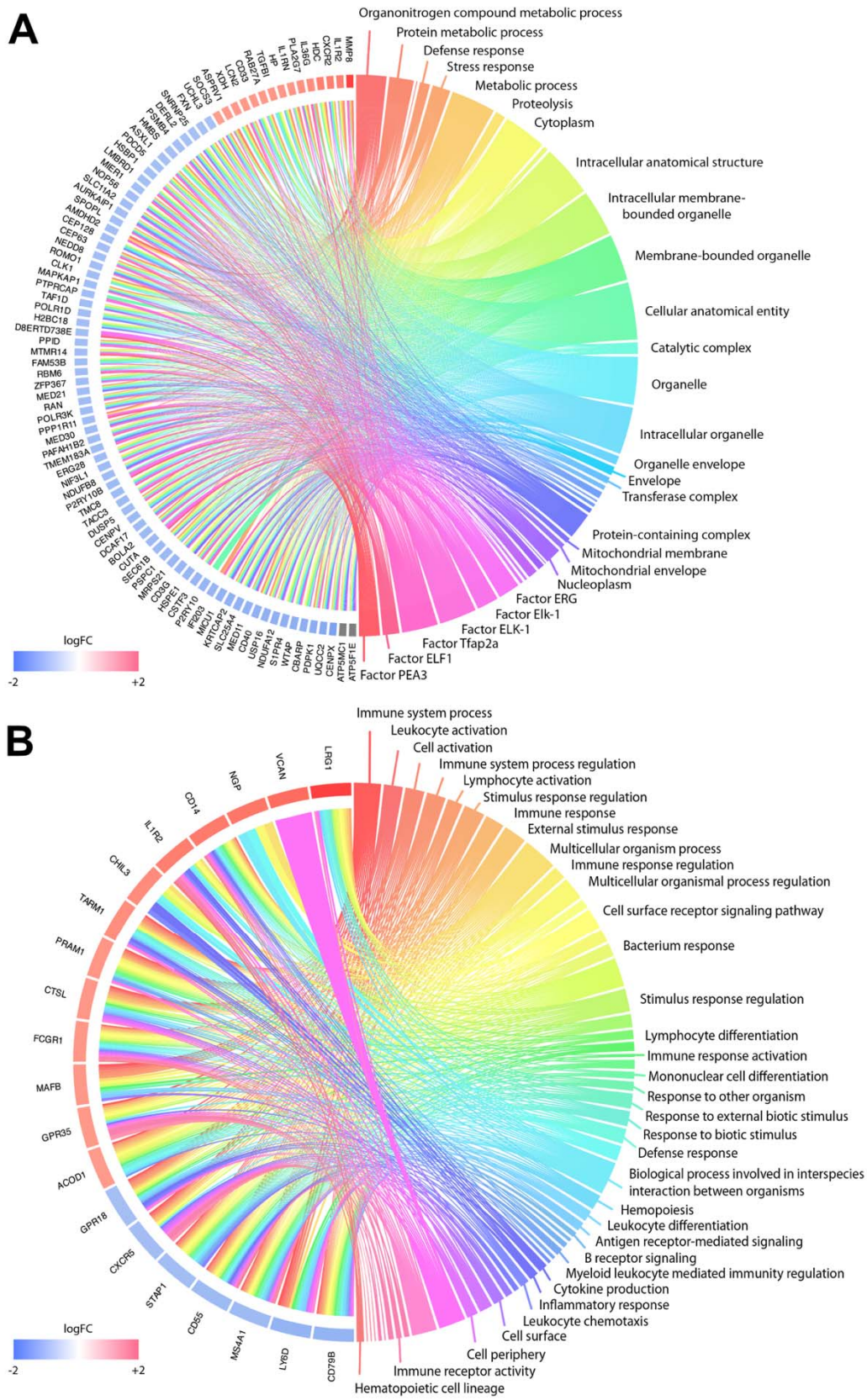
A
Organonitrogen compound metabolic process
Protein metabolic process
Defense response
Stress response
Metabolic process
Proteolysis
Cytoplasm
Intracellular anatomical structure
Intracellular membrane-bounded organelle
Membrane-bounded organelle
Cellular anatomical entity
Catalytic complex
Organelle
Intracellular organelle
Organelle envelope
Envelope
Transferase complex
Protein-containing complex
Mitochondrial membrane
Mitochondrial envelope
Nucleoplasm
Factor ERG
Factor Elk-1
Factor ELK-1
Factor Tfap2a
Factor ELF1
Factor PEA3
logFC
-2
+2
B
Immune system process
Leukocyte activation
Cell activation
Immune system process regulation
Lymphocyte activation
Stimulus response regulation
Immune response
External stimulus response
Multicellular organism process
Immune response regulation
Multicellular organismal process regulation
Cell surface receptor signaling pathway
Bacterium response
Stimulus response regulation
Lymphocyte differentiation
Immune response activation
Mononuclear cell differentiation
Response to other organism
Response to external biotic stimulus
Response to biotic stimulus
Defense response
Biological process involved in interspecies interaction between organisms
Hemopoiesis
Leukocyte differentiation
Antigen receptor-mediated signaling
B receptor signaling
Myeloid leukocyte mediated immunity regulation
Cytokine production
Inflammatory response
Leukocyte chemotaxis
Cell surface
Cell periphery
Immune receptor activity
Hematopoietic cell lineage
LRG1
VCAN
NGP
CD14
IL1R2
CHIL3
TARM1
PRAM1
CTSL
FCGR1
MAFB
GPR35
ACOD1
GPR18
CXCR5
STAP1
CD55
MS4A1
LY6D
CD79B
logFC
-2
+2

Figure 5. Gene ontology chord diagram showing core genes and significant pathways in **(A)** young and **(B)** aged MCAO+Recan mice. The diagram visualizes significant pathways on the right and their corresponding core genes on the left, with log fold change (logFC) indicated by coloured squares. Connections between the left (genes) and right (pathways) represent gene membership in a pathway's leading-edge subset. The gost() function was used to analyze gene ontology, utilizing gene identifiers from differential expression results. The analysis was conducted with Mus musculus as the organism, specifying evcodes=TRUE and significant=TRUE (p-value ≤ 0.05) to highlight relevant pathways and genes.

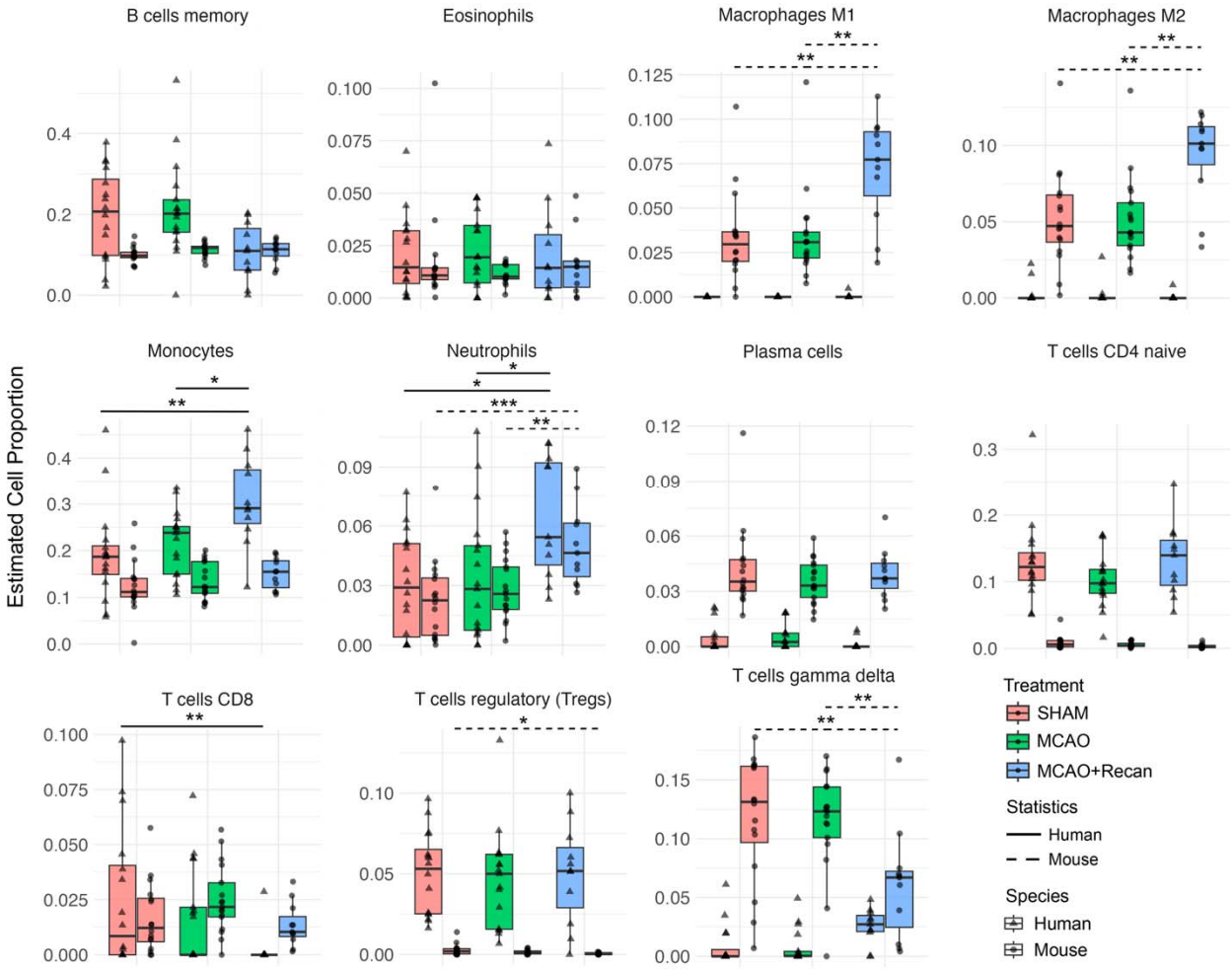

Figure 6. Relative immune cell proportions of cell types shared between immuCellAI-mouse (mouse reference database) and CIBERSORTx (human reference database) stratified by treatment. Results were obtained from immuCellAI-mouse and CIBERSORTx generated from microarray matrix. Statistical comparisons were performed using the Kruskal-Wallis, with p-

values adjusted using the Benjamini-Hochberg method for multiple comparisons. Dunnett's post-hoc pairwise multiple comparison was also performed (*$p \leq 0.05$, **$p \leq 0.01$, ***$p \leq 0.001$).

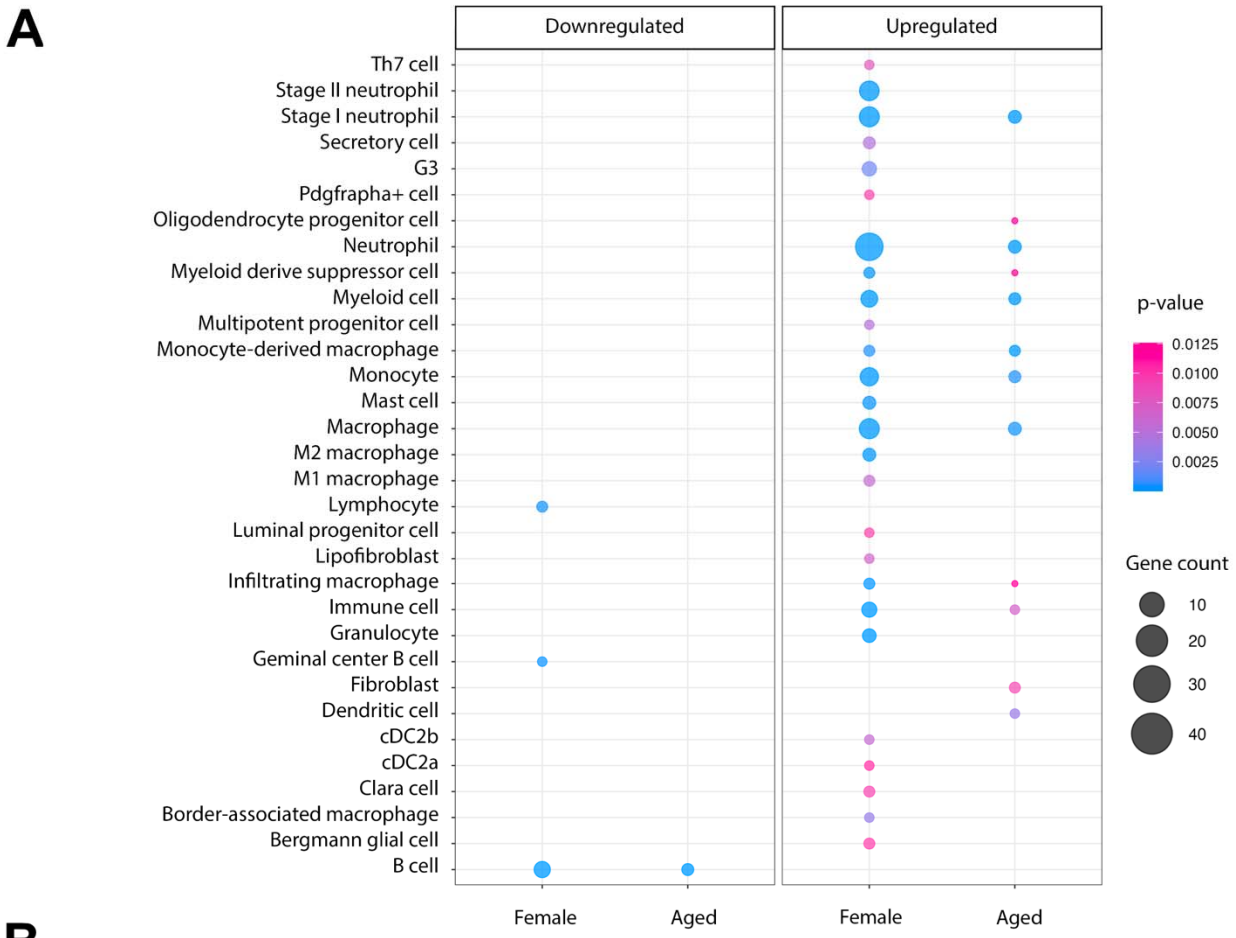
A
Downregulated
Upregulated
Th7 cell
Stage II neutrophil
Stage I neutrophil
Secretory cell
G3
Pdgfrapha+ cell
Oligodendrocyte progenitor cell
Neutrophil
Myeloid derive suppressor cell
Myeloid cell
Multipotent progenitor cell
Monocyte-derived macrophage
Monocyte
Mast cell
Macrophage
M2 macrophage
M1 macrophage
Lymphocyte
Luminal progenitor cell
Lipofibroblast
Infiltrating macrophage
Immune cell
Granulocyte
Geminal center B cell
Fibroblast
Dendritic cell
cDC2b
cDC2a
Clara cell
Border-associated macrophage
Bergmann glial cell
B cell
Female
Aged
Female
Aged
p-value
0.0125
0.0100
0.0075
0.0050
0.0025
Gene count
10
20
30
40

B
neutrophil migration regulation
myeloid leukocyte mediated immunity regulation
leukocyte proliferation regulation
leukocyte migration regulation
leukocyte chemotaxis regulation
leukocyte cell-cell adhsion regulation
leukocyte activation regulation
positive leukocyte migration regulation
positive leukocyte chemotaxis regulation
positive leukocyte cell-cell adhesion regulation
positive leukocyte activation regulation
neutrophil migration
neutrophil degranulation
neutrophil chemotaxis
myeloid leukocyte migration
myeloid leukocyte differentiation
myeloid leukocyte activation
leukocyte proliferation
leukocyte migration
leukocyte differentiation
leukocyte chemotaxis
leukocyte cell-cell adhesion
leukocyte aggregation
leukocyte activation
Female
Male
Aged
Young
p-value
0.04
0.03
0.02
0.01
Gene count
0
10
20

Figure 7 (A) Over-representation of cell markers from MCAO+Recan differentially expressed genes (DEGs). The Cell Marker 2.0 database and the clusterProfiler package were used to infer the cell types in which the identified DEGs might be expressed. The dot plot shows upregulated and downregulated DEGs mapped to specific cell types. **(B)** Enrichment of leukocyte and neutrophil activities in female and aged MCAO+Recan mice. Gene enrichment analysis was conducted using the gProfiler package. The enrichplot::dotplot function was used to visualize enriched pathways, with colour intensity indicating the significance of enrichment and dot size representing the gene count for MCAO+Recan samples. These highlight the significant involvement of leukocyte and neutrophil activities in the ischemic stroke model.

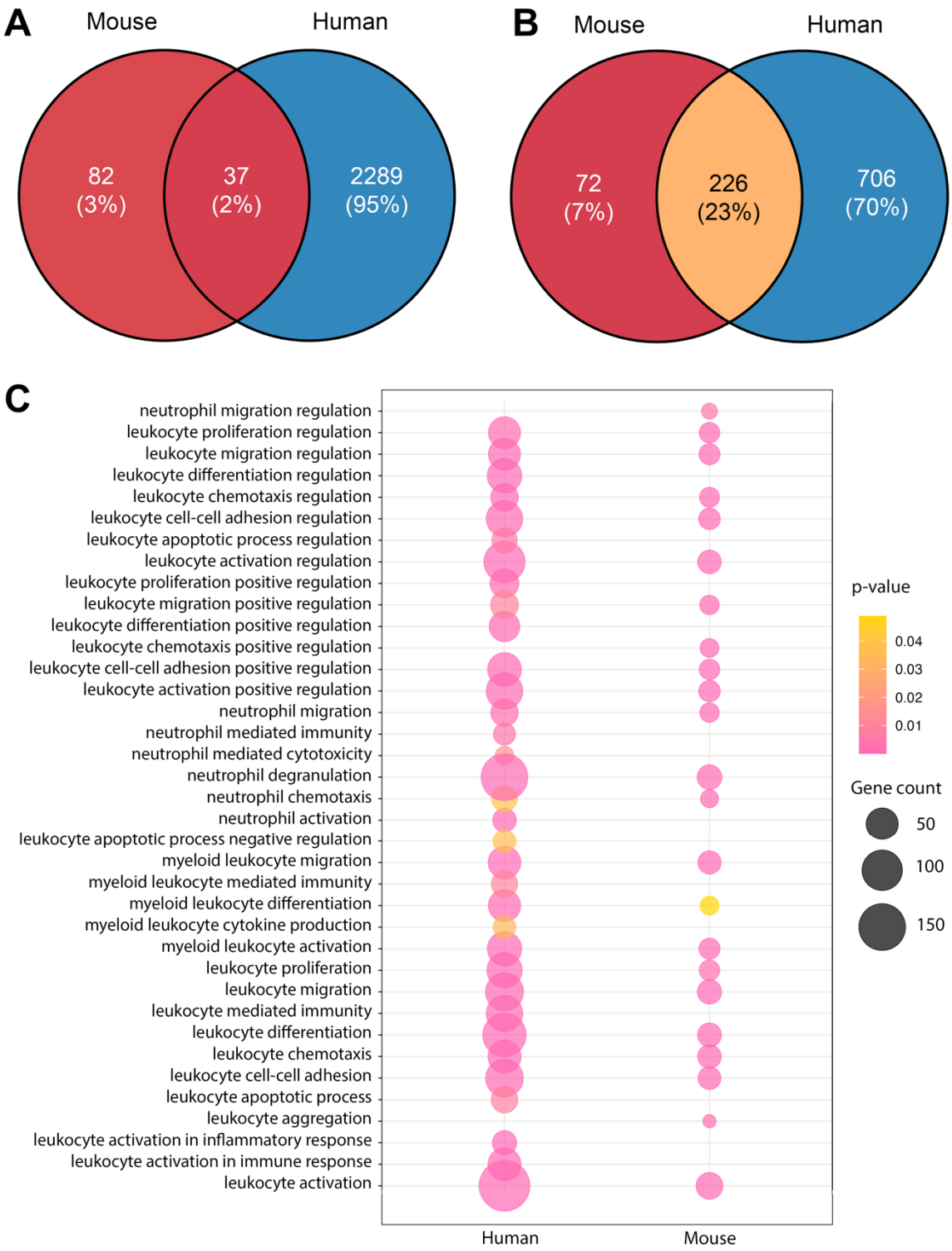

Figure 8 (A) Orthologue differentially expressed genes (DEGs) shared between MCAO+Recan female mice and clinical female patients. DEGs were identified in mouse and human datasets using the limma package ($|\log_2 FC| \geq 1.5$, p-value ≤ 0.05). The analysis highlights the common transcriptional responses to ischemic stroke and reperfusion (MCAO+Recan) across species. **(B)**

Shared gene ontology (GO) terms and KEGG pathways between MCAO+Recan mice and clinical patients. Functional enrichment analyses were performed using the gProfiler package to identify overlapping biological processes and pathways. Key shared pathways related to stroke, inflammation, and immune responses were identified, showing conserved functional responses across the species. **(C)** Conservation of leukocyte- and neutrophil-based pathways in human and mouse samples. Pathways related to leukocyte and neutrophil activity were conserved between human clinical patients and MCAO+Recan mice.

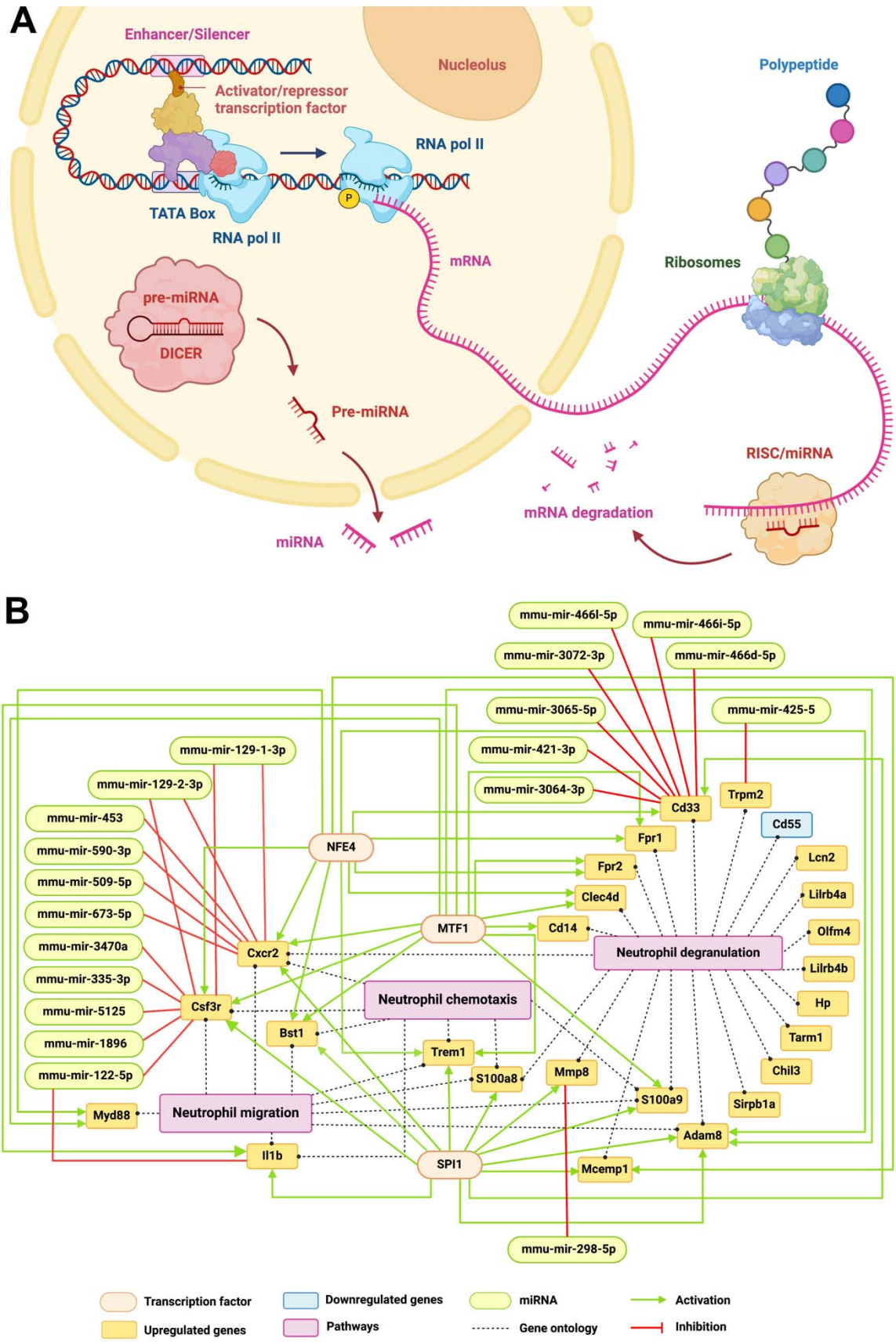
A
Enhancer/Silencer
Nucleolus
Polypeptide
Activator/repressor transcription factor
RNA pol II
TATA Box
RNA pol II
P
mRNA
Ribosomes
pre-miRNA
DICER
Pre-miRNA
RISC/miRNA
mRNA degradation
miRNA
B
mmu-mir-466l-5p
mmu-mir-466i-5p
mmu-mir-3072-3p
mmu-mir-466d-5p
mmu-mir-3065-5p
mmu-mir-425-5
mmu-mir-129-1-3p
mmu-mir-421-3p
mmu-mir-129-2-3p
mmu-mir-3064-3p
Trpm2
mmu-mir-453
Cd33
Cd55
mmu-mir-590-3p
NFE4
Fpr1
Lcn2
mmu-mir-509-5p
Fpr2
Lilrb4a
mmu-mir-673-5p
Clec4d
mmu-mir-3470a
MTF1
Cd14
Olfm4
Cxcr2
Neutrophil degranulation
mmu-mir-335-3p
Lilrb4b
mmu-mir-5125
Csf3r
Neutrophil chemotaxis
Hp
Bst1
mmu-mir-1896
Tarm1
Trem1
mmu-mir-122-5p
Chil3
S100a8
Mmp8
S100a9
Sirpb1a
Myd88
Neutrophil migration
Adam8
Il1b
SPI1
Mcemp1
mmu-mir-298-5p
Transcription factor
Downregulated genes
miRNA
Activation
Upregulated genes
Pathways
Gene ontology
Inhibition

Figure 9. (A) Transcriptional regulation by transcription factors (TFs) and miRNAs. mRNA is transcribed from DNA in the nucleus by the DNA polymerase II complex, a process regulated by TFs, which can act as activators or repressors. TFs bind to specific DNA regions, either enhancers or silencers, to increase or decrease gene transcription. In the cytoplasm, pre-miRNAs mature into miRNAs, which can cleave mRNA strands, destabilize mRNA, or inhibit translation. **(B)** Neutrophil signalling network. The neutrophil signalling network was generated using integrated results from gProfiler enrichment, NetworkAnalyst, and ChEA3 analyses. One TF can regulate several genes, and multiple TFs may regulate a single gene. Similarly, multiple miRNAs can regulate one gene, and each miRNA can target more than one gene. Graphs were created with BioRender.

Supplemental Material

Supplementary Table 1-3

Supplementary Figure 1-7

Supplementary Table 1. Differential gene expression and multivariate analysis results of MCAO, MCAO+Recan, Recan (MCAO+Recan vs. MCAO) ($|\log_2 FC| \geq 1.5$, p-value ≤ 0.05), Sex × MCAO+Recan interactions, and Age × MCAO+Recan interactions ($|\log_2 FC| \geq 1.5$, FDR ≤ 0.05). All analyses were performed using limma package in R Bioconductor.

Supplementary Table 2. Enrichment analysis gProfiler results for MCAO, MCAO+Recan, and Recan (MCAO+Recan vs. MCAO) groups. Columns include the group name, pathway category, term ID, description of the biological process, adjusted p-value (p.adjust), query size, count of genes in each pathway, total pathway size, effective domain size, and the list of associated genes (geneID). The gene ratio represents the proportion of query genes in the pathway, while the background ratio (BgRatio) represents the term size relative to the total background gene set.

Supplementary Table 3. The ARRIVE Guidelines 2.0: updated guidelines for reporting animal research. Form was obtained from https://www.goodreports.org/reporting-checklists/arrive2/ (28).

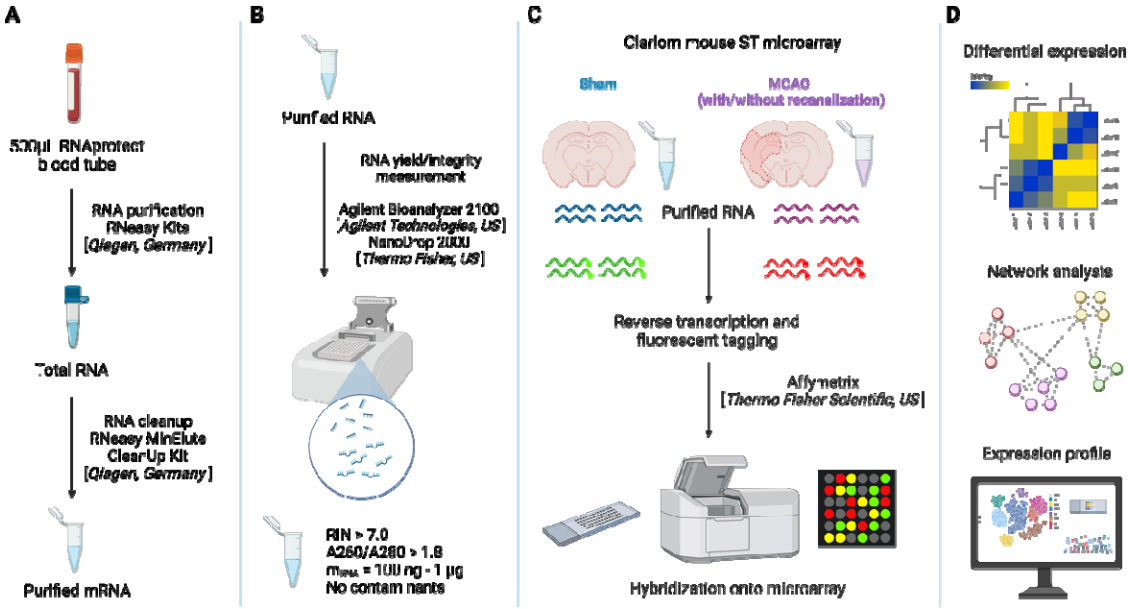

Supplementary Figure 1. Overview of RNA purification and microarray analysis procedures. **(A)** Sample collection and RNA extraction. Whole blood samples were obtained via retro-orbital sampling following sham and MCAO surgeries. Total RNA was extracted and purified using standardized QIAGEN protocols to ensure high-quality RNA for downstream analyses. **(B)** RNA selection for quality control. RNA samples were rigorously evaluated for yield and purity to ensure that only high-quality samples were used for microarray analysis. Stringent quality control measures were applied to select samples with optimal RNA integrity. **(C)** Microarray analysis using Affymetrix technology. Selected RNA samples were processed and analyzed on Affymetrix microarrays to generate comprehensive gene expression profiles. **(D)** Data normalization and differential expression analysis. Raw CEL files generated from the Affymetrix platform were normalized using robust statistical methods, followed by differential gene expression analysis with the limma package in RStudio. Enrichment analysis was performed using the gProfiler tool to identify biologically significant pathways enriched among the differentially expressed genes. These enriched pathways were subsequently visualized and interpreted using RStudio and Cytoscape to explore the molecular mechanisms underlying the gene expression changes.

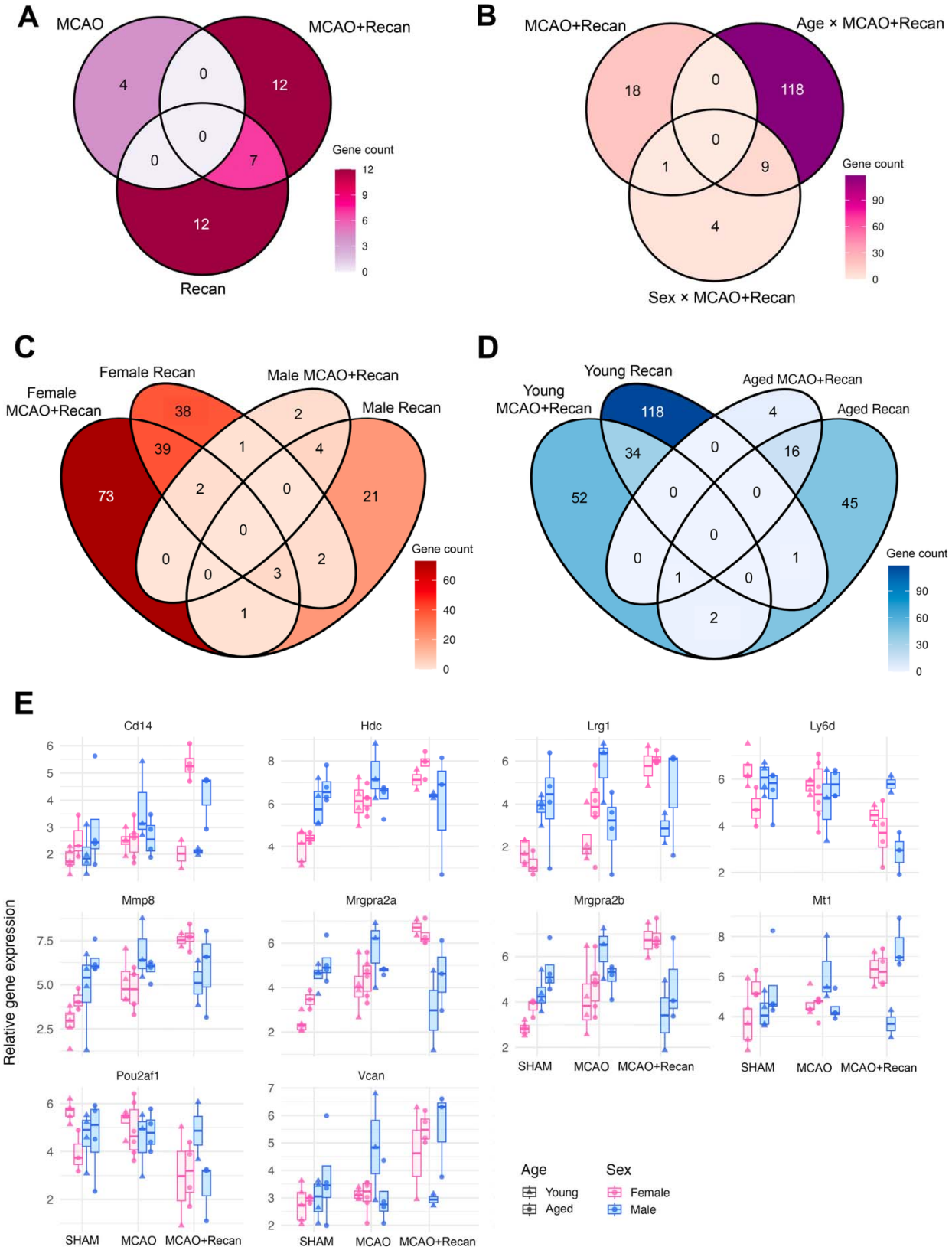
A
MCAO
MCAO+Recan
Recan
4
0
12
0
0
7
12
Gene count
12
9
6
3
0
B
MCAO+Recan
Age × MCAO+Recan
Sex × MCAO+Recan
18
0
118
0
1
9
4
Gene count
90
60
30
0
C
Female MCAO+Recan
Female Recan
Male MCAO+Recan
Male Recan
73
38
2
21
39
1
4
2
0
0
0
3
2
1
Gene count
60
40
20
0
D
Young MCAO+Recan
Young Recan
Aged MCAO+Recan
Aged Recan
52
118
4
45
34
0
16
0
0
0
1
0
1
2
Gene count
90
60
30
0
E
Cd14
Hdc
Lrg1
Ly6d
Mmp8
Mrgpra2a
Mrgpra2b
Mt1
Pou2af1
Vcan
Relative gene expression
SHAM
MCAO
MCAO+Recan
Age
Young
Aged
Sex
Female
Male

Supplementary Figure 2. (A) Venn diagram showing the overlap of DEGs between MCAO, MCAO+Recan, and Recan groups (|log2FC| ≥ 1.5, p-value ≤ 0.05). **(B)** Venn diagram showing the overlap of DEGs between MCAO+Recan, Sex × Treatment and Age × Treatment interactions groups (|log2FC| ≥ 1.5, p-value ≤ 0.05). **(C)** Venn diagram showing the overlap of DEGs between sex-specific MCAO+Recan and Recan groups (|log2FC| ≥ 1.5, p-value ≤ 0.05). **(D)** Venn diagram showing the overlap of DEGs between age-specific MCAO+Recan and Recan groups (|log2FC| ≥ 1.5, p-value ≤ 0.05). All analyses were performed using limma package in R Bioconductor. **(E)** Sex- and age-specific expression patterns of differentially expressed genes in MCAO+Recan group: *Cd14*, *Mmp8*, *Hdc*, *Lrg1*, *Ly6d*, *Mrgpra2a***,** *Mrgpra2b*, *Vcan*, *Mt1*, and *Pou2af1* determined by two-way interactions of Sex × Treatment and Age × Treatment multivariate analysis built-in in limma package (|$\log_2$FC| ≥ 1.5, p ≤ 0.05).

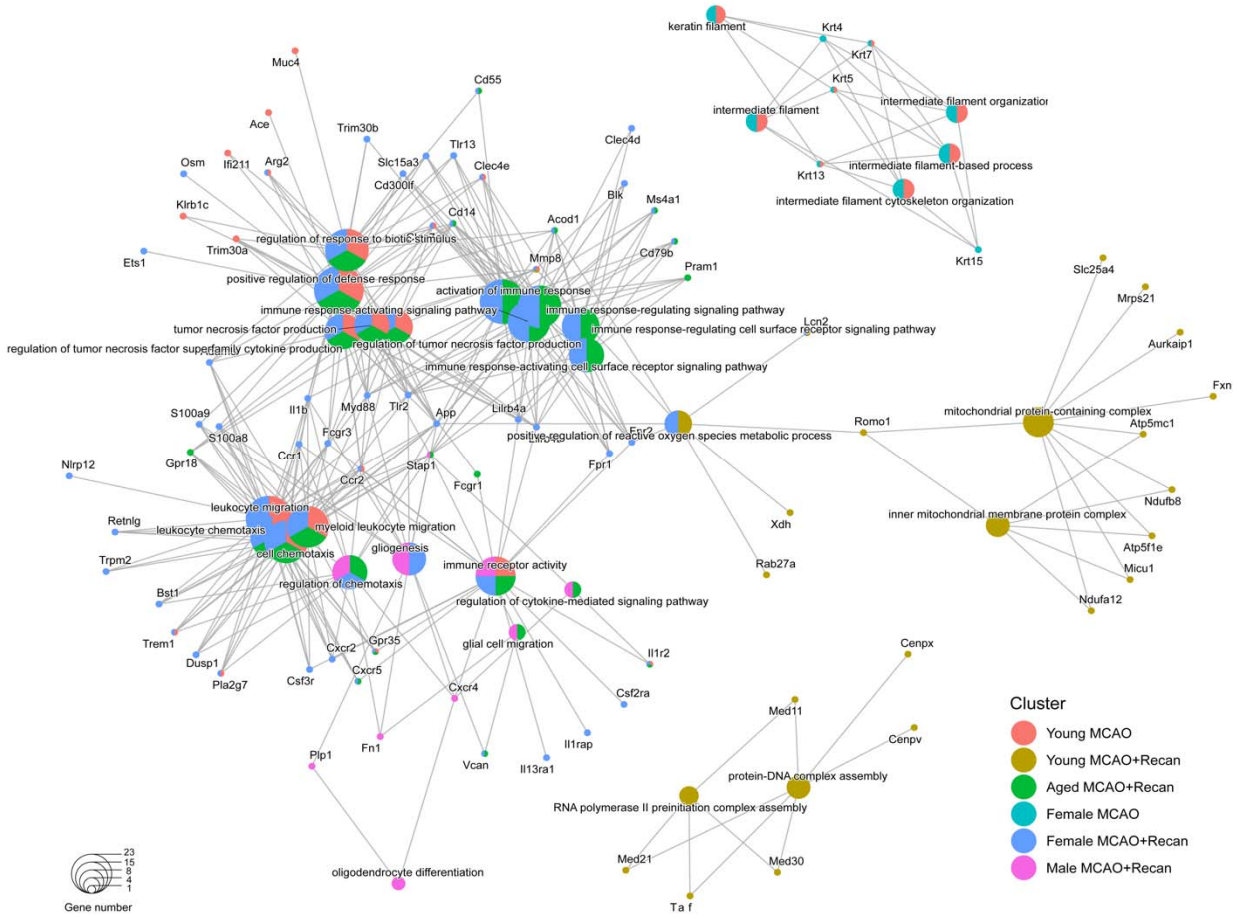

Supplementary Figure 3. *cnet* plot showing gene overlaps in enriched gene sets. Enrichment analysis was performed using the *clusterProfiler* R package and *cnetplot()* function, with the

Gene Ontology (GO) biological processes as the reference database. The plot visualizes the relationships between significantly enriched gene sets and their associated genes. Each node represents either a gene (small circles) or a gene set/pathway (larger colored circles). Edges indicate that a gene is part of a particular gene set. The size of each gene set node reflect the gene number.

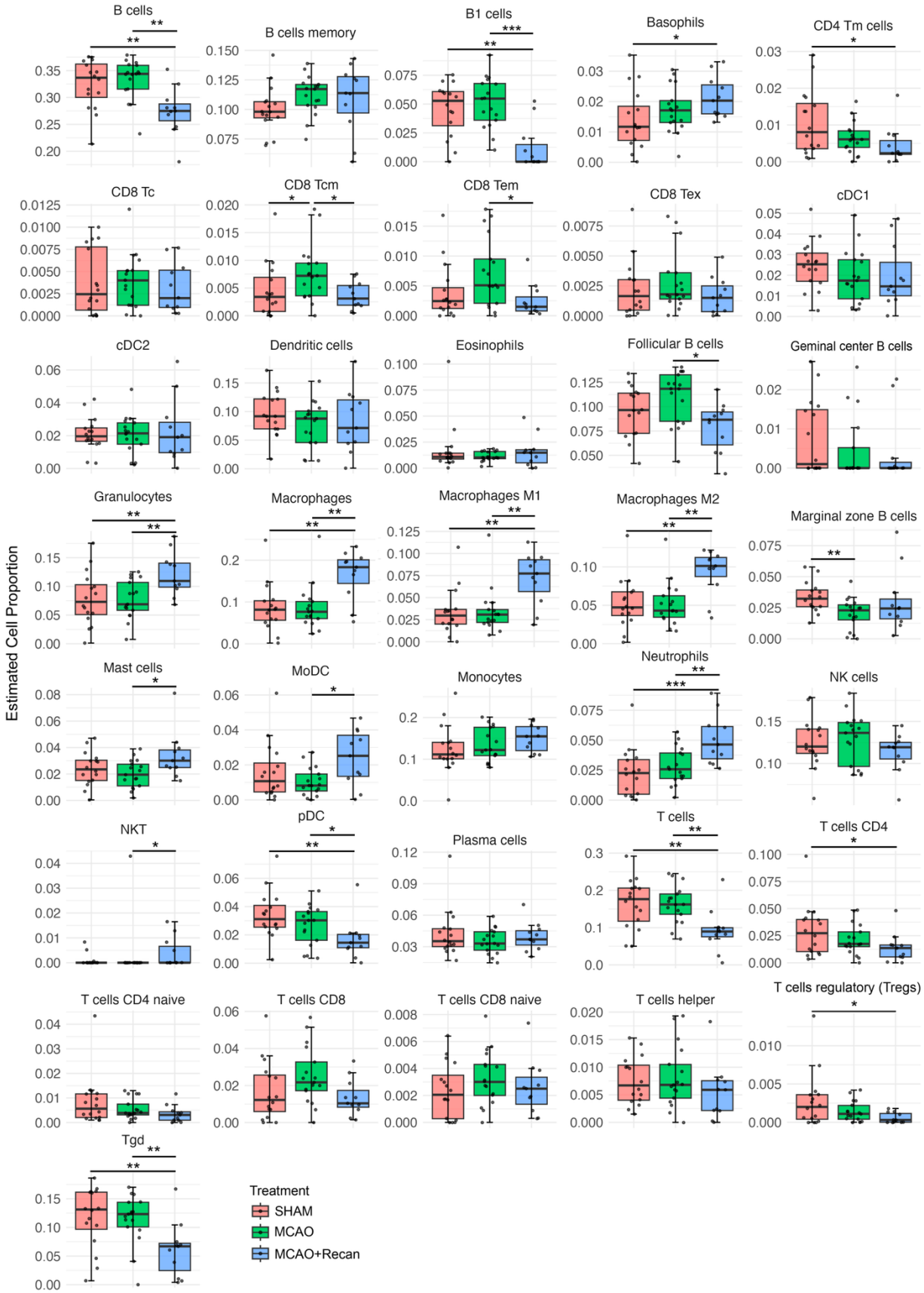
B cells
B cells memory
B1 cells
Basophils
CD4 Tm cells
CD8 Tc
CD8 Tcm
CD8 Tem
CD8 Tex
cDC1
cDC2
Dendritic cells
Eosinophils
Follicular B cells
Geminal center B cells
Granulocytes
Macrophages
Macrophages M1
Macrophages M2
Marginal zone B cells
Mast cells
MoDC
Monocytes
Neutrophils
NK cells
NKT
pDC
Plasma cells
T cells
T cells CD4
T cells CD4 naive
T cells CD8
T cells CD8 naive
T cells helper
T cells regulatory (Tregs)
Tgd
Estimated Cell Proportion
Treatment
SHAM
MCAO
MCAO+Recan

Supplementary Figure 4. Relative immune cell proportions of 36 immune cell types estimated by ImmunCellAI-mouse, stratified by treatment group. Box plots display the estimated proportions of immune cell types. Statistical comparisons were performed using the Kruskal-Wallis, with p-values adjusted using the Benjamini-Hochberg method for multiple comparisons. Dunnett's post-hoc pairwise multiple comparison was also performed (*$p \leq 0.05$, **$p \leq 0.01$, ***$p \leq 0.001$).

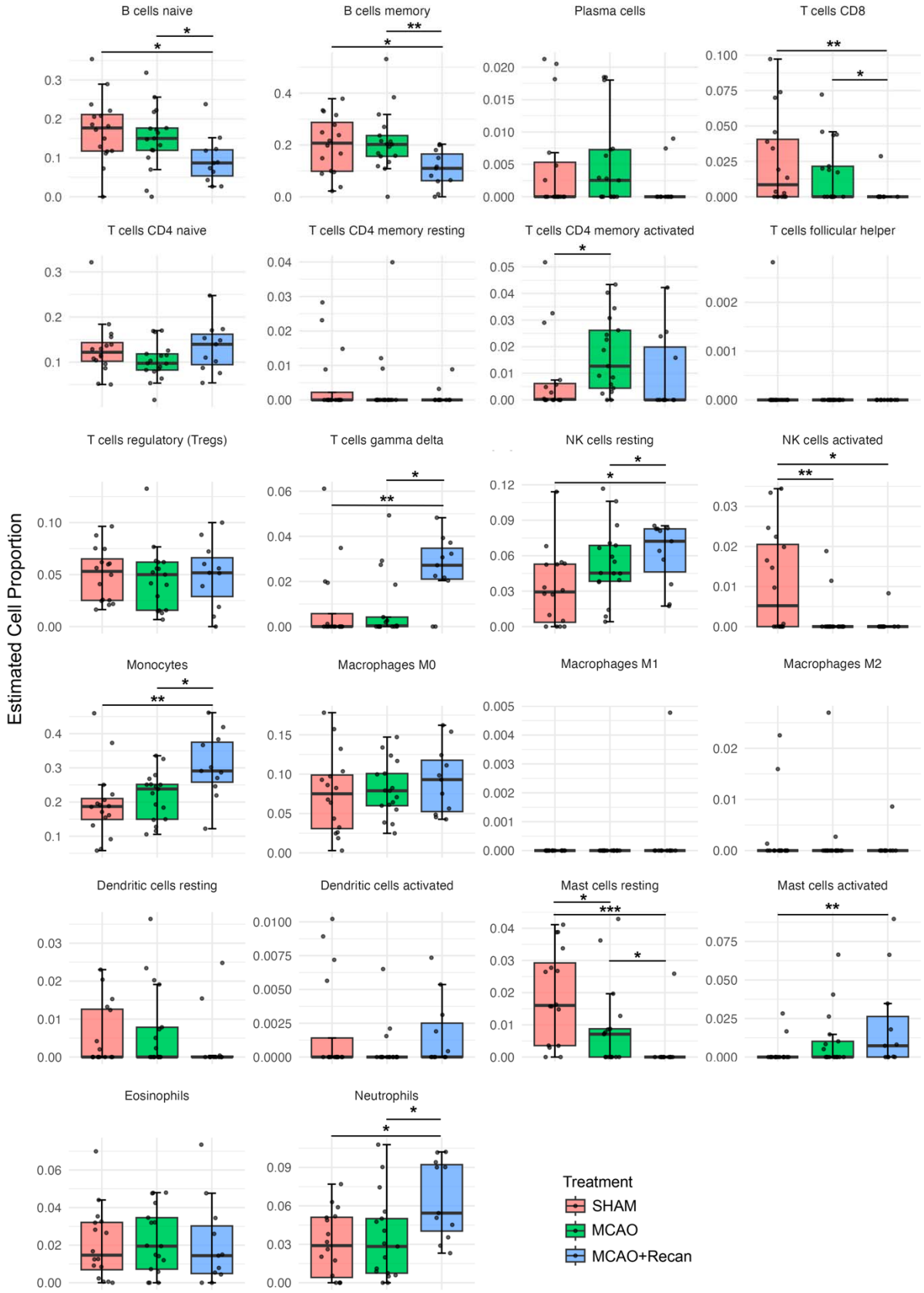
B cells naive
B cells memory
Plasma cells
T cells CD8
T cells CD4 naive
T cells CD4 memory resting
T cells CD4 memory activated
T cells follicular helper
T cells regulatory (Tregs)
T cells gamma delta
NK cells resting
NK cells activated
Monocytes
Macrophages M0
Macrophages M1
Macrophages M2
Dendritic cells resting
Dendritic cells activated
Mast cells resting
Mast cells activated
Eosinophils
Neutrophils
Estimated Cell Proportion
Treatment
SHAM
MCAO
MCAO+Recan

Supplementary Figure 5. Relative immune cell proportions of 22 immune cells estimated by CIBERSORT, stratified by treatment group. Box plots display the estimated proportions of immune cell types inferred using the CIBERSORT algorithm based on bulk RNA-sequencing data and LM22 human reference signature matrix. Statistical comparisons were performed using the Kruskal-Wallis, with p-values adjusted using the Benjamini-Hochberg method for multiple comparisons. Dunnett's post-hoc pairwise multiple comparison was also performed (*$p \leq 0.05$, **$p \leq 0.01$, ***$p \leq 0.001$).

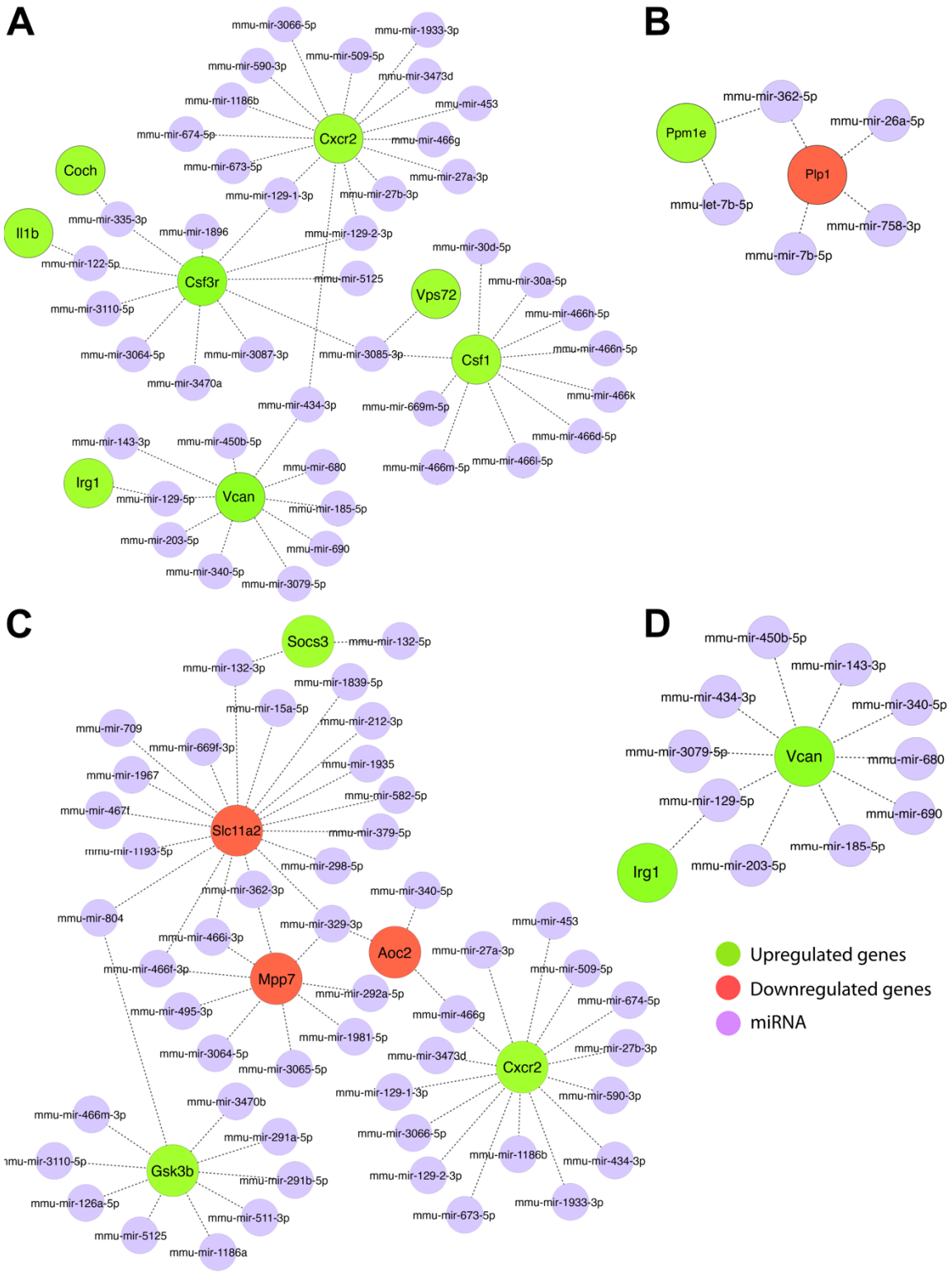

Supplementary Figure 6. miRNA-mRNA interactions in **(A)** female, **(B)** male, **(C)** young, and aged MCAO+Recan animals from NetworkAnalyst generated from lists of DEGs. One gene may be regulated by multiple miRNAs, and each miRNA can target more than one gene.

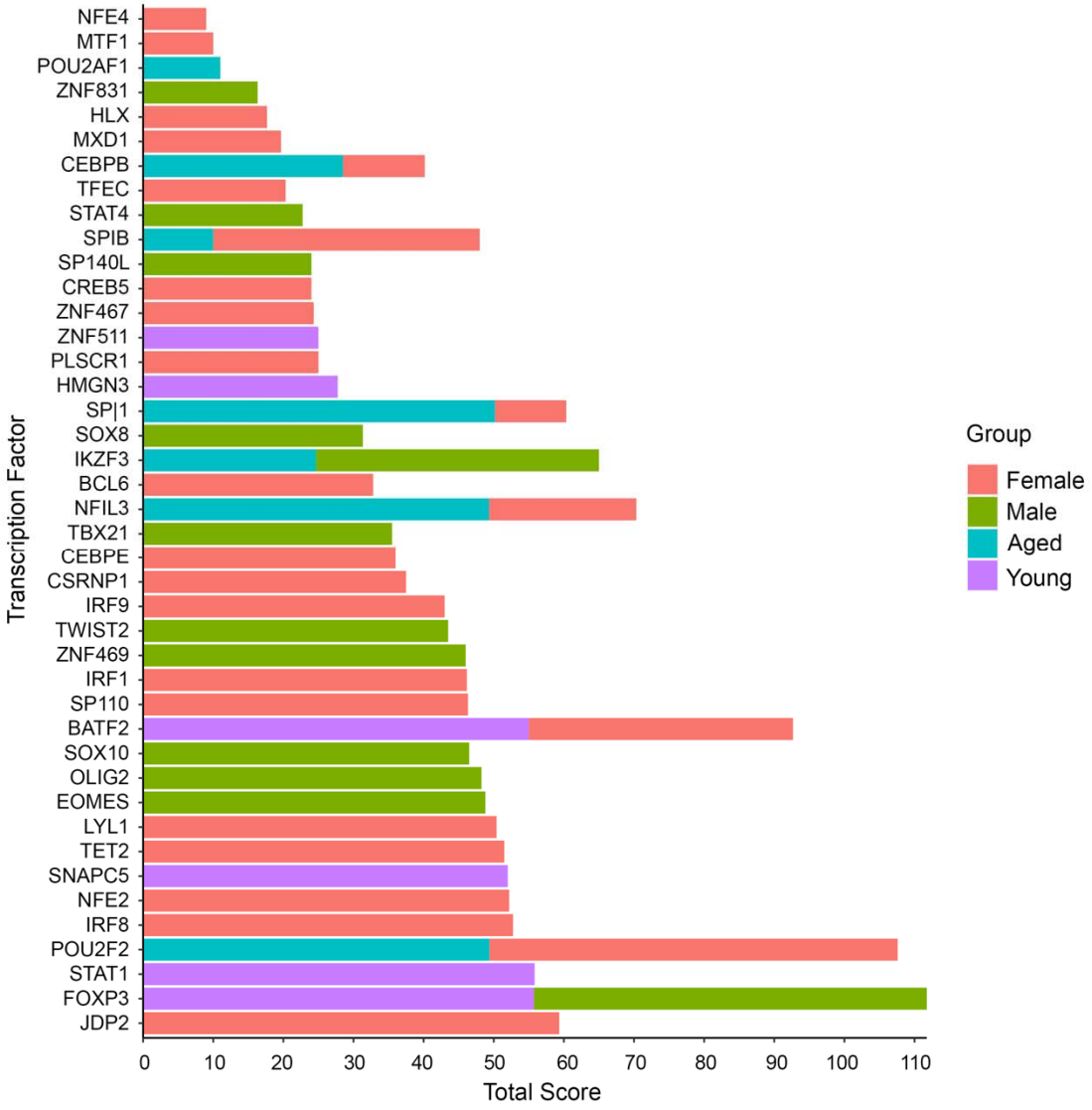

Supplementary Figure 7. Top 50 TFs identified by ChEA3. ChEA3 was used to predict TFs-mRNA regulatory network. Lists of DEGs of MCAO+Recan were submitted to the ChEA3 platform, and the top 50 TFs (organized by rank) were exported. One TF can regulate several genes, and multiple TFs may regulate one gene.

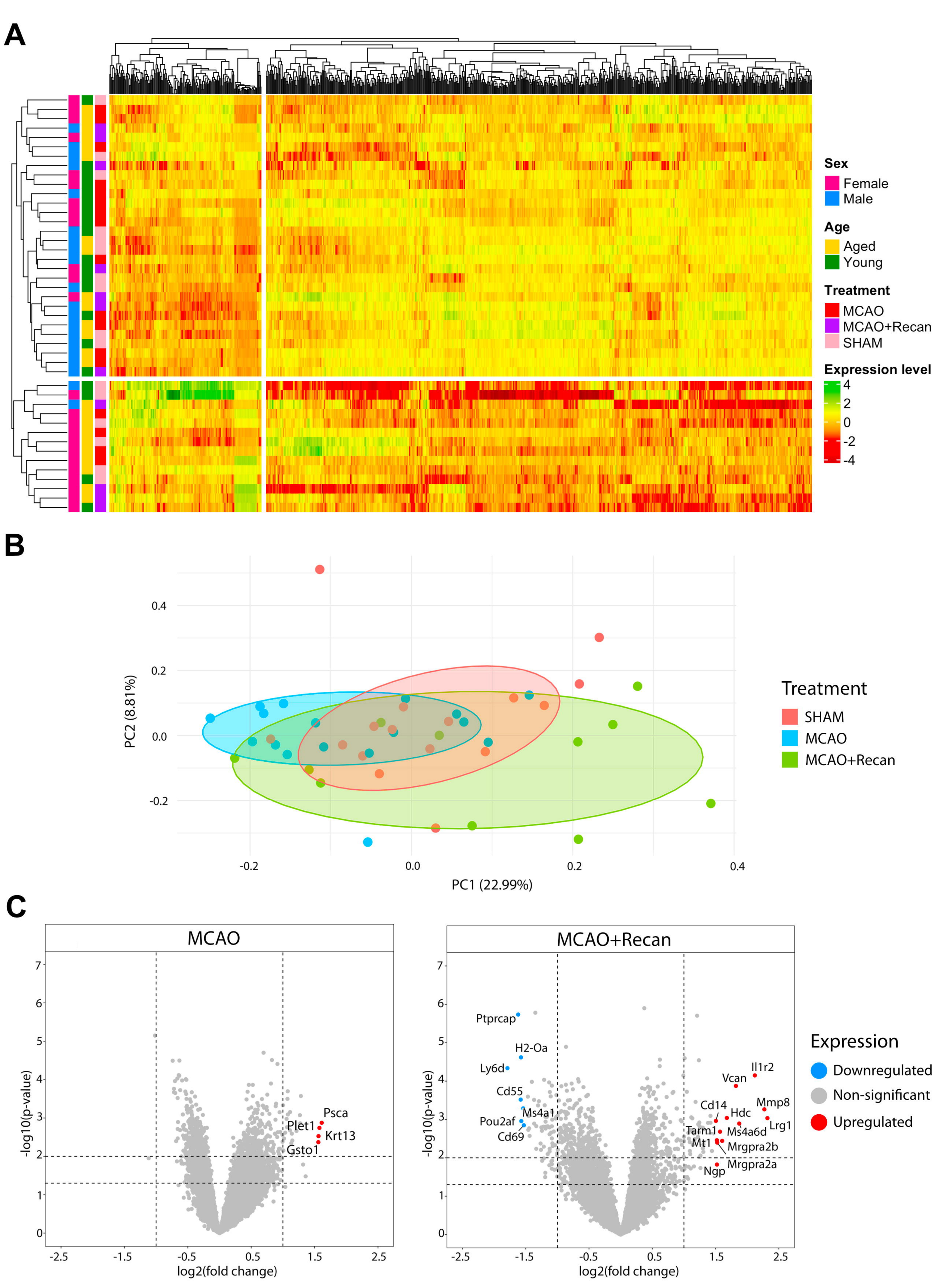
A
Sex
Female
Male
Age
Aged
Young
Treatment
MCAO
MCAO+Recan
SHAM
Expression level
4
2
0
-2
-4
B
PC2 (8.81%)
PC1 (22.99%)
Treatment
SHAM
MCAO
MCAO+Recan
C
MCAO
MCAO+Recan
-log10(p-value)
log2(fold change)
Psca
Plet1
Krt13
Gsto1
Ptprcap
H2-Oa
Ly6d
Cd55
Ms4a1
Pou2af
Cd69
Il1r2
Vcan
Cd14
Hdc
Mmp8
Lrg1
Tarm1
Ms4a6d
Mt1
Mrgpra2b
Mrgpra2a
Ngp
Expression
Downregulated
Non-significant
Upregulated

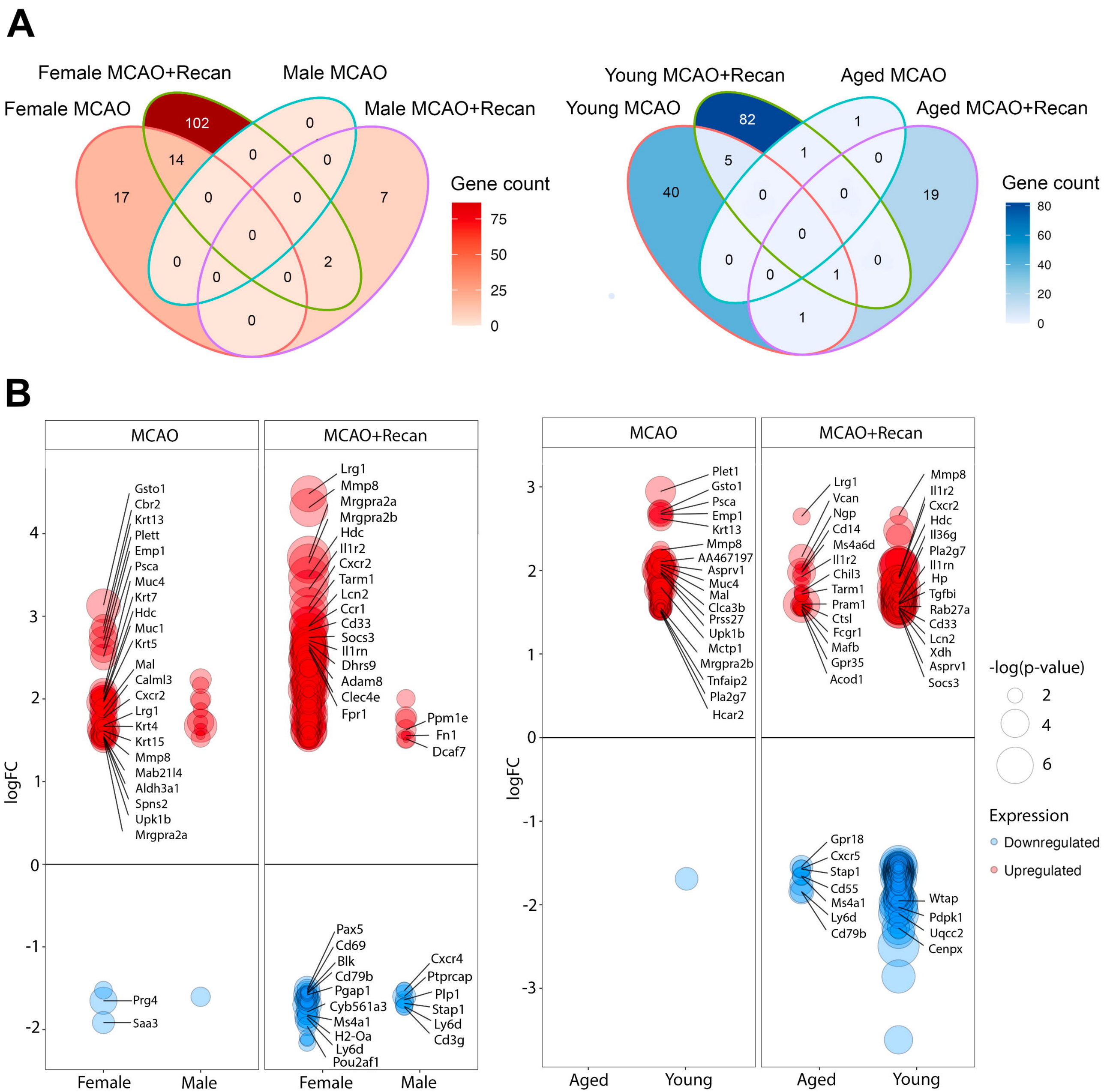
A
Female MCAO+Recan
Male MCAO
Female MCAO
Male MCAO+Recan
102
0
14
0
0
17
0
0
7
0
0
2
0
0
0
Gene count
75
50
25
0
Young MCAO+Recan
Aged MCAO
Young MCAO
Aged MCAO+Recan
82
1
5
1
0
40
0
0
19
0
0
0
0
1
1
Gene count
80
60
40
20
0
B
MCAO
MCAO+Recan
logFC
Gsto1
Cbr2
Krt13
Plett
Emp1
Psca
Muc4
Krt7
Hdc
Muc1
Krt5
Mal
Calml3
Cxcr2
Lrg1
Krt4
Krt15
Mmp8
Mab21l4
Aldh3a1
Spns2
Upk1b
Mrgpra2a
Prg4
Saa3
Lrg1
Mmp8
Mrgpra2a
Mrgpra2b
Hdc
Il1r2
Cxcr2
Tarm1
Lcn2
Ccr1
Cd33
Socs3
Il1rn
Dhrs9
Adam8
Clec4e
Fpr1
Ppm1e
Fn1
Dcaf7
Pax5
Cd69
Blk
Cd79b
Pgap1
Cyb561a3
Ms4a1
H2-Oa
Ly6d
Pou2af1
Cxcr4
Ptprcap
Plp1
Stap1
Ly6d
Cd3g
Female
Male
Female
Male
MCAO
MCAO+Recan
logFC
Plet1
Gsto1
Psca
Emp1
Krt13
Mmp8
AA467197
Asprv1
Muc4
Mal
Clca3b
Prss27
Upk1b
Mctp1
Mrgpra2b
Tnfaip2
Pla2g7
Hcar2
Lrg1
Vcan
Ngp
Cd14
Ms4a6d
Il1r2
Chil3
Tarm1
Pram1
Ctsl
Fcgr1
Mafb
Gpr35
Acod1
Mmp8
Il1r2
Cxcr2
Hdc
Il36g
Pla2g7
Il1rn
Hp
Tgfbi
Rab27a
Cd33
Lcn2
Xdh
Asprv1
Socs3
Gpr18
Cxcr5
Stap1
Cd55
Ms4a1
Ly6d
Cd79b
Wtap
Pdpk1
Uqcc2
Cenpx
Aged
Young
Aged
Young
-log(p-value)
2
4
6
Expression
Downregulated
Upregulated

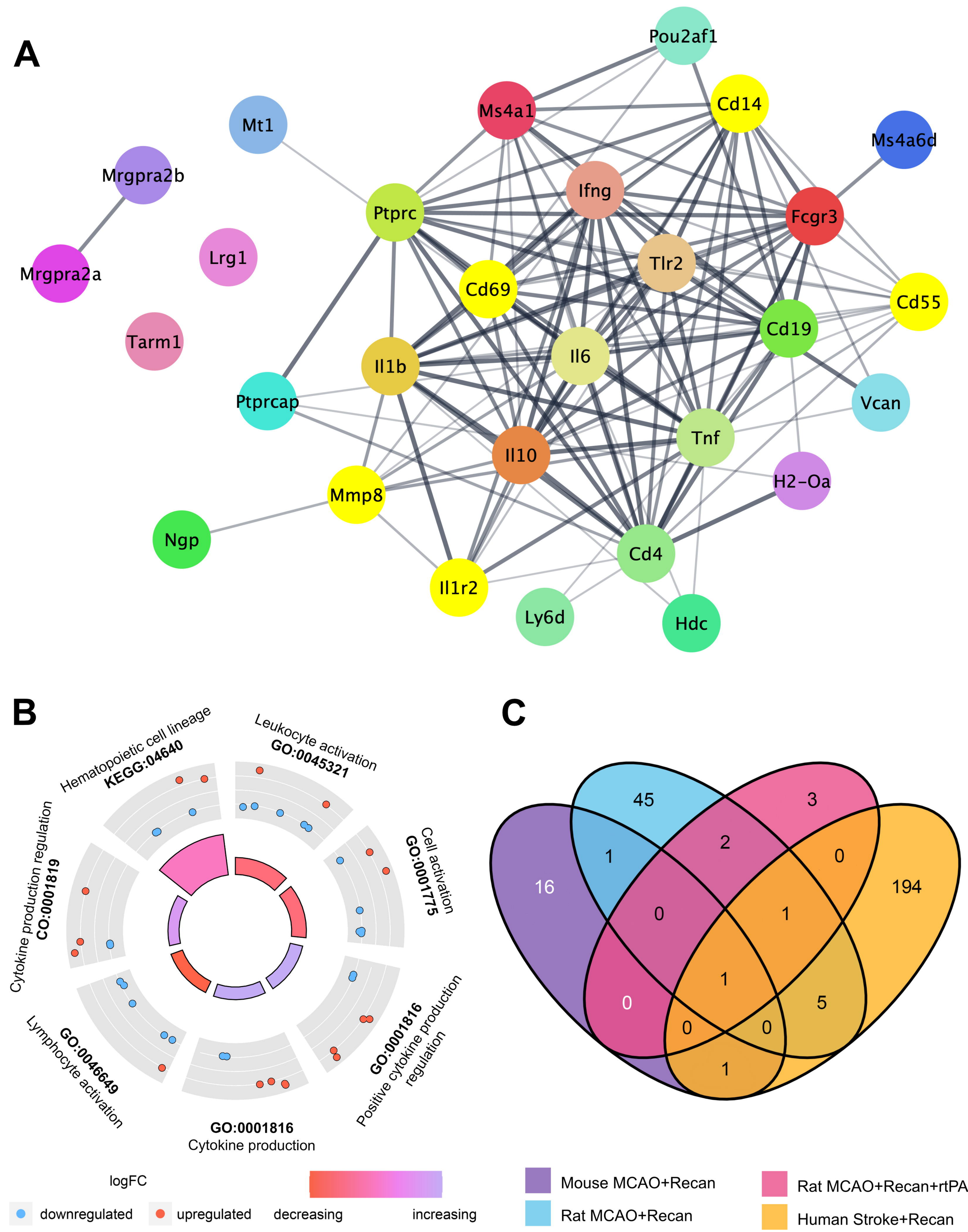
A
Pou2af1
Ms4a1
Cd14
Mt1
Ms4a6d
Mrgpra2b
Ifng
Ptprc
Fcgr3
Lrg1
Tlr2
Mrgpra2a
Cd69
Cd55
Cd19
Tarm1
Il6
Il1b
Ptprcap
Vcan
Tnf
Il10
H2-Oa
Mmp8
Ngp
Cd4
Il1r2
Ly6d
Hdc
B
Hematopoietic cell lineage
KEGG:04640
Leukocyte activation
GO:0045321
Cell activation
GO:0001775
GO:0001816
Positive cytokine production regulation
GO:0001816
Cytokine production
GO:0046649
Lymphocyte activation
Cytokine production regulation
CO:0001819
C
45
3
1
2
0
16
0
1
194
1
0
5
0
0
1
logFC
downregulated
upregulated
decreasing
increasing
Mouse MCAO+Recan
Rat MCAO+Recan
Rat MCAO+Recan+rtPA
Human Stroke+Recan

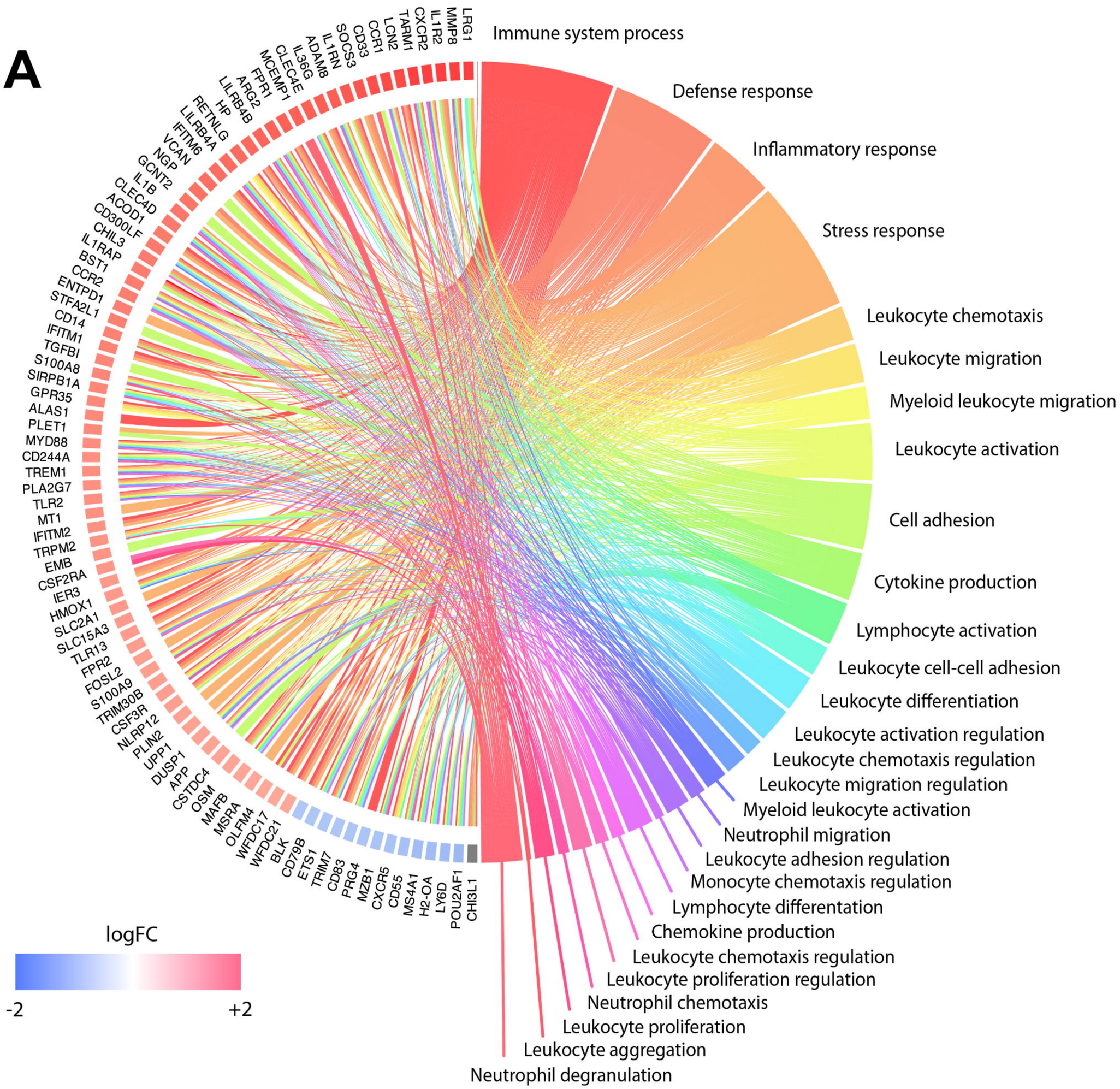
A
Immune system process
Defense response
Inflammatory response
Stress response
Leukocyte chemotaxis
Leukocyte migration
Myeloid leukocyte migration
Leukocyte activation
Cell adhesion
Cytokine production
Lymphocyte activation
Leukocyte cell-cell adhesion
Leukocyte differentiation
Leukocyte activation regulation
Leukocyte chemotaxis regulation
Leukocyte migration regulation
Myeloid leukocyte activation
Neutrophil migration
Leukocyte adhesion regulation
Monocyte chemotaxis regulation
Lymphocyte differentation
Chemokine production
Leukocyte chemotaxis regulation
Leukocyte proliferation regulation
Neutrophil chemotaxis
Leukocyte proliferation
Leukocyte aggregation
Neutrophil degranulation
LRG1
MMP8
IL1R2
CXCR2
TARM1
LCN2
CCR1
CD33
SOCS3
IL1RN
ADAM8
IL36G
CLEC4E
MCEMP1
FPR1
ARG2
LILRB4B
HP
RETNLG
LILRB4A
IFITM6
VCAN
NGP
GCNT2
IL1B
CLEC4D
ACOD1
CD300LF
CHIL3
IL1RAP
BST1
CCR2
ENTPD1
STFA2L1
CD14
IFITM1
TGFBI
S100A8
SIRPB1A
GPR35
ALAS1
PLET1
MYD88
CD244A
TREM1
PLA2G7
TLR2
MT1
IFITM2
TRPM2
EMB
CSF2RA
IER3
HMOX1
SLC2A1
SLC15A3
TLR13
FPR2
FOSL2
S100A9
TRIM30B
CSF3R
NLRP12
PLIN2
UPP1
DUSP1
APP
CSTDC4
OSM
MAFB
MSRA
OLFM4
WFDC17
WFDC21
BLK
CD79B
ETS1
TRIM7
CD83
PRG4
MZB1
CXCR5
CD55
MS4A1
H2-OA
LY6D
POU2AF1
CHI3L1
logFC
-2
+2
B
Chemotaxis regulation
FN1
CXCR4
STAP1
C-X-C motif chemokine 12 receptor activity
logFC
-2
+2

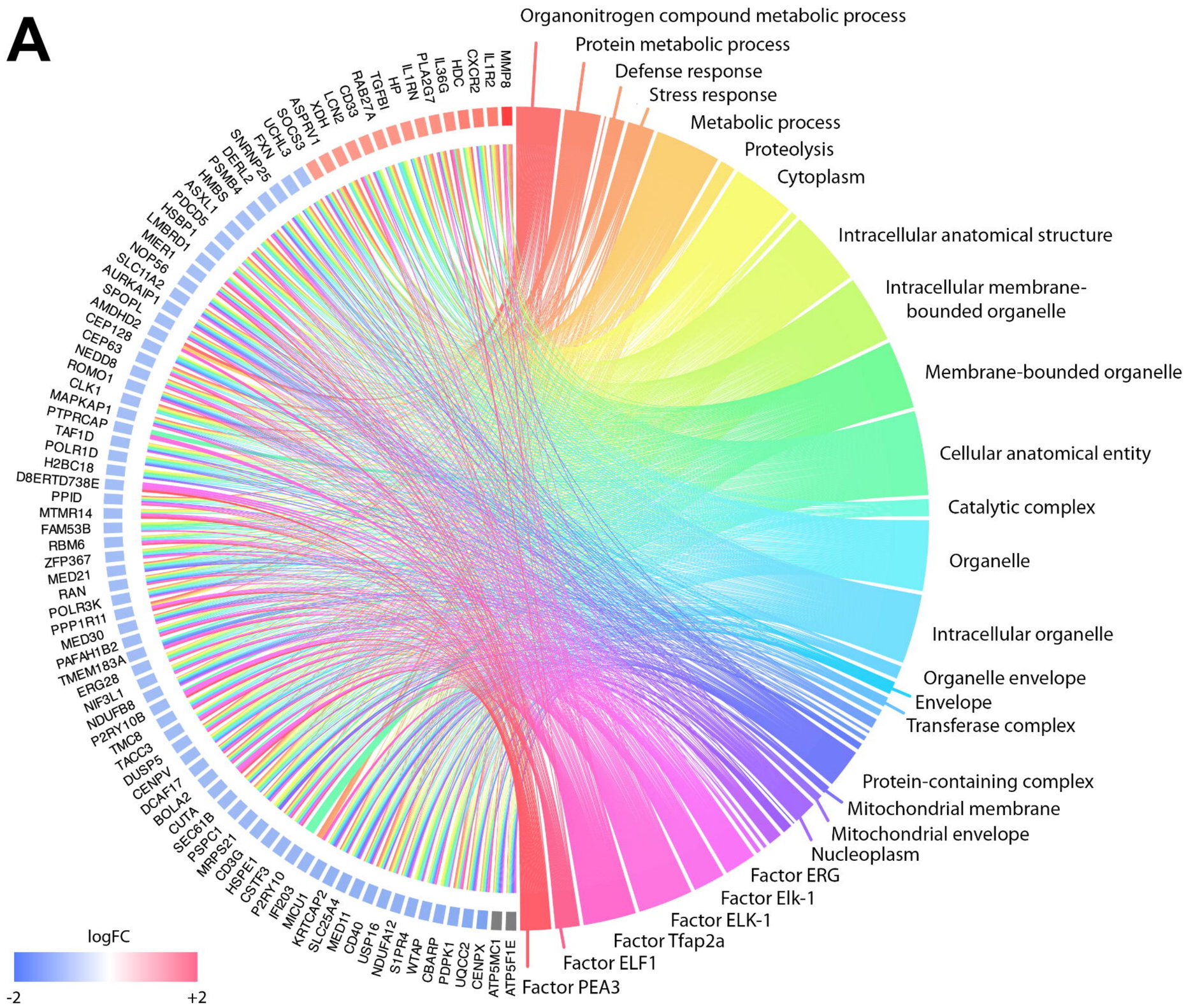
A
Organonitrogen compound metabolic process
Protein metabolic process
Defense response
Stress response
Metabolic process
Proteolysis
Cytoplasm
Intracellular anatomical structure
Intracellular membrane-bounded organelle
Membrane-bounded organelle
Cellular anatomical entity
Catalytic complex
Organelle
Intracellular organelle
Organelle envelope
Envelope
Transferase complex
Protein-containing complex
Mitochondrial membrane
Mitochondrial envelope
Nucleoplasm
Factor ERG
Factor Elk-1
Factor ELK-1
Factor Tfap2a
Factor ELF1
Factor PEA3
MMP8
IL1R2
CXCR2
HDC
IL36G
PLA2G7
IL1RN
HP
TGFBI
RAB27A
CD33
LCN2
XDH
ASPRV1
SOCS3
UCHL3
FXN
SNRNP25
DERL2
PSMB4
HMBS
ASXL1
PDCD5
HSBP1
LMBRD1
MIER1
NOP56
SLC11A2
AURKAIP1
SPOPL
AMDHD2
CEP128
CEP63
NEDD8
ROMO1
CLK1
MAPKAP1
PTPRCAP
TAF1D
POLR1D
H2BC18
D8ERTD738E
PPID
MTMR14
FAM53B
RBM6
ZFP367
MED21
RAN
POLR3K
PPP1R11
MED30
PAFAH1B2
TMEM183A
ERG28
NIF3L1
NDUFB8
P2RY10B
TMC8
TACC3
DUSP5
CENPV
DCAF17
BOLA2
CUTA
SEC61B
PSPC1
MRPS21
CD3G
HSPE1
CSTF3
P2RY10
IFI203
MICU1
KRTCAP2
SLC25A4
MED11
CD40
USP16
NDUFA12
S1PR4
WTAP
CBARP
PDPK1
UQCC2
CENPX
ATP5MC1
ATP5F1E
logFC
-2
+2

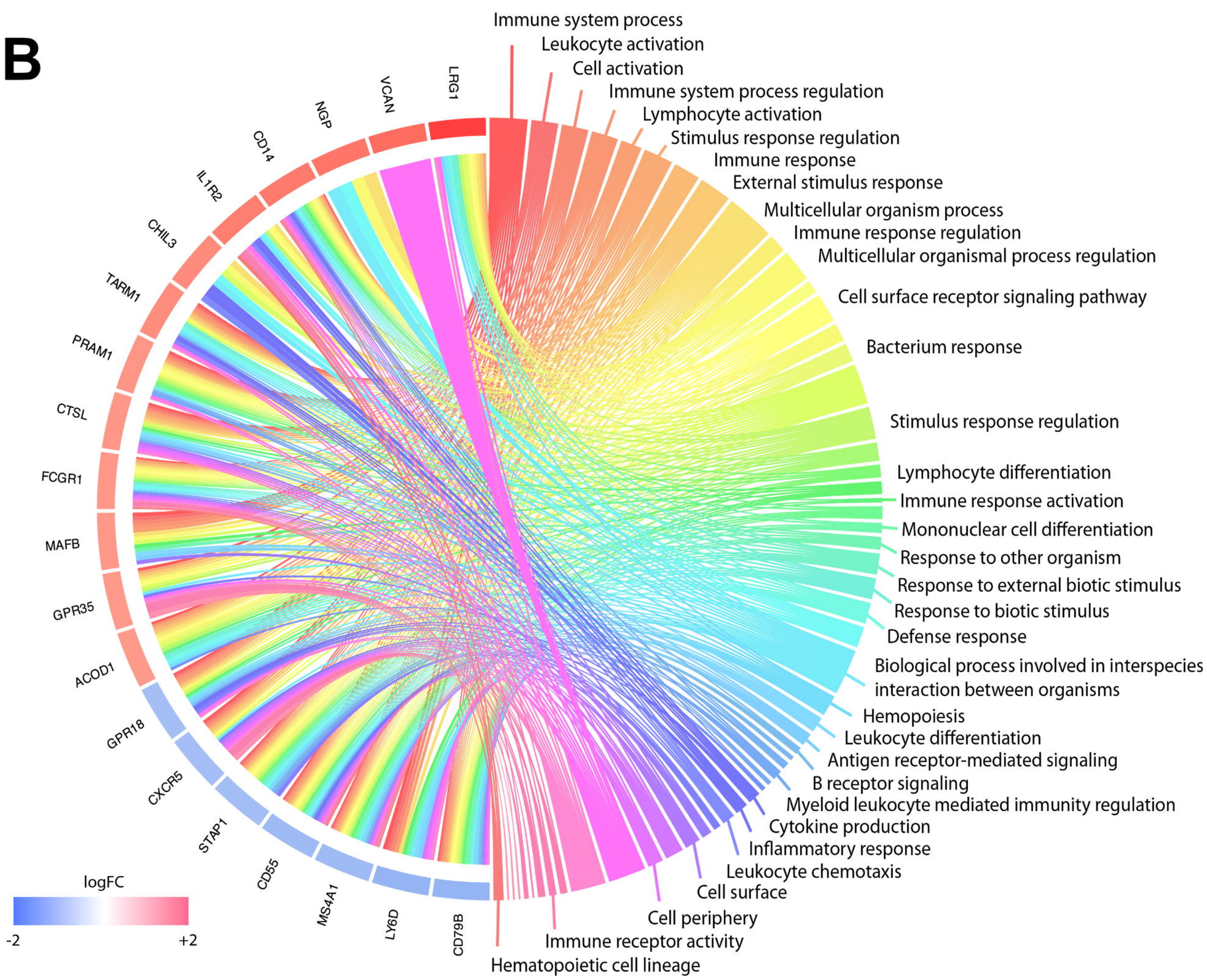
B
Immune system process
Leukocyte activation
Cell activation
Immune system process regulation
Lymphocyte activation
Stimulus response regulation
Immune response
External stimulus response
Multicellular organism process
Immune response regulation
Multicellular organismal process regulation
Cell surface receptor signaling pathway
Bacterium response
Stimulus response regulation
Lymphocyte differentiation
Immune response activation
Mononuclear cell differentiation
Response to other organism
Response to external biotic stimulus
Response to biotic stimulus
Defense response
Biological process involved in interspecies interaction between organisms
Hemopoiesis
Leukocyte differentiation
Antigen receptor-mediated signaling
B receptor signaling
Myeloid leukocyte mediated immunity regulation
Cytokine production
Inflammatory response
Leukocyte chemotaxis
Cell surface
Cell periphery
Immune receptor activity
Hematopoietic cell lineage
LRG1
VCAN
NGP
CD14
IL1R2
CHIL3
TARM1
PRAM1
CTSL
FCGR1
MAFB
GPR35
ACOD1
GPR18
CXCR5
STAP1
CD55
MS4A1
LY6D
CD79B
logFC
-2
+2

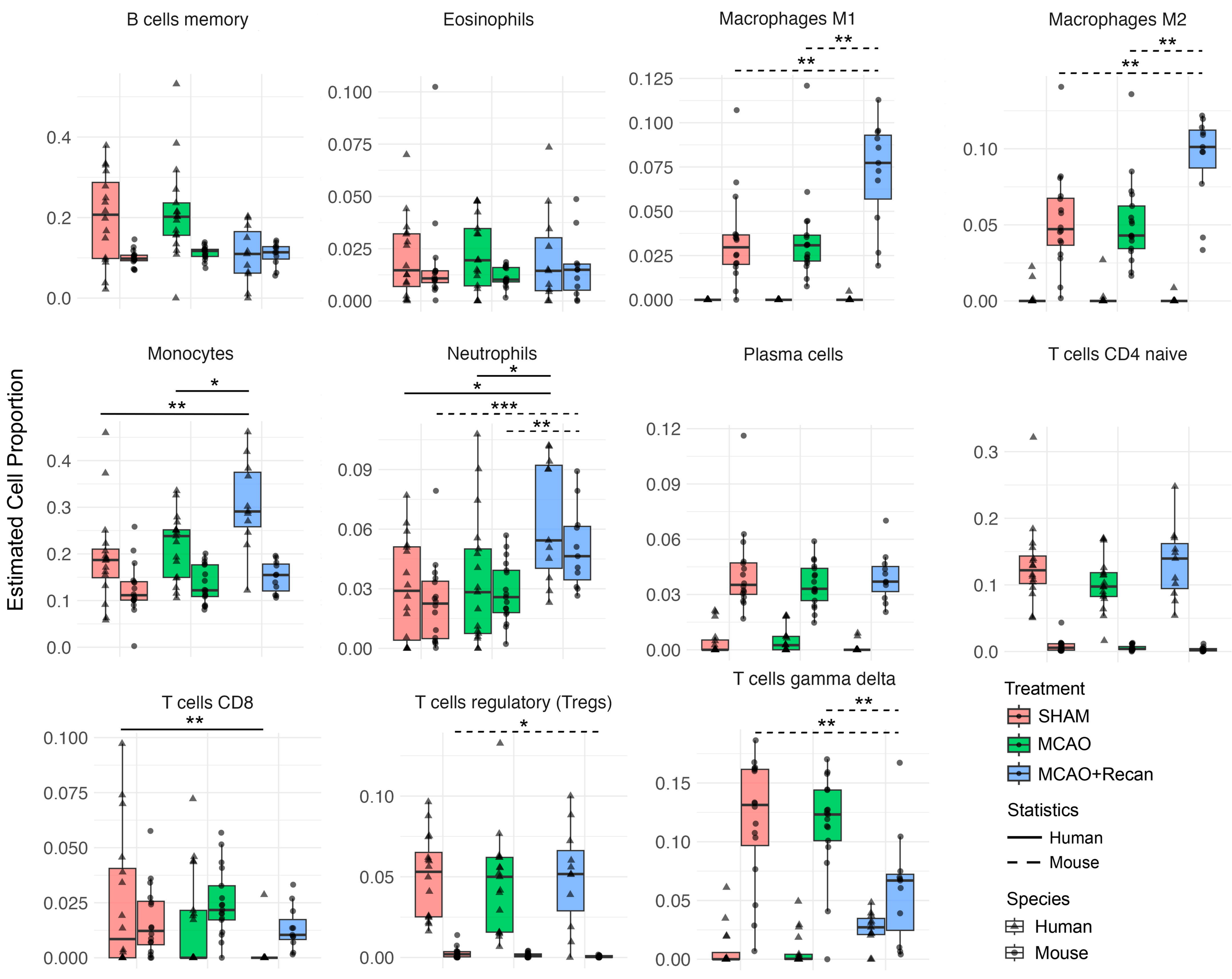
B cells memory
Eosinophils
Macrophages M1
Macrophages M2
Monocytes
Neutrophils
Plasma cells
T cells CD4 naive
T cells CD8
T cells regulatory (Tregs)
T cells gamma delta
Estimated Cell Proportion
Treatment
SHAM
MCAO
MCAO+Recan
Statistics
Human
Mouse
Species
Human
Mouse

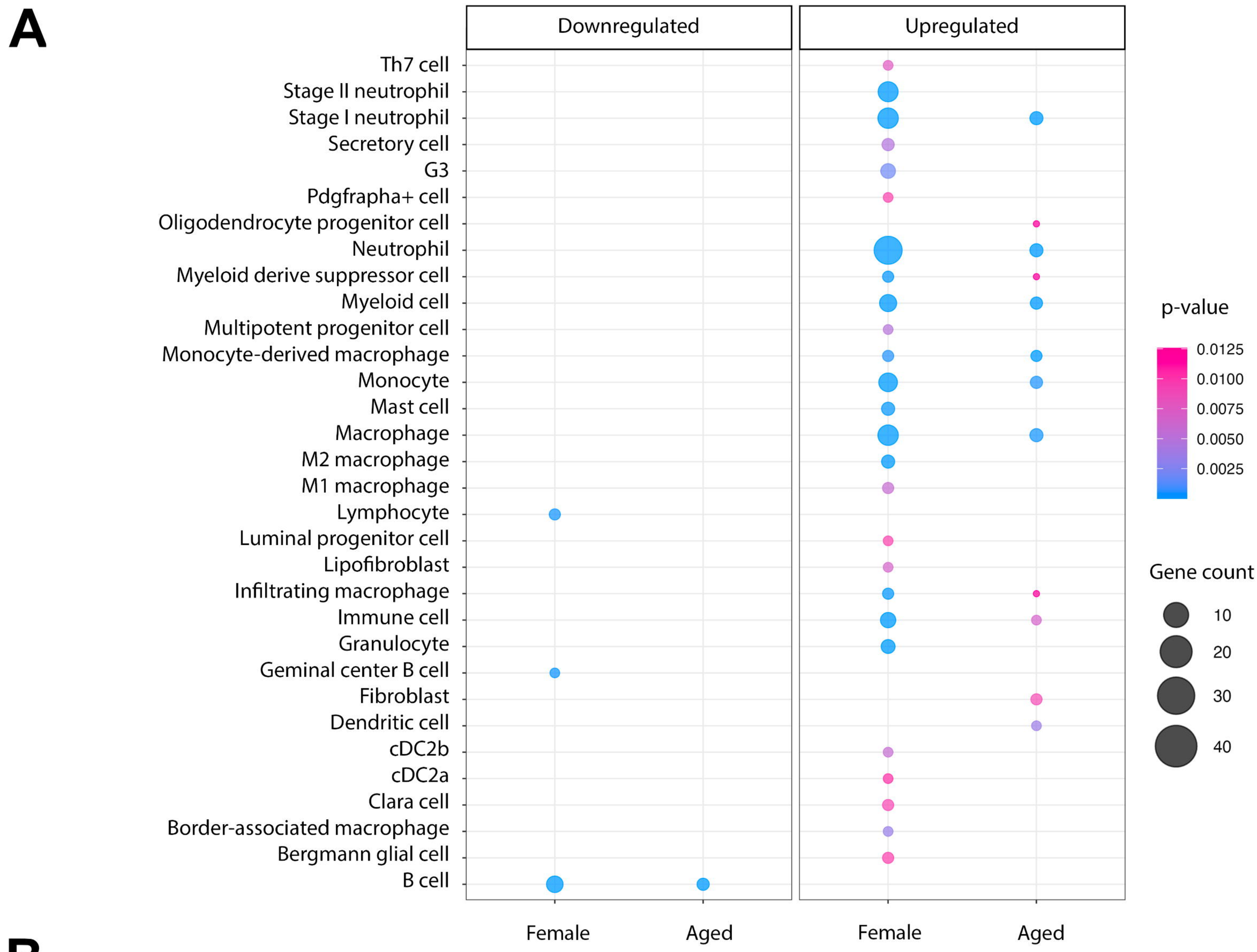
A
Downregulated
Upregulated
Th7 cell
Stage II neutrophil
Stage I neutrophil
Secretory cell
G3
Pdgfrapha+ cell
Oligodendrocyte progenitor cell
Neutrophil
Myeloid derive suppressor cell
Myeloid cell
Multipotent progenitor cell
Monocyte-derived macrophage
Monocyte
Mast cell
Macrophage
M2 macrophage
M1 macrophage
Lymphocyte
Luminal progenitor cell
Lipofibroblast
Infiltrating macrophage
Immune cell
Granulocyte
Geminal center B cell
Fibroblast
Dendritic cell
cDC2b
cDC2a
Clara cell
Border-associated macrophage
Bergmann glial cell
B cell
Female
Aged
Female
Aged
p-value
0.0125
0.0100
0.0075
0.0050
0.0025
Gene count
10
20
30
40

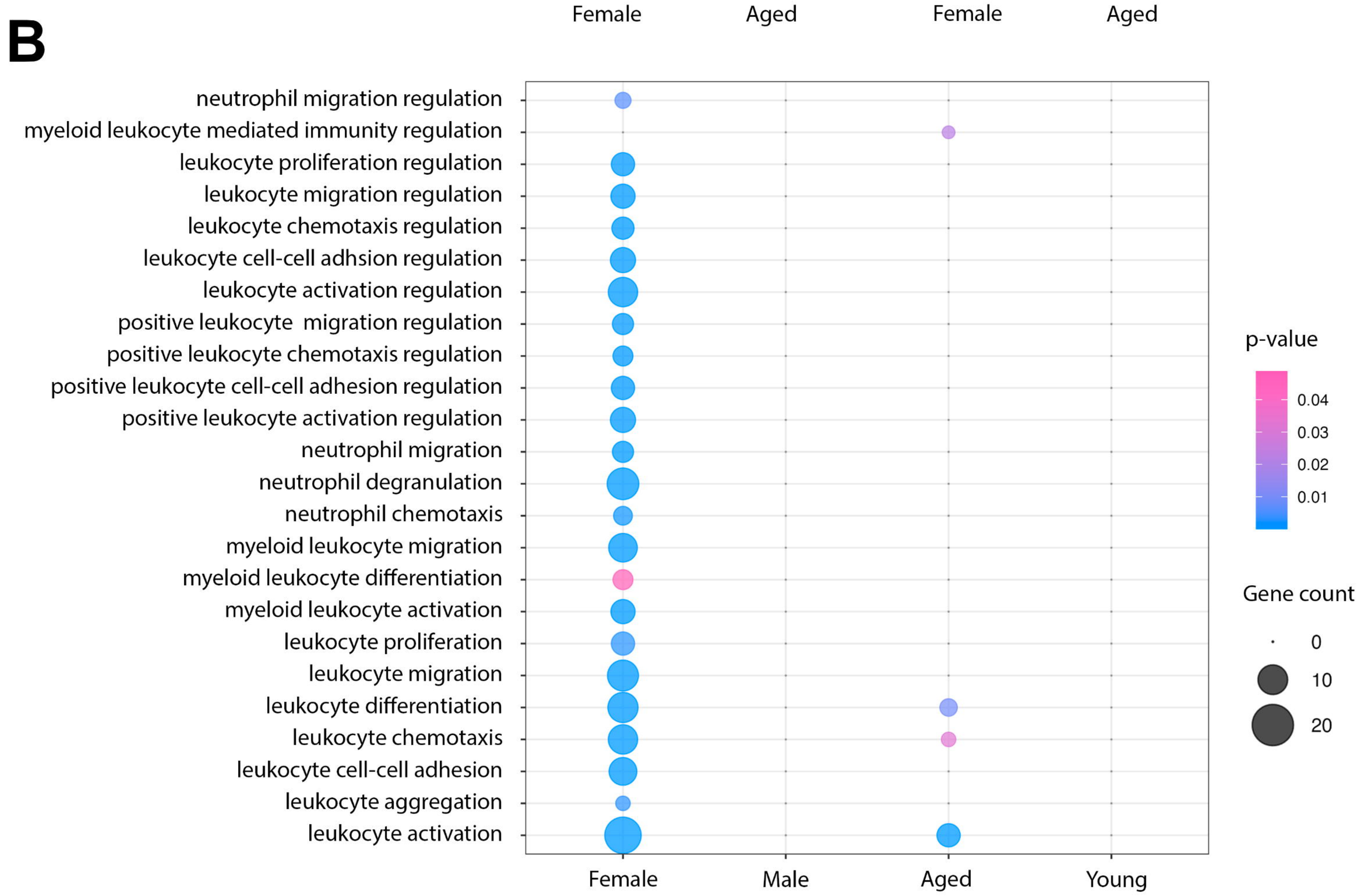
B
neutrophil migration regulation
myeloid leukocyte mediated immunity regulation
leukocyte proliferation regulation
leukocyte migration regulation
leukocyte chemotaxis regulation
leukocyte cell-cell adhsion regulation
leukocyte activation regulation
positive leukocyte migration regulation
positive leukocyte chemotaxis regulation
positive leukocyte cell-cell adhesion regulation
positive leukocyte activation regulation
neutrophil migration
neutrophil degranulation
neutrophil chemotaxis
myeloid leukocyte migration
myeloid leukocyte differentiation
myeloid leukocyte activation
leukocyte proliferation
leukocyte migration
leukocyte differentiation
leukocyte chemotaxis
leukocyte cell-cell adhesion
leukocyte aggregation
leukocyte activation
Female
Male
Aged
Young
p-value
0.04
0.03
0.02
0.01
Gene count
0
10
20

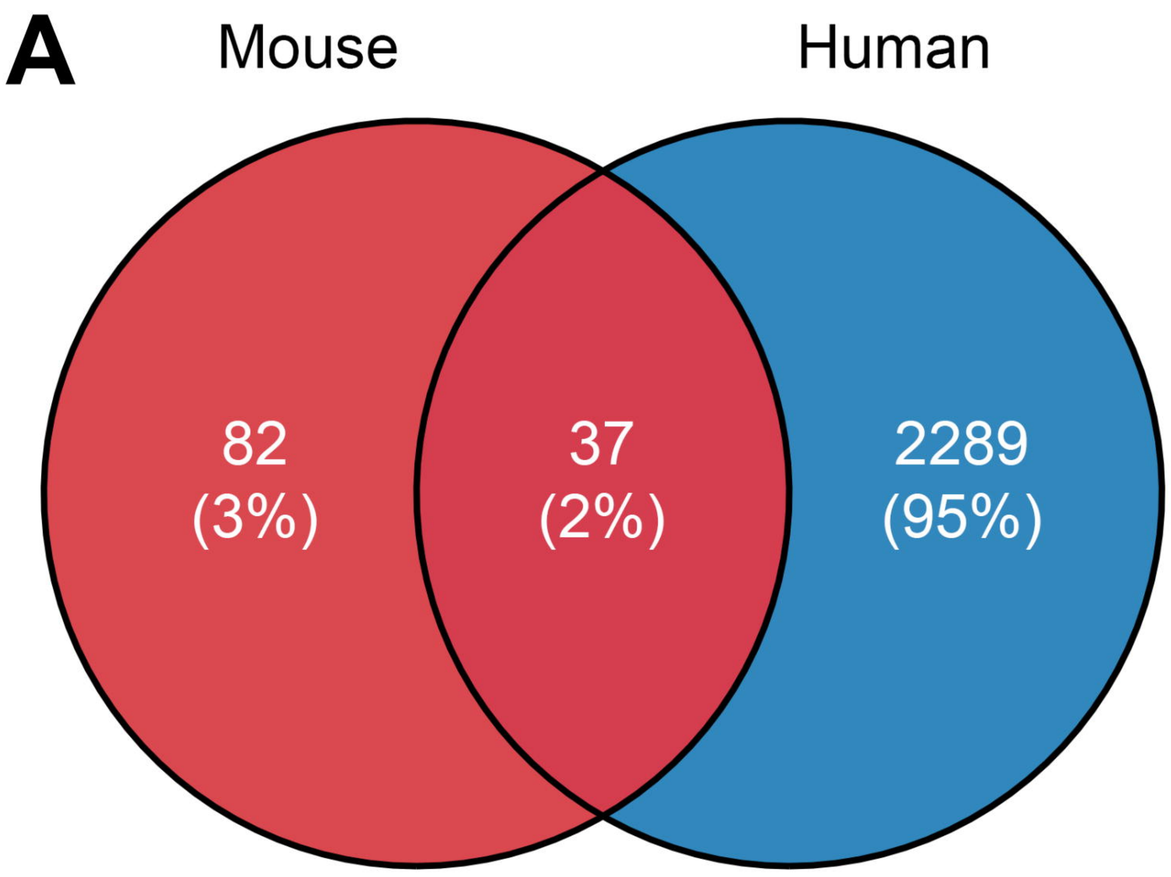
A
Mouse
Human
82
(3%)
37
(2%)
2289
(95%)

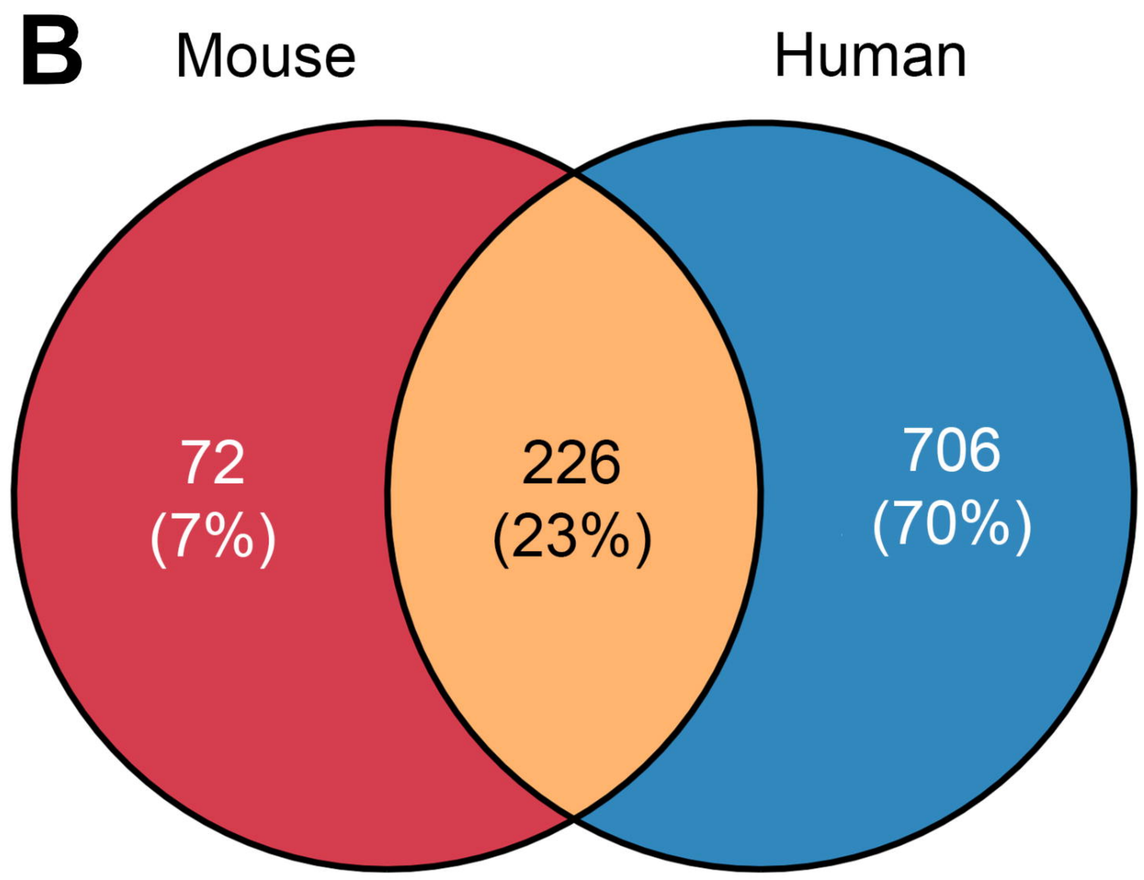
B
Mouse
Human
72
(7%)
226
(23%)
706
(70%)

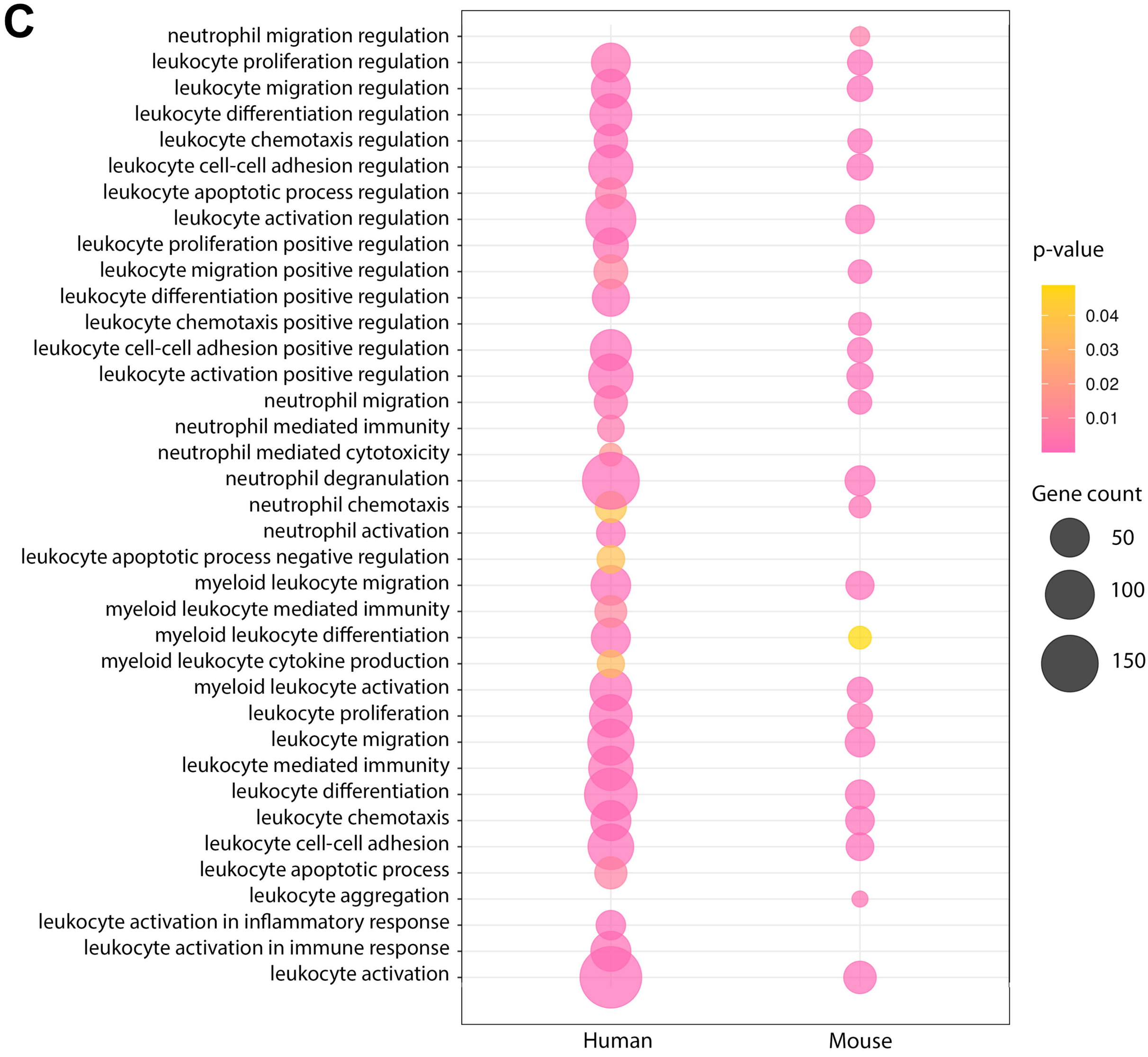
C
neutrophil migration regulation
leukocyte proliferation regulation
leukocyte migration regulation
leukocyte differentiation regulation
leukocyte chemotaxis regulation
leukocyte cell-cell adhesion regulation
leukocyte apoptotic process regulation
leukocyte activation regulation
leukocyte proliferation positive regulation
leukocyte migration positive regulation
leukocyte differentiation positive regulation
leukocyte chemotaxis positive regulation
leukocyte cell-cell adhesion positive regulation
leukocyte activation positive regulation
neutrophil migration
neutrophil mediated immunity
neutrophil mediated cytotoxicity
neutrophil degranulation
neutrophil chemotaxis
neutrophil activation
leukocyte apoptotic process negative regulation
myeloid leukocyte migration
myeloid leukocyte mediated immunity
myeloid leukocyte differentiation
myeloid leukocyte cytokine production
myeloid leukocyte activation
leukocyte proliferation
leukocyte migration
leukocyte mediated immunity
leukocyte differentiation
leukocyte chemotaxis
leukocyte cell-cell adhesion
leukocyte apoptotic process
leukocyte aggregation
leukocyte activation in inflammatory response
leukocyte activation in immune response
leukocyte activation
Human
Mouse
p-value
0.04
0.03
0.02
0.01
Gene count
50
100
150

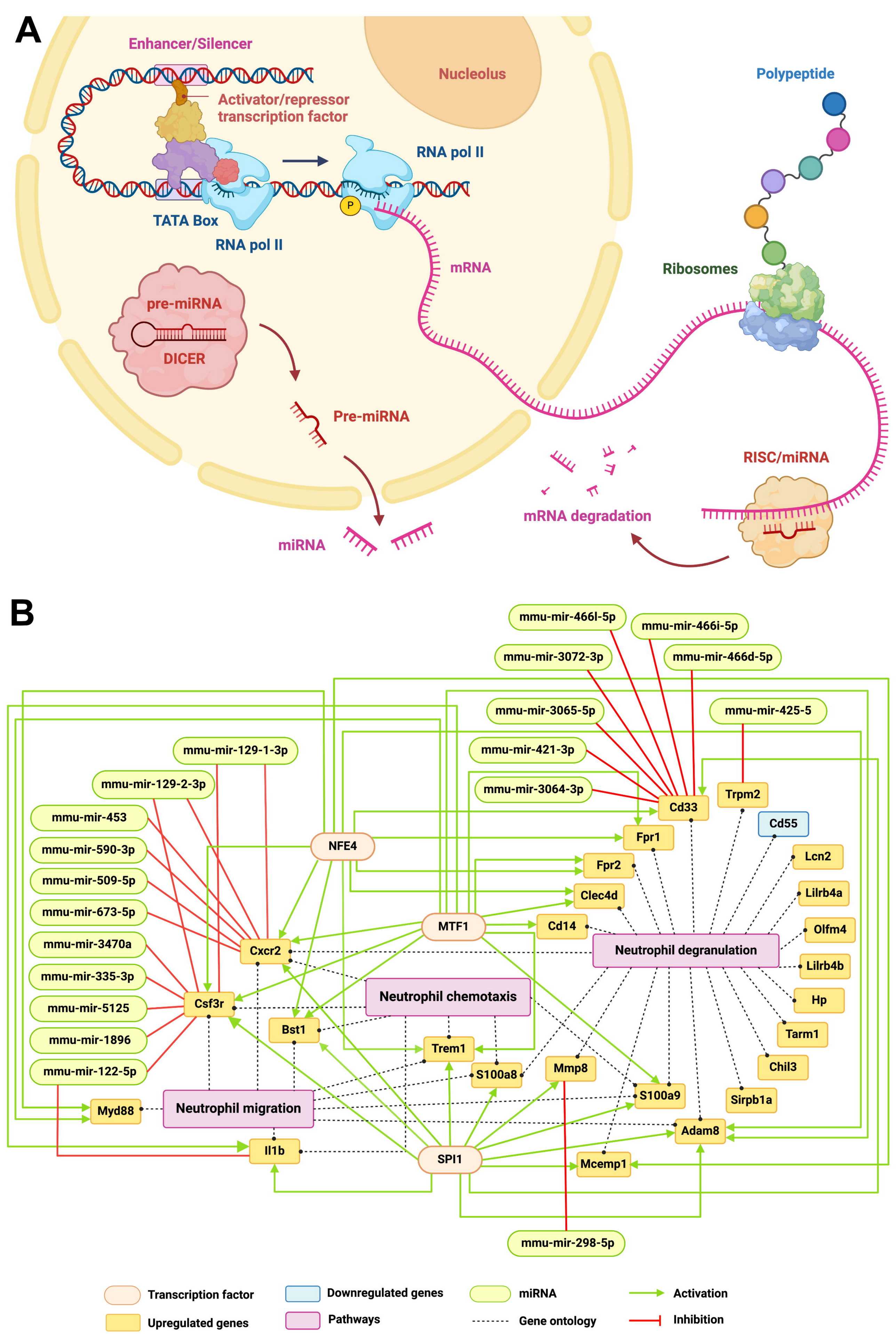
A
Enhancer/Silencer
Nucleolus
Polypeptide
Activator/repressor transcription factor
RNA pol II
TATA Box
RNA pol II
P
mRNA
Ribosomes
pre-miRNA
DICER
Pre-miRNA
RISC/miRNA
mRNA degradation
miRNA
B
mmu-mir-466l-5p
mmu-mir-466i-5p
mmu-mir-3072-3p
mmu-mir-466d-5p
mmu-mir-3065-5p
mmu-mir-425-5
mmu-mir-129-1-3p
mmu-mir-421-3p
mmu-mir-129-2-3p
mmu-mir-3064-3p
mmu-mir-453
mmu-mir-590-3p
mmu-mir-509-5p
mmu-mir-673-5p
mmu-mir-3470a
mmu-mir-335-3p
mmu-mir-5125
mmu-mir-1896
mmu-mir-122-5p
Cd33
Trpm2
Cd55
Fpr1
NFE4
Fpr2
Lcn2
Clec4d
Lilrb4a
MTF1
Cd14
Olfm4
Cxcr2
Neutrophil degranulation
Lilrb4b
Neutrophil chemotaxis
Csf3r
Hp
Bst1
Tarm1
Trem1
Chil3
S100a8
Mmp8
S100a9
Sirpb1a
Myd88
Neutrophil migration
Adam8
Il1b
SPI1
Mcemp1
mmu-mir-298-5p
Transcription factor
Downregulated genes
miRNA
Activation
Upregulated genes
Pathways
Gene ontology
Inhibition